Draft version November 29, 2021
Typeset using LaTeX **twocolumn** style in AASTeX631

Searches for Gravitational Waves from Known Pulsars at Two Harmonics in the Second and Third LIGO-Virgo Observing Runs

The LIGO Scientific Collaboration, the Virgo Collaboration, and the KAGRA Collaboration

(Dated: November 29, 2021)

ABSTRACT

We present a targeted search for continuous gravitational waves (GWs) from 236 pulsars using data from the third observing run of LIGO and Virgo (O3) combined with data from the second observing run (O2). Searches were for emission from the $l = m = 2$ mass quadrupole mode with a frequency at only twice the pulsar rotation frequency (single harmonic) and the $l = 2, m = 1, 2$ modes with a frequency of both once and twice the rotation frequency (dual harmonic). No evidence of GWs was found so we present 95% credible upper limits on the strain amplitudes h_0 for the single harmonic search along with limits on the pulsars' mass quadrupole moments Q_{22} and ellipticities ε. Of the pulsars studied, 23 have strain amplitudes that are lower than the limits calculated from their electromagnetically measured spin-down rates. These pulsars include the millisecond pulsars J0437−4715 and J0711−6830 which have spin-down ratios of 0.87 and 0.57 respectively. For nine pulsars, their spin-down limits have been surpassed for the first time. For the Crab and Vela pulsars our limits are factors of ~ 100 and ~ 20 more constraining than their spin-down limits, respectively. For the dual harmonic searches, new limits are placed on the strain amplitudes C_{21} and C_{22}. For 23 pulsars we also present limits on the emission amplitude assuming dipole radiation as predicted by Brans-Dicke theory.

1. INTRODUCTION

To date, the LIGO and Virgo observatories have made detections of numerous sources of gravitational radiation. These detections have been of transient gravitational waves (GWs) from the inspiral and subsequent mergers of compact binary objects including binary black holes and binary neutron stars (Abbott et al. 2021a). Recently, the list of observed events expanded to include neutron star-black hole binaries (Abbott et al. 2021b). There remain other types of GW sources that are yet to be observed such as continuous GW (CW) sources. Unlike transients, CW signals are almost monochromatic, with their amplitude and frequency changing very slowly over year-long timescales. The mass quadrupoles of these sources, such as deformed neutron stars, are expected to be far smaller than those involved in compact binaries and therefore only local galactic sources are likely to produce detectable signals.

Likely candidates for producing such signals are neutron stars spinning with some non-axisymmetric deformation (Zimmermann & Szedenits 1979). This may be a solid deformation such as mountains on the crust produced during cooling (Ushomirsky et al. 2000), from binary accretion (Gittins & Andersson 2021) or due to strong magnetic fields (Bonazzola & Gourgoulhon 1996; Cutler 2002). GW radiation can also be caused by fluid modes of oscillation beneath the crust such as r-modes (Andersson 1998; Friedman & Morsink 1998). By detecting CWs, light can be shed on the structure of the star. Additionally, detections of such GWs can be used to test general relativity via the constraint of non-standard GW polarization (Isi et al. 2017; Abbott et al. 2019a). A more thorough discussion of various methods of GW emission from neutron stars can be found in Riles (2017); Glampedakis & Gualtieri (2018).

The structure of this paper is as follows. Section 1.1 outlines the types of CW searches. Section 1.2 describes the types of signal models used in this analysis. Section 2 describes the search methods used. Section 3 covers both the GW and EM data used. We present our results in Section 4 with conclusions in Section 5.

1.1. *Continuous-wave searches*

There are broadly three types of CW searches. Targeted searches look for signals from known pulsars for which their rotational phases can be accurately deter-

mined from electromagnetic (EM) observations (e.g., Abbott et al. 2017a, 2019b; Nieder et al. 2019, 2020; Abbott et al. 2020, 2021c). This simplifies the search as the EM observations can be used to derive a timing solution and it is assumed that the GW phase evolution is locked to the EM evolution. This means the search is over a small parameter space, generally limited to the unknown signal amplitude and orientation of the source, which allows a more sensitive search than other methods. In some targeted searches, the assumption that the GW evolution follows the EM evolution is relaxed and the search is performed in a narrow band around the expected frequency and spin-down rate (Abbott et al. 2017b, 2019c). In this case, the search is more computationally expensive due to the larger parameter range being searched and slightly less sensitive because of a higher trials factor. To overcome this, narrow-band searches often look at fewer targets. Directed searches look for signals from small sky regions that are believed to have a high probability of containing a neutron star, such as supernova remnants (e.g., Abbott et al. 2019d; Ming et al. 2019; Lindblom & Owen 2020; Papa et al. 2020; Abbott et al. 2021d). As the timing solution cannot be derived from EM observations, a wide range of rotational parameters must be searched. All-sky searches look for signals in all sky directions and over a wide range of rotational parameters (e.g., Abbott et al. 2018, 2019e; Dergachev & Papa 2020; Abbott et al. 2021e; Steltner et al. 2021). Both these methods suffer increasing computational costs and decreasing sensitivity of the searches as parameter space increases.

Searches of all three types have been performed and so far no convincing evidence for CWs has been observed. However, searches have probed new regimes, such as providing upper limits on emission that are more stringent (i.e., smaller) than those based on energetics arguments. For example, for several pulsars including the Crab pulsar, Vela pulsar (Abbott et al. 2019b), J0537−6910 (Abbott et al. 2021c,f) and two millisecond pulsars (Abbott et al. 2020) the direct upper limits set on the GW amplitude are more constraining than limits based on the assumption that all the pulsars' spin-down luminosity is radiated through GWs, known as the spin-down limit.

In this paper we report the new results of a targeted search for CW signals from 236 pulsars using the most recent LIGO and Virgo datasets including the second and third observing runs (O2 and O3 respectively). LIGO (Aasi et al. 2015) consists of two gravitational-wave detectors situated in Hanford, Washington (H1) and Livingston, Louisiana (L1) while Virgo (Acernese et al. 2015) is located in Cascina, Pisa (V1). The ephemerides for the pulsars have been derived from observations using the CHIME, Hobart, Jodrell Bank, MeerKAT, Nancay, NICER and UTMOST observatories. More details on these observations can be found in Section 3.2.

1.2. *Signal models*

We assume that the gravitational-wave (GW) emission is locked to the rotational phase of the pulsar. For the ideal case of a triaxial star rotating steadily about a principal moment of inertia axis, the GW emission is at twice the star's spin frequency, $f_{\rm rot}$. However, there are mechanisms that can produce variations to this $2f_{\rm rot}$ frequency. For example, a superfluid component with a misaligned spin axis within the star could produce a dual-harmonic emission at both once and twice the rotation frequency without leaving an imprint on the EM emission (Jones 2010). Therefore we perform two searches: one at just twice the pulsar rotation frequency and one at both one and two times the frequency, which is referred to as a dual harmonic search.

The waveform used in the dual harmonic search is detailed in Jones (2010) and used in Pitkin et al. (2015); Abbott et al. (2017a, 2019b, 2020). The signals h_{21} and h_{22} at once and twice the pulsar rotation frequency can be defined as

$$h_{21} = -\tfrac{C_{21}}{2}\Big[F_+^D(\alpha,\delta,\psi;t)\sin\iota\cos\iota\cos\left(\Phi(t)+\Phi_{21}^C\right) + F_\times^D(\alpha,\delta,\psi;t)\sin\iota\sin\left(\Phi(t)+\Phi_{21}^C\right)\Big], \quad (1)$$

$$h_{22} = -C_{22}\Big[F_+^D(\alpha,\delta,\psi;t)(1+\cos^2\iota)\cos\left(2\Phi(t)+\Phi_{22}^C\right) + 2F_\times^D(\alpha,\delta,\psi;t)\cos\iota\sin\left(2\Phi(t)+\Phi_{22}^C\right)\Big], \quad (2)$$

where C_{21} and C_{22} are the dimensionless constants that give the component amplitudes, the angles (α,δ) are the right ascension and declination of the source, while the angles (ι,ψ) describe the orientation of the source's spin axis with respect to the observer in terms of inclination and polarization, Φ_{21}^C and Φ_{22}^C are phase angles at a defined epoch and $\Phi(t)$ is the rotational phase of the source. The antenna functions F_+^D and $F_\times^D$ describe how the two polarization components (plus and cross) are projected onto the detector.

For the ideal case of a steadily spinning triaxial star emitting GWs only at twice the rotation frequency, the equatorial ellipticity can be defined as

$$\varepsilon \equiv \frac{|I_{xx}-I_{yy}|}{I_{zz}}, \quad (3)$$

where (I_{xx}, I_{yy}, I_{zz}) are the source's principal moments of inertia, with the star rotating about the z-axis. The mass quadrupole of the source Q_{22} is often quoted and

is related to the ellipticity as

$$Q_{22} = I_{zz}\varepsilon\sqrt{\frac{15}{8\pi}}. \quad (4)$$

For single harmonic emission, C_{21} from equation (1) can be set as 0, leaving only C_{22} in equation (2). The amplitude can then be parameterised as the dimensionless h_0: the amplitude of the circularly polarised signal that would be observed if the source lay directly above or below the plane of the detector and had its spin axis pointed directly towards or away from the detector. The following equations are defined in Aasi et al. (2014).

$$h_0 = 2C_{22} = \frac{16\pi^2 G}{c^4}\frac{I_{zz}\varepsilon f_{\rm rot}^2}{d}, \quad (5)$$

where d is the distance of the source. The spin-down limit $h_0^{\rm sd}$ of a source is given by:

$$h_0^{\rm sd} = \frac{1}{d}\left(\frac{5GI_{zz}}{2c^3}\frac{|\dot{f}_{\rm rot}|}{f_{\rm rot}}\right)^{1/2}, \quad (6)$$

where $\dot{f}_{\rm rot}$ is the first derivative of the rotational frequency, i.e., the spin-down rate, and provides an amplitude limit assuming that all of the rotational energy lost by the pulsar is converted to gravitational-wave energy (Owen 2005). When the directly observed h_0 is smaller than $h_0^{\rm sd}$, the spin-down limit can be said to have been surpassed. This information is most often represented by quoting the "spin-down ratio", i.e., the ratio between h_0 and $h_0^{\rm sd}$. If assuming that there is no mechanism (e.g., accretion) providing some additional spin-up torque, the direct amplitude constraints probe a new physical regime only when the spin-down limit is surpassed. There are two types of spin-down rate: intrinsic and observed. The observed spin-down rate can be affected by the transverse velocity of the source, e.g., the Shlovskii effect (Shklovskii 1970), so where possible the intrinsic spin-down rate is used to calculate the spin-down limit.

1.2.1. *Non-GR polarization signal*

In this paper we also perform a search for GWs with polarizations as predicted in a modification of the standard general relativity (GR) proposed by Brans and Dicke. The Brans-Dicke theory (Brans & Dicke 1961) predicts three independent polarization states: two tensor polarizations, as in GR, and an additional scalar polarization. The dominant scalar radiation in Brans-Dicke theory originates from the time-dependent dipole moment (see Verma 2021, for details). The signal h_{11} due to dipole radiation is given by (see Eqs. (63) - (67) and (70) - (71) of Verma 2021)

$$h_{11} = -h_0^d\, c(\alpha,\delta;t)\,\sin\iota\sin(\Phi(t)+\Phi_0), \quad (7)$$

where $c(\alpha,\delta;t)$ is the amplitude modulation function and Φ_0 is the phase angle at time $t = 0$. The explicit formula for $c(\alpha,\delta;t)$ is given by Eq. (64) of Verma (2021). We see that the dipole radiation comes at the rotational frequency of the pulsar. We assume that the only non-vanishing component D of the dipole moment in the pulsar's frame is in the x-direction. Then the amplitude h_0^d of the signal is given by

$$h_0^d = \frac{4\pi G}{c^3}\zeta\frac{Df_{\rm rot}}{d}, \quad (8)$$

where ζ is the parameter of the Brans-Dicke theory (see Section 3 of Verma 2021, for details).

2. ANALYSIS

As in Abbott et al. (2017a, 2019b), three largely independent analysis methods were used for the searches in this paper: the *Time-domain Bayesian method* (Section 2.1), the $\mathcal{F}/\mathcal{G}/\mathcal{D}$-statistic method (Section 2.2), and the *5n-vector method* (Section 2.3). The $\mathcal{F}/\mathcal{G}/\mathcal{D}$-statistic and the 5n-vector methods are only used in searches for pulsars deemed to be high-value: those which surpass their spin-down limits in the Bayesian analysis. The Bayesian and $\mathcal{F}/\mathcal{G}/\mathcal{D}$-statistic methods search for two signal models: a single harmonic signal emitted by the $l = m = 2$ mass quadrupole mode at twice the pulsar rotation frequency and a dual harmonic signal emitted by the $l = m = 2$ *and* $l = 2, m = 1$ modes at twice and once the frequency. The 5n-vector method restricts the latter search to the $l = 2, m = 1$ mode only. Only one method, the $\mathcal{D}$-statistic, is used for the Brans-Dicke polarization search. The GW emission is assumed to precisely follow the phase evolution determined through EM observations, although uncertainties in values from the EM observations are not accounted for here.

2.1. *Time-domain Bayesian method*

The raw GW strain data are heterodyned using their expected phase evolution, which includes corrections for the relative motion of the source with respect to the detector and relativistic effects (Dupuis & Woan 2005). They are then low-pass filtered using a cut-off frequency of 0.25 Hz and then down-sampled to one sample per minute (1/60 Hz bandwidth) centred about the expected signal frequency now at 0 Hz. For the dual harmonic search this is repeated so that a time series is obtained centred at both $f_{\rm rot}$ and $2f_{\rm rot}$. Bayesian inference is used to estimate the remaining unknown signal parameters and the evidence for the signal model (Pitkin et al. 2017). For the parameter inference, the prior distributions used were those given in Appendix 2 of Abbott

et al. (2017a). They were uninformative uniform priors for the orientation angles, unless restricted ranges were appropriate as discussed in Section 2.1.2. For the amplitude parameters, Fermi-Dirac distribution priors were used (see Section 2.3.5 of Pitkin et al. 2017). The Fermi-Dirac distributions for each pulsar were set such that they were close to flat over the bulk of the likelihood while penalizing very large values. To avoid basing the priors on current detector data the priors were constructed by choosing Fermi-Dirac parameters that gave distributions for which the 95% probability upper bound was equivalent to the estimated upper limit sensitivity of the combined LIGO S6 and Virgo VSR4 science runs at the particular pulsar GW signal frequency.[1]

This method also considers the effect of glitches on the pulsars (Section 2.1.1) and can perform searches with restrictions on the pulsar orientation (Section 2.1.2).

2.1.1. *Glitches*

Although their frequency is usually very stable, pulsars occasionally experience a transient increase in rotation frequency and frequency derivative. Such events are called glitches and are most common in young, non-recycled pulsars, although they do rarely occur in millisecond pulsars (Cognard & Backer 2004; McKee et al. 2016). Some of our sample of pulsars glitched during the course of O2 and O3. We assume that glitches affect the GW phase identically to the EM phase, but with the addition of an unknown phase offset at the time of the glitch. This phase offset is included in the parameter inference. For glitches that occur before or after the range of the data, no phase offset is needed. The pulsars which experienced glitching during the course of this analysis are J0534+2200, also known as the Crab pulsar (Shaw et al. 2021), J0908−4913 (Lower et al. 2019) and J1105−6107. They are shown in Table 1 along with the time (MJD) of the glitch.

2.1.2. *Restricted orientations*

Occasionally, the orientation of a pulsar can be determined from modeling of X-ray observations of its pulsar wind nebula (Ng & Romani 2004, 2008). In such cases, these values can be included as narrow priors on inclination and polarization angle rather than using an uninformative uniform prior. Results still assuming uniform priors are also included. Such pulsars are shown in Table 2 below along with their restricted prior ranges (Abbott et al. 2017a), which are assumed to be Gaussian about the given mean and standard deviation.

In the case of the Crab pulsar, which both experienced a glitch and has sufficient observations for restricted priors, four individual analyses are performed. Each analysis accounts for the glitch, with combinations of dual/single harmonic search and restricted/unrestricted priors.

[1] For the dual harmonic search for pulsars with signal components below 20 Hz, the C_{21} priors were constructed without using the estimated VSR4 Virgo sensitivity. This was to prevent prior from dominating over the likelihood in this frequency region.

2.2. *$\mathcal{F}/\mathcal{G}/\mathcal{D}$-statistic method*

The time-domain $\mathcal{F}/\mathcal{G}/\mathcal{D}$-statistic method uses the $\mathcal{F}$-statistic derived in Jaranowski et al. (1998) and the $\mathcal{G}$ statistic derived in Jaranowski & Królak (2010). The input data for the analysis using this method are the heterodyned data used in the time-domain Bayesian analysis. The $\mathcal{F}$-statistic is used when the amplitude, phase and polarization of the signal are unknown, whereas the $\mathcal{G}$-statistic is applied when only amplitude and phase are unknown, and the polarization of the signal is known (as described in Section 2.1.2). The methods have been used in several analyses of LIGO and Virgo data (Abadie et al. 2011; Aasi et al. 2014; Abbott et al. 2017a, 2020). The method also uses the $\mathcal{D}$-statistic developed in Verma (2021) to search for dipole radiation in Brans-Dicke theory. The $\mathcal{D}$-statistic search is the first search of LIGO and Virgo data for dipole radiation as predicted by Brans-Dicke theory.

In this method a signal is detected in the data if the value of the $\mathcal{F}$-, $\mathcal{G}$- or $\mathcal{D}$-statistic exceeds a certain threshold corresponding to an acceptable false alarm probability. We consider the false alarm probability of 1% for the signal to be significant. The $\mathcal{F}$-, $\mathcal{G}$-, and $\mathcal{D}$-statistics are computed for each detector and each inter-glitch period separately. The results from different detectors or different inter-glitch periods are then combined incoherently by adding the respective statistics. When the values of the statistics are not statistically significant, we set upper limits on the amplitude of the gravitational-wave signal.

2.3. *The 5n-vector method*

The 5n-vector method, derived in Astone et al. (2012), is a multi-detector matched filter in the frequency domain, based on the sidereal modulation of the expected signal amplitude and phase. The method has been used in several analysis of LIGO and Virgo detector data (Abadie et al. 2011; Aasi et al. 2014; Abbott et al. 2017a, 2020), and recently Abbott et al. (2021a) combined with the Band-Sample Data (BSD) framework (Piccinni et al. 2018). This is based on the construction of BSD files, i.e., complex time series that cover 10 Hz and 1 month of the original dataset. Using the BSD files, the compu-

Table 1. Pulsars with glitches occurring during the course of the runs used in this analysis.

PSR	Epoch (MJD)
J0534+2200 (Crab)	58687.6448 ± 0.0033
J0908−4913	58767.34 ± 4.5
J1105−6107	58582.24

Table 2. Pulsars with observations sufficient to restrict their orientation priors in terms of inclination and polarization and the values used as the constraints.

PSR	Ψ (rad)	ι_1 (rad)	ι_2 (rad)
J0534+2200 (Crab)	2.1844 ± 0.0016	1.0850 ± 0.0149	2.0566 ± 0.0149
J0835-4510 (Vela)	2.2799 ± 0.0015	1.1048 ± 0.0105	2.0368 ± 0.0105
J1952+3252	0.2007 ± 0.1501		
J2229+6114	1.7977 ± 0.0454	0.8029 ± 0.1100	2.3387 ± 0.1100

tational cost of the analysis is reduced to a few CPU-minutes per source per detector.

The $5n$-vector method uses a frequentist approach: the significance of a certain candidate, characterised by a value of the detection statistic, is established through the p-value, that is the probability to obtain a larger value for the statistics in the hypothesis of noise only. The statistic distribution can be inferred considering a range of off-source frequencies, as in Astone et al. (2014). In case of no detection, upper limits on the amplitude for the single harmonic search are set following Abbott et al. (2019b). For the dual harmonic search, for simplicity, we only consider the emission at once the rotation frequency, so we set upper limit on the C_{21} parameter alone.

For the pulsars which experienced glitching, each inter-glitch period is analysed independently and then the resulting statistics are combined incoherently. For pulsars for which an estimation of the polarization parameters can be derived from EM observations, see Table 2, two searches are carried on: one assuming uninformative uniform priors on ψ and ι and one using restricted Gaussian priors. Only O3 data from LIGO and Virgo detectors have been used in this search.

3. DATA SETS USED

3.1. *Gravitational-wave data*

The data set used O2 and O3 runs. The O2 run took place between 2016 October 30 (MJD: 57722.667) and 2017 August 25 (MJD: 57990.917). Virgo joined O2 on 2017 August 1. The duty factors for L1, H1, and V1, were 57%, 59%, and 80%, respectively. O3 took place between 2019 April 1 (MJD: 58574.625) and 2020 March 27 (MJD: 58935.708). Virgo was operational for the whole of the O3 run. The duty factors for this run were 76%, 71%, and 76% for L1, H1, and V1, respectively. The uncertainties on the amplitude and phase calibration of the detectors for O2 can be found in Cahillane et al. (2017); Acernese et al. (2018) and those for O3 can be found in Sun et al. (2020, 2021); Acernese et al. (2021). For O2, the maximum 1σ amplitude uncertainties over the range 10-2000 Hz were between about $[-2.5, +7.5]\%$ and $[-8, +4]\%$ for H1 and L1, respectively, and for Virgo the the maximum uncertainty was 5.1%. For O3, the maximum 1σ amplitude uncertainties over the range 10-2000 Hz were between about $[-5, +7]\%$ and $[-5.5, +5.5]\%$ for H1 and L1, respectively, and for Virgo the maximum uncertainty was 5%. These ranges are the maximum upper and lower bound over the full frequency range and over different measurement epochs over the run, so at specific frequencies/times the uncertainty can be far smaller.

The data used underwent cleaning processes (Davis et al. 2019; Viets & Wade 2021; Acernese et al. 2021), specifically the removal of narrowband spectral artifacts at the calibration line frequencies and power line frequencies. A discussion on the consequences of performing a search using LIGO data with the narrowband cleaning of Viets & Wade (2021) applied compared to that without it applied can be found in Appendix A.

3.2. *Electromagnetic data*

EM observations of pulsars produce the timing solutions used as input to the GW searches. These observations have been made in radio and X-ray wavelengths. The observatories which have contributed to the data set are: the Canadian Hydrogen Intensity Mapping Experiment (CHIME) (as part of the CHIME Pulsar Project; Amiri et al. 2021), the Mount Pleasant Observatory 26 m telescope, the 42 ft telescope and Lovell telescope at Jodrell Bank, the MeerKAT project (as part of the MeerTime project; Bailes et al. 2020), the Nançay Decimetric Radio Telescope, the Neutron Star Interior Composition Explorer (NICER) and the Molon-

glo Observatory Synthesis Telescope (as part of the UTMOST pulsar timing programme; Jankowski et al. 2019; Lower et al. 2020). Pulsar timing solutions were determined from this data using TEMPO (Nice et al. 2015) or TEMPO2 (Edwards et al. 2006; Hobbs et al. 2006, 2009) to fit the model parameters.

We select pulsars whose rotation frequency is greater than 10 Hz so they are within the sensitivity band of the GW detectors. This leads to primarily targeting millisecond pulsars and fast spinning young pulsars. Of the 236 pulsars in this analysis, 74 are different from the 221 used in the O2 analysis (Abbott et al. 2019b). There are 168 pulsars in binary systems and 161 are millisecond pulsars with frequencies above about 100 Hz. The pulsar J0537−6910 is not included due to the recently published searches for it in Abbott et al. (2021f,c).

For some pulsars, ephemerides were only available for the course of O3. In such cases, only GW data from O3 was used. This was the case for 102 out of the 236 pulsars in this analysis.

4. ANALYSIS RESULTS

No evidence for gravitational-wave signals from any of the included pulsars was found. The results for all except the high-value targets are shown in Table 3. The high-value pulsars are shown in Table 4 and discussed in Section 4.1. As no CWs were observed, we present the 95% credible upper limits on the gravitational-wave amplitudes C_{22} and C_{21} for the dual harmonic run (searching for the mass quadrupole modes $l = 2$, $m = 1, 2$) and the gravitational-wave amplitude h_0 for the single harmonic ($l = 2$, $m = 2$) search. These were all calculated using coherently combined data from all three detectors over the O2 and O3 observing runs or just the O3 run, as appropriate. Due to the calibration amplitude systematic uncertainties for the detectors, the amplitude estimates can have uncertainties of up to $\sim 8\%$.

Figure 1 shows the 95% credible upper limits on the gravitational-wave amplitudes C_{22} and C_{21} for all pulsars using the time-domain Bayesian method. In addition, it shows joint detector sensitivity estimates for the two amplitudes based on the representative power spectral densities for the detectors over the course of O3. For an explanation of how these estimates were calculated, see Appendix C in Abbott et al. (2019b).

The 95% credible upper limits for the GW amplitude h_0 from the single harmonic analysis for all pulsars, again using the results from the time-domain Bayesian method, are shown as stars in Figure 2. The spin-down limit for each pulsar is represented as a grey triangle. If the observed upper limit for a pulsar is below the spin-down limit, this is shown via a dotted green line from the spin-down limit to the h_0 limit which is plotted within a shaded circle. The solid line gives the joint detector sensitivity estimate over the course of O3.[2]

Figure 3 shows a histogram of the spin-down ratio $h_0^{95\%}/h_0^{\rm sd}$ from the Bayesian analysis for every pulsar for which calculating a spin-down rate was possible.[3] These values rely on the pulsar distance and period derivative which can have associated errors. These are not taken into account in this study but their presence should be kept in mind. The mass quadrupole Q_{22} (see equation 4) also relies on these values and the ellipticity ε (equation (5)) additionally requires the fiducial moment of inertia $I_{zz}^{\rm fid}$ which is taken to be $10^{38}\,{\rm kg\,m^2}$. The values for distance and period derivative used can be found in Table 3 and Table 4.

The single harmonic search was used to place limits on the mass quadrupole $Q_{22}^{95\%}$ which can be used to find the pulsar's ellipticity $\varepsilon^{95\%}$ using equations (5) and (4). However, for pulsars that did not surpass their spin-down limits these Q_{22} and ε values would lead to spin-down rates $\dot{P}_{rot}$ that are greater than (and thus are in violation of) their measured values. The results for the Bayesian analysis are shown in terms of the mass quadrupole Q_{22} and ellipticity ε in Figure 4. Also included are histograms of the upper limits and spin-down limits as well as contour lines of equal characteristic age τ calculated under the assumption that all spin-down is due to energy loss through GW emission, i.e., the braking index is $n = 5$.

From the Bayesian search twenty-three pulsars have direct upper limits that are below their spin-down limit, with 89 pulsars within a factor of 10 of their spin-down limit. There were 90 millisecond pulsars with a spin-down ratio less than 10. For the dual harmonic search, the most constraining upper limit for C_{21} was J2302+4442 with 7.05×10^{-27}. The smallest C_{22} upper limit was 2.05×10^{-27} for J1537−5312. As physically meaningful constraints for the single harmonic search are only achieved once the spin-down limit has been surpassed, the following best limits are taken from the 23 pulsars that had $h_0^{95\%}/h_0^{sd} < 1$. The smallest spin-down limit was 0.009 for J0534+2200 (the Crab pulsar). The pulsar with the smallest upper limit on h_0 was J1745−0952 with 4.72×10^{-27}. The best Q_{22} upper limit was achieved by J0711−6830 with $4.07\times10^{29}\,{\rm kg\,m^2}$ which led to the best limit on ellipticity of 5.26×10^{-9}.

[2] The sensitivity estimate for O3 alone is used as it dominates compared to the estimate for the O2 run.

[3] Spin-down rates cannot be calculated for pulsars with insufficient distance, frequency or frequency derivative data (see equation (6)).

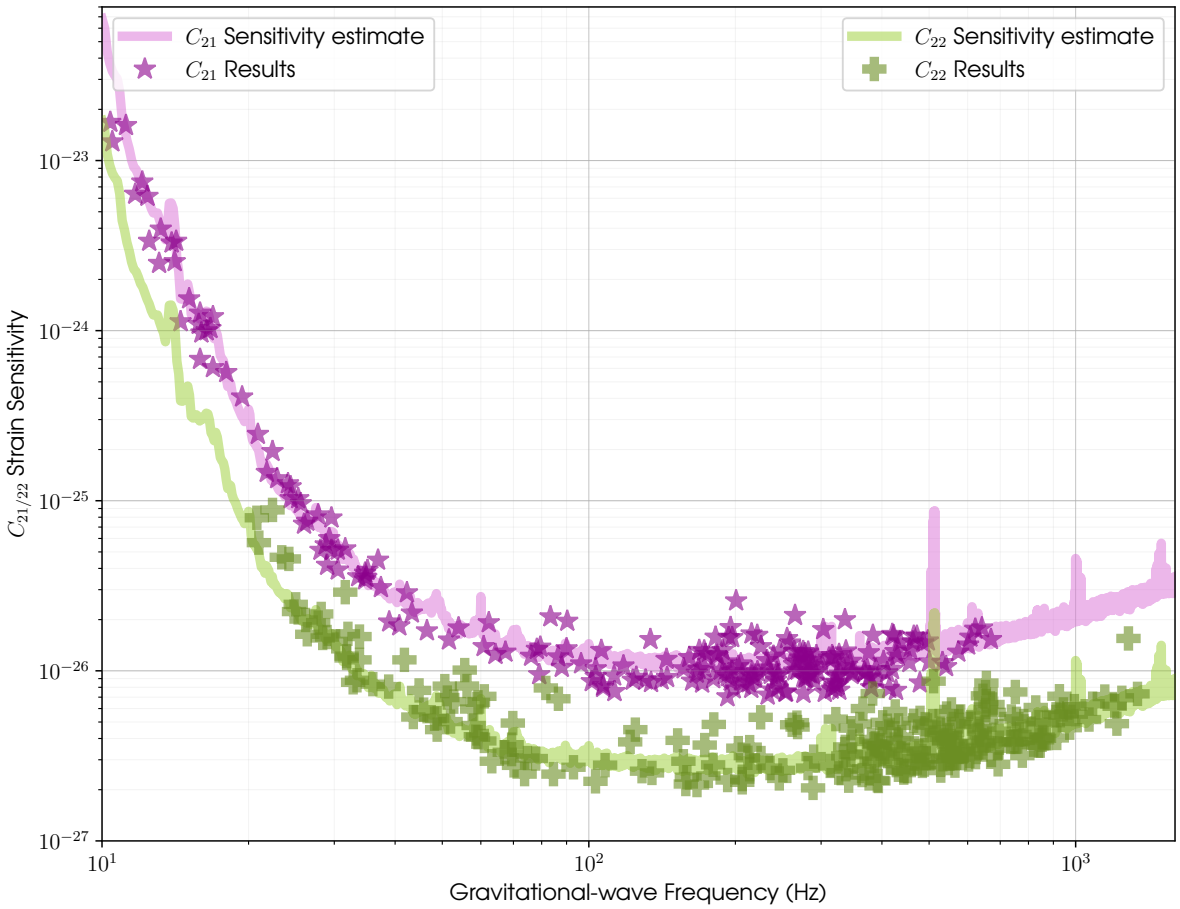

Figure 1. The 95% credible upper limits on the gravitational-wave amplitudes for all 236 pulsars using the time-domain Bayesian method. The pink stars and green crosses show the 95% credible upper limits for the GW amplitudes (C_{22} and C_{21}) for the dual harmonic search. The solid lines show the estimated sensitivity of all three detectors combined over the course of O3.

For each pulsar, we performed a model comparison between the assumption of the data being consistent with a coherent signal compared to the assumption of an incoherent signal *or* noise. This was calculated for both the dual harmonic ($l = 2$, $m = 1, 2$) and single harmonic ($l = 2$, $m = 2$) searches. Specifically, the base-10 logarithm of the Bayesian odds between models is calculated, which will be referred to as $\mathcal{O}$. Of all the pulsars in this search, none had $\mathcal{O} > 0$, meaning in all cases incoherent noise was more likely than a coherent signal. The pulsar with the highest odds overall was J2010−1323 with −0.77.

4.1. *High-value targets*

Table 4 shows the results for the analyses on the high-value targets for the *Bayesian*, the *$\mathcal{F}/\mathcal{G}$-statistic* and the *5n-vectors* analyses. In this case, Statistic[a] and Statistic[b] change depending on which analysis method was used. For the Bayesian analysis Statistic[a] and Statistic[b] represent the base-10 logarithm of the Bayesian odds, $\mathcal{O}$, for the dual- and single-harmonic searches, respectively. This is the same as for the results in Table 3. For the *$\mathcal{F}/\mathcal{G}$-statistic* and *5n-vector* analysis methods they represent the false-alarm probabilities at the $l = 2, m = 1$ and $l = m = 2$ modes respectively.

By definition, all high-value pulsars surpassed their spin-down limits in the Bayesian analysis. Several pulsars glitched during the course of the runs: J0534+2200 (Crab pulsar), J0908−4913 and J1105−6107. The times of the glitches are shown in Table 1 and the process for dealing with them is outlined in Section 2.1.1. Additionally, some have sufficient information from EM observations on their orientation to restrict their priors: J0534+2200 (Crab pulsar), J0835−4510 (Vela), J1952+3252 and J2229+6114. This is discussed in 2.1.2 and the pulsars' restricted ranges are quoted in Table 2. For each pulsar with either a glitch or restricted priors, individual analyses were performed assuming GW emission at both $2f_{\rm rot}$ and $f_{\rm rot}$ and just $2f_{\rm rot}$. In the

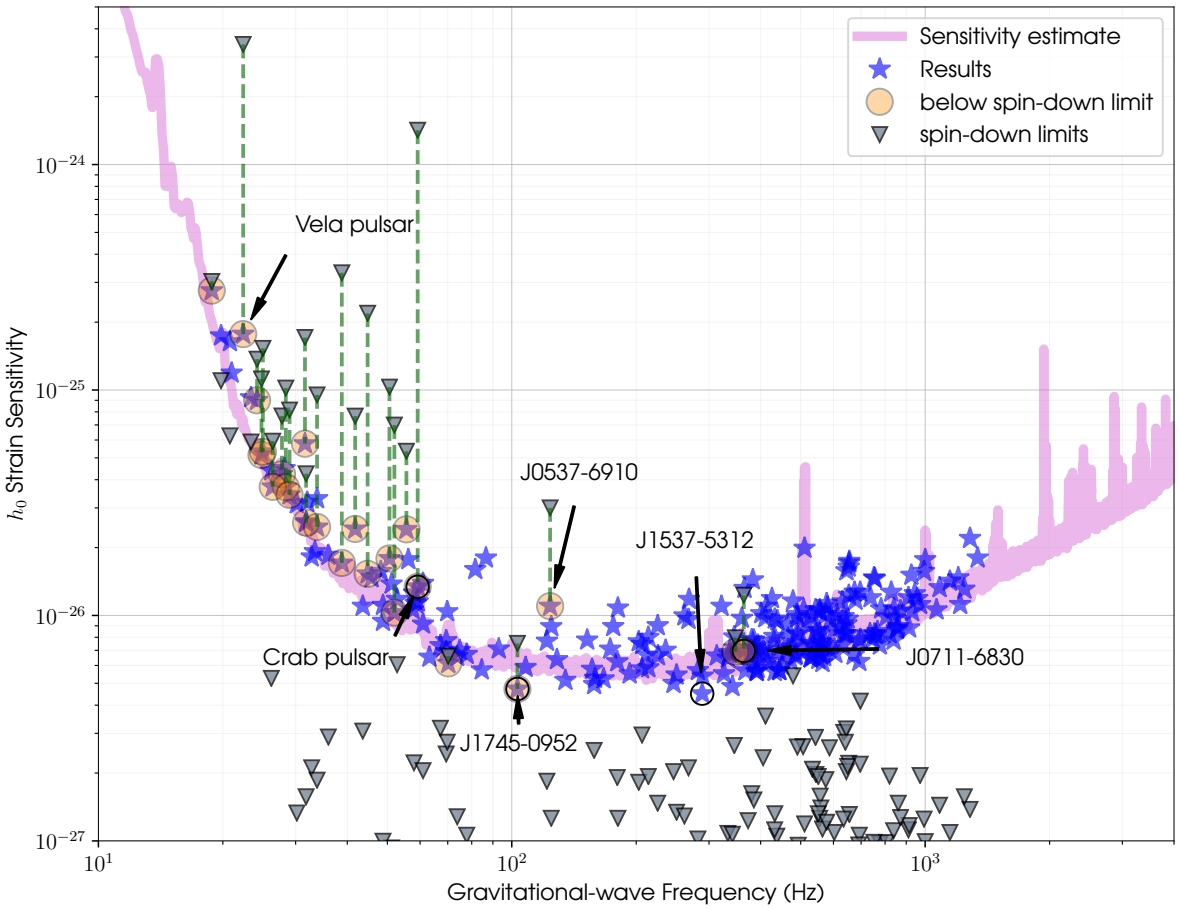

Figure 2. Upper limits on h_0 for the 236 pulsars in this analysis using the time-domain Bayesian method. The stars show 95% credible upper limits on the amplitudes of h_0. Grey triangles represent the spin-down limits for each pulsar (based on the distance measurement stated in Table 3 and assuming the canonical moment of inertia). For those pulsars which surpass their spin-down limits, their results are plotted within shaded circles. The pink curve gives an estimate of the expected strain sensitivity of all three detectors combined during the course of O3. The highlighted pulsars are those with the best h_0, Q_{22} and spin-down ratio out of the pulsars which surpassed their spin-down limit, as well as the best h_0 limit out of the whole sample. The Vela pulsar is highlighted and the pulsar J0537−6910 upper and spin-down limits calculated in Abbott et al. (2021c) are also included for completeness.

case of the Crab pulsar, which both experienced a glitch and has sufficient observations for restricted priors, four individual analyses were performed. Each analysis accounted for the glitch, with combinations of dual/single harmonic search and restricted/unrestricted priors. The values shown in Table 4 are from the searches with glitches accounted for via an unknown phase offset. When a pulsar had a restricted prior search, the results are shown in parentheses next to the unrestricted results.

The Crab pulsar is of interest due to its high spin-down luminosity. For the single harmonic Bayesian analysis and with the glitch accounted for by a phase offset, its upper limit as a fraction of the spin-down limit is only 0.0094(0.0085) meaning that GWs contribute to less than 0.009% of the available spin-down luminosity. This is consistent with previous studies that also surpassed the spin-down limit (Abbott et al. 2019b, 2017b). Its $h_0^{95\%}$ upper limit was found to be $1.3(1.2) \times 10^{-26}$. With a distance of 2 kpc and period derivative of $4.2 \times 10^{-13}\,\mathrm{s\,s^{-1}}$, the upper limits on the mass quadrupole and ellipticity were calculated to be $Q_{22}^{95\%} = 5.6(5.0)\times10^{32}$ kg m^2 and $\varepsilon^{95\%} = 7.2(6.5)\times10^{-6}$. The base-10 logarithm of the Bayesian odds for this analysis favouring a coherent signal over incoherent noise is -2.6(-2.7).

The Vela pulsar also has a very high spin-down luminosity and is considered another source of interest. Unlike the Crab pulsar, the Vela pulsar did not experience any glitches over the course of this analysis. In the single harmonic Bayesian analysis, the spin-down limit was surpassed with a ratio of 0.052(0.051), with

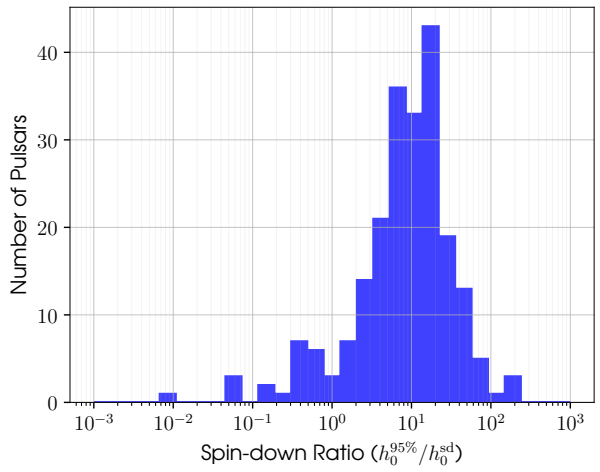

Figure 3. A histogram of the spin-down ratio for all pulsars for which a spin-down ratio was calculated.

$h_0^{95\%} = 1.8(1.7)\times10^{-25}$. This ratio corresponds to a maximum of 0.27% of the spin-down luminosity being emitted by GWs. The previous known pulsar search by Abbott et al. (2019b) found the spin-down ratio to be 0.042 with $h_0^{95\%} = 1.4\times10^{-25}$ which is lower than in this analysis. This is due to significant noise in the LIGO Hanford detector at twice Vela's rotational frequency, with an angular sensing control dither line being the most likely culprit.[4] However, this analysis is an improvement on the more recent measurement of the spin-down ratio of 0.067 and $h_0^{95\%} = 2.2\times10^{-25}$ produced in Abbott et al. (2020). The upper limits on the mass quadrupole $Q_{22}^{95\%}$ and ellipticity ε were calculated to be $7.2(7.1)\times10^{33}$ kg m^2 and $9.3(9.2)\times10^{-5}$, respectively. These values were calculated assuming a distance of 0.28 kpc and a period derivative of $1.2\times10^{-13}\,\mathrm{s\,s^{-1}}$. The base-10 logarithm of the Bayesian odds for this pulsar in the single harmonic analysis was -1.1(-1.0).

The pulsar J0537−6910 has the highest spin-down luminosity but has not been included in this search due to recently published searches for it in Abbott et al. (2021c,f). The limits, which can be found in Table 3 of Abbott et al. (2021c), are shown for comparison. They found $h_0^{95\%} = 1.1(1.0)\times10^{-26}$ with a spin-down ratio of $h_0^{95\%}/h_0^{sd} = 0.37(0.33)$. $\varepsilon^{95\%} = 3.4(3.1)\times10^{-5}$ while for the dual harmonic search $C_{21}^{95\%} = 2.2(1.8)\times10^{-26}$ and $C_{22}^{95\%} = 5.6(5.0)\times10^{-27}$.

Table 5 shows the results for the analyses on the high-value targets using the $\mathcal{D}$-statistic analyses to search for dipole radiation predicted by Brans-Dicke theory. No significant signal was detected and consequently upper limits are obtained. The 95% confidence upper limits are given in the second last column of Table 5 and the last column gives the false alarm probability, i.e., the probability that the obtained values of the $\mathcal{D}$-statistic result only from the noise in the data. The most constraining upper limit for dipole radiation is obtained for the millisecond pulsar J0437−4715.

[4] This contamination was removed for the final third of O3, although its presence at earlier times still has a detrimental effect on the result.

5. CONCLUSIONS

In this paper, we have searched for evidence of GWs from 236 pulsars over the course of the LIGO and Virgo O2 and O3 runs and across all three detectors (LIGO Hanford, LIGO Livingston and Virgo). This is an improvement on the 221 pulsars from the O1 and O2 analysis in Abbott et al. (2019b). Searches were carried out for two different emission models. One assumed GW emission from the $l = m = 2$ mass quadrupole mode and the other assumed emission from the $l = 2, m = 1, 2$ modes. For the single harmonic search, new upper limits on h_0 were produced and a total of 23 pulsars surpassed their spin-down limits (24 if one includes J0537-6910 from Abbott et al. (2021c)). This is an improvement from the 20 pulsars in Abbott et al. (2019b) and includes 9 pulsars for which their spin-down limit had not previously been surpassed. For the dual harmonic search, new limits on C_{21} and C_{22} are found. For pulsars which were deemed high-value, two more analysis methods were included for robustness: the *$\mathcal{F}/\mathcal{G}$-statistic* method and the *5n-vector* method.

The millisecond pulsars that surpassed their spin-down limits, J0437−4715 and J0711−6830, have ellipticity upper limits of 8.5×10^{-9} and 5.3×10^{-9}, respectively. Comparing these values to the left-hand panel of Figure 3 in Gittins & Andersson (2021) finds that our results are lower than the maximum values predicted for a variety of neutron star equations of state. Our results are therefore providing new constraints in physically realistic parts of the ellipticity parameter space.

No search found strong evidence of GW emission from any of the pulsars. However, with so many pulsars now surpassing their spin-down limit, including the millisecond pulsars J0437−4715 and J0711−6830 (Abbott et al. 2020), the next observing run O4 could add more pulsars to this count and bring us closer to observing CWs from pulsars for the first time. In addition to the search for CW signals consisting of the tensorial polarizations predicted by GR, this paper provides the first search explicitly targeting emission of scalar polarization modes predicted by Brans-Dicke theory.

6. ACKNOWLEDGEMENTS

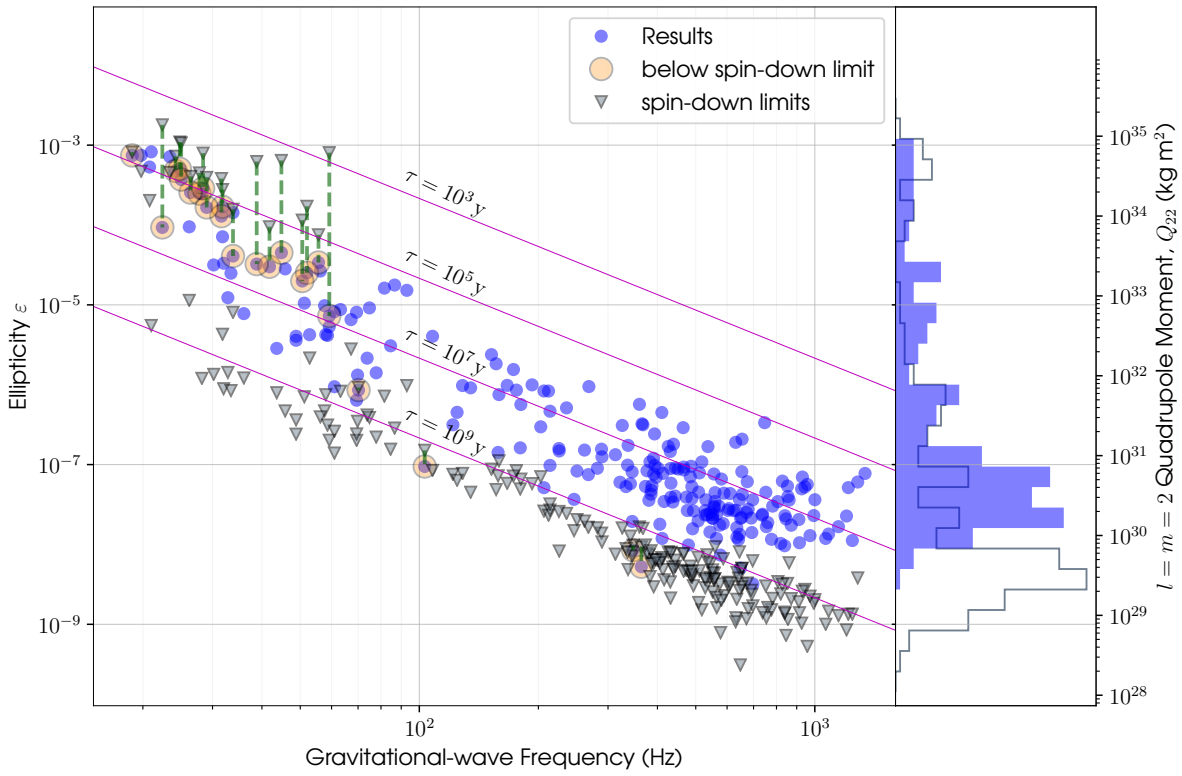

Figure 4. 95% credible upper limits on ellipticity ε and mass quadrupole Q_{22} for all 236 pulsars. The upper limits for each pulsar are represented by blue circles while their spin-down limits are shown as grey triangles. Pulsars for which our direct upper limits have surpassed their spin-down limits are highlighted within a shaded circle with a dotted green line linking the limit to its spin-down limit. Also included are pink contour lines of equal characteristic age $\tau = P/4\dot{P}$ assuming that GW emission alone is causing spin-down. To the right of the plot, histograms of both these direct limits and spin-down limits are shown by filled and empty bars respectively.

This material is based upon work supported by NSF's LIGO Laboratory which is a major facility fully funded by the National Science Foundation. The authors also gratefully acknowledge the support of the Science and Technology Facilities Council (STFC) of the United Kingdom, the Max-Planck-Society (MPS), and the State of Niedersachsen/Germany for support of the construction of Advanced LIGO and construction and operation of the GEO600 detector. Additional support for Advanced LIGO was provided by the Australian Research Council. The authors gratefully acknowledge the Italian Istituto Nazionale di Fisica Nucleare (INFN), the French Centre National de la Recherche Scientifique (CNRS) and the Netherlands Organization for Scientific Research (NWO), for the construction and operation of the Virgo detector and the creation and support of the EGO consortium. The authors also gratefully acknowledge research support from these agencies as well as by the Council of Scientific and Industrial Research of India, the Department of Science and Technology, India, the Science & Engineering Research Board (SERB), India, the Ministry of Human Resource Development, India, the Spanish Agencia Estatal de Investigación (AEI), the Spanish Ministerio de Ciencia e Innovación and Ministerio de Universidades, the Conselleria de Fons Europeus, Universitat i Cultura and the Direcció General de Política Universitaria i Recerca del Govern de les Illes Balears, the Conselleria d'Innovació, Universitats, Ciència i Societat Digital de la Generalitat Valenciana and the CERCA Programme Generalitat de Catalunya, Spain, the National Science Centre of Poland and the European Union – European Regional Development Fund; Foundation for Polish Science (FNP), the Swiss National Science Foundation (SNSF), the Russian Foundation for Basic Research, the Russian Science Foundation, the European Commission, the European Social Funds (ESF), the European Regional Development Funds (ERDF), the Royal Society, the Scottish Funding Council, the Scottish Universities Physics Alliance, the Hungarian Scientific Research Fund (OTKA), the French Lyon Institute of Origins (LIO), the Belgian Fonds de la Recherche Scientifique (FRS-FNRS), Actions de Recherche Concertées (ARC) and Fonds Wetenschappelijk Onderzoek – Vlaanderen

(FWO), Belgium, the Paris Île-de-France Region, the National Research, Development and Innovation Office Hungary (NKFIH), the National Research Foundation of Korea, the Natural Science and Engineering Research Council Canada, Canadian Foundation for Innovation (CFI), the Brazilian Ministry of Science, Technology, and Innovations, the International Center for Theoretical Physics South American Institute for Fundamental Research (ICTP-SAIFR), the Research Grants Council of Hong Kong, the National Natural Science Foundation of China (NSFC), the Leverhulme Trust, the Research Corporation, the Ministry of Science and Technology (MOST), Taiwan, the United States Department of Energy, and the Kavli Foundation. The authors gratefully acknowledge the support of the NSF, STFC, INFN and CNRS for provision of computational resources.

This work was supported by MEXT, JSPS Leading-edge Research Infrastructure Program, JSPS Grant-in-Aid for Specially Promoted Research 26000005, JSPS Grant-in-Aid for Scientific Research on Innovative Areas 2905: JP17H06358, JP17H06361 and JP17H06364, JSPS Core-to-Core Program A. Advanced Research Networks, JSPS Grant-in-Aid for Scientific Research (S) 17H06133 and 20H05639 , JSPS Grant-in-Aid for Transformative Research Areas (A) 20A203: JP20H05854, the joint research program of the Institute for Cosmic Ray Research, University of Tokyo, National Research Foundation (NRF) and Computing Infrastructure Project of KISTI-GSDC in Korea, Academia Sinica (AS), AS Grid Center (ASGC) and the Ministry of Science and Technology (MoST) in Taiwan under grants including AS-CDA-105-M06, Advanced Technology Center (ATC) of NAOJ, Mechanical Engineering Center of KEK.

The Nançay Radio Observatory is operated by the Paris Observatory, associated with the French Centre National de la Recherche Scientifique (CNRS). We acknowledge financial support from "Programme National de Cosmologie et Galaxies" (PNCG) and "Programme National Hautes Energies" (PNHE) of CNRS/INSU, France.

We are grateful to the staff of the Dominion Radio Astrophysical Observatory, which is operated by the National Research Council of Canada. CHIME is funded by a grant from the Canada Foundation for Innovation (CFI) 2012 Leading Edge Fund (Project 31170) and by contributions from the provinces of British Columbia, Québec and Ontario. The CHIME/FRB Project, which enabled development in common with the CHIME/Pulsar instrument, is funded by a grant from the CFI 2015 Innovation Fund (Project 33213) and by contributions from the provinces of British Columbia and Québec, and by the Dunlap Institute for Astronomy and Astrophysics at the University of Toronto. Additional support was provided by the Canadian Institute for Advanced Research (CIFAR), McGill University and the McGill Space Institute thanks to the Trottier Family Foundation, and the University of British Columbia. The CHIME/Pulsar instrument hardware was funded by NSERC RTI-1 grant EQPEQ 458893-2014. This research was enabled in part by support provided by WestGrid (www.westgrid.ca) and Compute Canada (www.computecanada.ca). J.W.M. is a CITA Postdoctoral Fellow: This work was supported by the Natural Sciences and Engineering Research Council of Canada (NSERC), funding reference #CITA 490888-16. Pulsar research at UBC is supported by an NSERC Discovery Grant and by the Canadian Institute for Advanced Research (I.H.S.). K.C. is supported by a UBC Four Year Fellowship (6456).

D.An. acknowledges support from an EPSRC/STFC fellowship (EP/T017325/1). W.C.G.H. acknowledges support through grants 80NSSC19K1444 and 80NSSC21K0091 from NASA. This work is supported by NASA through the NICER mission and the Astrophysics Explorers Program and uses data and software provided by the High Energy Astrophysics Science Archive Research Center (HEASARC), which is a service of the Astrophysics Science Division at NASA/GSFC and High Energy Astrophysics Division of the Smithsonian Astrophysical Observatory.

We would like to thank all of the essential workers who put their health at risk during the COVID-19 pandemic, without whom we would not have been able to complete this work.

APPENDIX

A. CLEANED VERSUS UNCLEANED DATA COMPARISON

The data used in this analysis was subject to a cleaning process described in Viets & Wade (2021) which focused on the removal of various narrow-band spectral artifacts at calibration line frequencies. For any pulsars very close to these lines, this cleaning would be expected to provide an improvement in sensitivity. In this appendix we present the comparison of results using this cleaned data against results using data without this cleaning process (which we will refer to as "uncleaned") for a sample of pulsars.

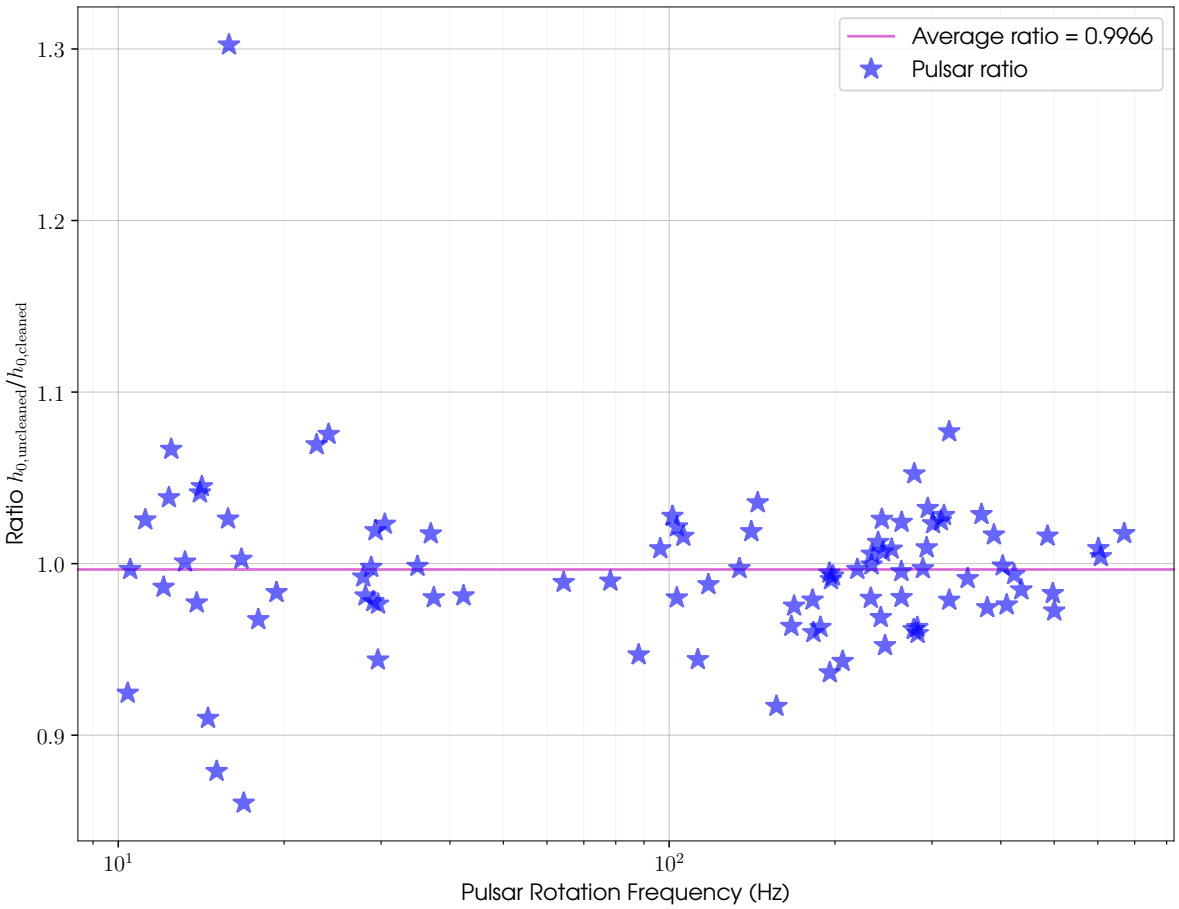

Figure 5. The ratio of uncleaned versus cleaned upper limits against pulsar rotational frequency. The h_0 upper limits for both data sets are calculated from the C_{22} limit determined in dual harmonic searches using O3 data only. The mean ratio is represented by the solid pink line.

Uncleaned O3 LIGO data is used for a dual harmonic Bayesian analysis of 95 pulsars which had ephemeris data only overlapping with O3. This is compared to the O3-only analysis performed in this paper using the cleaned data. The Virgo data used was the same in both cases. For comparison, the ratio of h_0 upper limits for each pulsar using uncleaned $h_{0,\mathrm{uncleaned}}$ versus cleaned $h_{0,\mathrm{cleaned}}$ data are shown in Figure 5.

The mean ratio of upper limit for uncleaned data versus cleaned data was 0.9966 (with a standard deviation of 0.0486) which suggests no major effect of the line cleaning on the majority results. It should be noted that for this analysis there is a statistical uncertainty on the upper limits of around 1% due to the use of a finite number of posterior samples when calculating them (Abbott et al. 2020). If performing parameter estimation on h_0 using multiple data sets consisting of independent noise realizations drawn from the same distribution, empirically it is found that the resultant upper limits will vary by on order of 30%. Due to the cleaning, the cleaned and uncleaned datasets will contain different, albeit highly correlated, noise. So, a spread of upper limit ratios that are larger than expected from the pure statistical uncertainty on each limit, but smaller that one would get from independent data is to be expected.

As the upper limit ratio spread can be explained as being consistent with expectations from statistical fluctuations, it suggests that very few pulsars are close enough to the cleaned lines for the cleaning to have a significant effect overall. However, it makes sense to apply consistency in using the same dataset for all pulsars being analyzed. In this analysis we chose to use the narrow-band cleaned data.

REFERENCES

Aasi, J., Abadie, J., Abbott, B. P., et al. 2014, ApJ, 785, 119, doi: 10.1088/0004-637X/785/2/119

Aasi, J., Abbott, B. P., Abbott, R., et al. 2015, CQGra, 32, 074001, doi: 10.1088/0264-9381/32/7/074001

Abadie, J., Abbott, B. P., Abbott, R., et al. 2011, ApJ, 737, 93, doi: 10.1088/0004-637X/737/2/93
Abbott, B. P., Abbott, R., Abbott, T. D., et al. 2017a, ApJ, 839, 12, doi: 10.3847/1538-4357/aa677f
—. 2017b, PhRvD, 96, 122006, doi: 10.1103/PhysRevD.96.122006
—. 2018, PhRvD, 97, 102003, doi: 10.1103/PhysRevD.97.102003
—. 2019a, PhRvD, 100, 104036, doi: 10.1103/PhysRevD.100.104036
—. 2019b, ApJ, 879, 10, doi: 10.3847/1538-4357/ab20cb
—. 2019c, PhRvD, 99, 122002, doi: 10.1103/PhysRevD.99.122002
—. 2019d, ApJ, 875, 122, doi: 10.3847/1538-4357/ab113b
—. 2019e, PhRvD, 100, 024004, doi: 10.1103/PhysRevD.100.024004
Abbott, R., Abbott, T. D., Abraham, S., et al. 2020, ApJL, 902, L21, doi: 10.3847/2041-8213/abb655
—. 2021a, PhRvX, 11, 021053, doi: 10.1103/PhysRevX.11.021053
—. 2021b, ApJL, 915, L5, doi: 10.3847/2041-8213/ac082e
—. 2021c, ApJL, 913, L27, doi: 10.3847/2041-8213/abffcd
—. 2021d, ApJ, 921, 80, doi: 10.3847/1538-4357/ac17ea
—. 2021e, arXiv:2107.00600
—. 2021f, arXiv e-prints, arXiv:2104.14417. https://arxiv.org/abs/2104.14417
Acernese, F., Agathos, M., Agatsuma, K., et al. 2015, CQGra, 32, 024001, doi: 10.1088/0264-9381/32/2/024001
Acernese, F., Adams, T., Agatsuma, K., et al. 2018, CQGra, 35, 205004, doi: 10.1088/1361-6382/aadf1a
Acernese, F., Agathos, M., Ain, A., et al. 2021, arXiv:2107.03294
Amiri, M., Bandura, K. M., Boyle, P. J., et al. 2021, ApJS, 255, 5, doi: 10.3847/1538-4365/abfdcb
Andersson, N. 1998, ApJ, 502, 708, doi: 10.1086/305919
Antoniadis, J., Freire, P. C. C., Wex, N., et al. 2013, Sci, 340, 448, doi: 10.1126/science.1233232
Arzoumanian, Z., Brazier, A., Burke-Spolaor, S., et al. 2018, ApJS, 235, 37, doi: 10.3847/1538-4365/aab5b0
Astone, P., Colla, A., D'Antonio, S., Frasca, S., & Palomba, C. 2012, JPhCS, 363, 012038, doi: 10.1088/1742-6596/363/1/012038
Astone, P., Colla, A., D'Antonio, S., et al. 2014, Phys. Rev. D, 89, 062008, doi: 10.1103/PhysRevD.89.062008
Bailes, M., Jameson, A., Abbate, F., et al. 2020, PASA, 37, e028, doi: 10.1017/pasa.2020.19
Bassa, C. G., Antoniadis, J., Camilo, F., et al. 2016, MNRAS, 455, 3806, doi: 10.1093/mnras/stv2607
Bates, S. D., Thornton, D., Bailes, M., et al. 2015, MNRAS, 446, 4019, doi: 10.1093/mnras/stu2350
Bonazzola, S., & Gourgoulhon, E. 1996, A&A, 312, 675
Braga, V. F., Dall'Ora, M., Bono, G., et al. 2015, ApJ, 799, 165, doi: 10.1088/0004-637X/799/2/165
Brans, C., & Dicke, R. H. 1961, PhRv, 124, 925, doi: 10.1103/PhysRev.124.925
Brownsberger, S., & Romani, R. W. 2014, ApJ, 784, 154, doi: 10.1088/0004-637X/784/2/154
Cahillane, C., Betzwieser, J., Brown, D. A., et al. 2017, PhRvD, 96, 102001, doi: 10.1103/PhysRevD.96.102001
Camilo, F., Ransom, S. M., Halpern, J. P., & Roshi, D. A. 2021, ApJ, 917, 67, doi: 10.3847/1538-4357/ac0720
Cognard, I., & Backer, D. C. 2004, ApJL, 612, L125, doi: 10.1086/424692
Cutler, C. 2002, PhRvD, 66, 084025, doi: 10.1103/PhysRevD.66.084025
Davis, D., Massinger, T., Lundgren, A., et al. 2019, Classical and Quantum Gravity, 36, 055011, doi: 10.1088/1361-6382/ab01c5
Deller, A. T., Boyles, J., Lorimer, D. R., et al. 2013, ApJ, 770, 145, doi: 10.1088/0004-637X/770/2/145
Dergachev, V., & Papa, M. A. 2020, PhRvL, 125, 171101, doi: 10.1103/PhysRevLett.125.171101
Desvignes, G., Caballero, R. N., Lentati, L., et al. 2016, MNRAS, 458, 3341, doi: 10.1093/mnras/stw483
Dupuis, R. J., & Woan, G. 2005, PhRvD, 72, 102002, doi: 10.1103/PhysRevD.72.102002
Edwards, R. T., Hobbs, G. B., & Manchester, R. N. 2006, MNRAS, 372, 1549, doi: 10.1111/j.1365-2966.2006.10870.x
Espinoza, C. M., Guillemot, L., Çelik, Ö., et al. 2013, MNRAS, 430, 571, doi: 10.1093/mnras/sts657
Ferdman, R. D., Stairs, I. H., Kramer, M., et al. 2014, MNRAS, 443, 2183, doi: 10.1093/mnras/stu1223
Fonseca, E., Stairs, I. H., & Thorsett, S. E. 2014, ApJ, 787, 82, doi: 10.1088/0004-637X/787/1/82
Fonseca, E., Cromartie, H. T., Pennucci, T. T., et al. 2021, ApJL, 915, L12, doi: 10.3847/2041-8213/ac03b8
Freire, P. C. C., Wex, N., Esposito-Farèse, G., et al. 2012, MNRAS, 423, 3328, doi: 10.1111/j.1365-2966.2012.21253.x
Friedman, J. L., & Morsink, S. M. 1998, ApJ, 502, 714, doi: 10.1086/305920
Gittins, F., & Andersson, N. 2021, MNRAS, 507, 116, doi: 10.1093/mnras/stab2048
Glampedakis, K., & Gualtieri, L. 2018, Gravitational Waves from Single Neutron Stars: An Advanced Detector Era Survey, ed. L. Rezzolla, P. Pizzochero, D. I. Jones, N. Rea, & I. Vidaña, Vol. 457, 673, doi: 10.1007/978-3-319-97616-7_12

Gotthelf, E. V., Halpern, J. P., Terrier, R., & Mattana, F. 2011, ApJL, 729, L16, doi: 10.1088/2041-8205/729/2/L16
Guillemot, L., Smith, D. A., Laffon, H., et al. 2016, A&A, 587, A109, doi: 10.1051/0004-6361/201527847
Halpern, J. P., Bogdanov, S., & Gotthelf, E. V. 2013, ApJ, 778, 120, doi: 10.1088/0004-637X/778/2/120
Halpern, J. P., Gotthelf, E. V., Leighly, K. M., & Helfand, D. J. 2001, ApJ, 547, 323, doi: 10.1086/318361
Harris, W. E. 2010, arXiv:1012.3224
Hobbs, G., Edwards, R., & Manchester, R. 2006, Chinese Journal of Astronomy and Astrophysics Supplement, 6, 189
Hobbs, G., Jenet, F., Lee, K. J., et al. 2009, MNRAS, 394, 1945, doi: 10.1111/j.1365-2966.2009.14391.x
Isi, M., Pitkin, M., & Weinstein, A. J. 2017, PhRvD, 96, 042001, doi: 10.1103/PhysRevD.96.042001
Jankowski, F., Bailes, M., van Straten, W., et al. 2019, MNRAS, 484, 3691, doi: 10.1093/mnras/sty3390
Jaranowski, P., & Królak, A. 2010, CQGra, 27, 194015, doi: 10.1088/0264-9381/27/19/194015
Jaranowski, P., Królak, A., & Schutz, B. F. 1998, PhRvD, 58, 063001, doi: 10.1103/PhysRevD.58.063001
Jones, D. I. 2010, MNRAS, 402, 2503, doi: 10.1111/j.1365-2966.2009.16059.x
Lin, L. C.-C., Takata, J., Hwang, C.-Y., & Liang, J.-S. 2009, MNRAS, 400, 168, doi: 10.1111/j.1365-2966.2009.15468.x
Lindblom, L., & Owen, B. J. 2020, PhRvD, 101, 083023, doi: 10.1103/PhysRevD.101.083023
Lorimer, D. R., Kawash, A. M., Freire, P. C. C., et al. 2021, arXiv:2108.03946
Lower, M. E., Bailes, M., Shannon, R. M., et al. 2019, RNAAS, 3, 192, doi: 10.3847/2515-5172/ab621d
—. 2020, MNRAS, 494, 228, doi: 10.1093/mnras/staa615
Matthews, A. M., Nice, D. J., Fonseca, E., et al. 2016, ApJ, 818, 92, doi: 10.3847/0004-637X/818/1/92
McKee, J. W., Janssen, G. H., Stappers, B. W., et al. 2016, MNRAS, 461, 2809, doi: 10.1093/mnras/stw1442
Ming, J., Papa, M. A., Singh, A., et al. 2019, PhRvD, 100, 024063, doi: 10.1103/PhysRevD.100.024063
Negueruela, I., Ribó, M., Herrero, A., et al. 2011, ApJL, 732, L11, doi: 10.1088/2041-8205/732/1/L11
Ng, C.-Y., & Romani, R. W. 2004, ApJ, 601, 479, doi: 10.1086/380486
—. 2008, ApJ, 673, 411, doi: 10.1086/523935
Nice, D., Demorest, P., Stairs, I., et al. 2015, Tempo: Pulsar timing data analysis. http://ascl.net/1509.002
Nieder, L., Clark, C. J., Bassa, C. G., et al. 2019, ApJ, 883, 42, doi: 10.3847/1538-4357/ab357e
Nieder, L., Clark, C. J., Kandel, D., et al. 2020, ApJL, 902, L46, doi: 10.3847/2041-8213/abbc02
Owen, B. J. 2005, Physical Review Letters, 95, 211101, doi: 10.1103/PhysRevLett.95.211101
Papa, M. A., Ming, J., Gotthelf, E. V., et al. 2020, ApJ, 897, 22, doi: 10.3847/1538-4357/ab92a6
Piccinni, O. J., Astone, P., D'Antonio, S., et al. 2018, Classical and Quantum Gravity, 36, 015008, doi: 10.1088/1361-6382/aaefb5
Pitkin, M., Gill, C., Jones, D. I., Woan, G., & Davies, G. S. 2015, MNRAS, 453, 4399, doi: 10.1093/mnras/stv1931
Pitkin, M., Isi, M., Veitch, J., & Woan, G. 2017, arXiv:1705.08978v1
Reardon, D. J., Hobbs, G., Coles, W., et al. 2016, MNRAS, 455, 1751, doi: 10.1093/mnras/stv2395
Reardon, D. J., Shannon, R. M., Cameron, A. D., et al. 2021, MNRAS, 507, 2137, doi: 10.1093/mnras/stab1990
Reynoso, E. M., Johnston, S., Green, A. J., & Koribalski, B. S. 2006, MNRAS, 369, 416, doi: 10.1111/j.1365-2966.2006.10325.x
Riles, K. 2017, MLPA, 32, 1730035, doi: 10.1142/S021773231730035X
Shaw, B., Keith, M. J., Lyne, A. G., et al. 2021, MNRAS, 505, L6, doi: 10.1093/mnrasl/slab038
Shklovskii, I. S. 1970, Soviet Ast., 13, 562
Spiewak, R., Bailes, M., Barr, E. D., et al. 2018, MNRAS, 475, 469, doi: 10.1093/mnras/stx3157
Steltner, B., Papa, M. A., Eggenstein, H. B., et al. 2021, ApJ, 909, 79, doi: 10.3847/1538-4357/abc7c9
Sun, L., Goetz, E., Kissel, J. S., et al. 2020, CQGra, 37, 225008, doi: 10.1088/1361-6382/abb14e
—. 2021, arXiv:2107.00129
Swiggum, J. K., Kaplan, D. L., McLaughlin, M. A., et al. 2017, ApJ, 847, 25, doi: 10.3847/1538-4357/aa8994
Testa, V., Corsi, C. E., Andreuzzi, G., et al. 2001, AJ, 121, 916, doi: 10.1086/318752
Ushomirsky, G., Cutler, C., & Bildsten, L. 2000, MNRAS, 319, 902, doi: 10.1046/j.1365-8711.2000.03938.x
Verbiest, J. P. W., & Lorimer, D. R. 2014, MNRAS, 444, 1859, doi: 10.1093/mnras/stu1560
Verbiest, J. P. W., Weisberg, J. M., Chael, A. A., Lee, K. J., & Lorimer, D. R. 2012, ApJ, 755, 39, doi: 10.1088/0004-637X/755/1/39
Verma, P. 2021, Universe, 7, 351, doi: 10.3390/universe7070235
Viets, A., & Wade, M. 2021, LIGO T2100058 https://dcc.ligo.org/LIGO-T2100058/public
Vigeland, S. J., Deller, A. T., Kaplan, D. L., et al. 2018, ApJ, 855, 122, doi: 10.3847/1538-4357/aaaa73

Yao, J. M., Manchester, R. N., & Wang, N. 2017, ApJ, 835, 29, doi: 10.3847/1538-4357/835/1/29

Zimmermann, M., & Szedenits, Jr., E. 1979, PhRvD, 20, 351, doi: 10.1103/PhysRevD.20.351

Table 3. Limits on Gravitational-wave Amplitude, and Other Derived Quantities, for 213 Pulsars from the *Bayesian* Analysis.

Pulsar Name (J2000)	$f_{\rm rot}$ (Hz)	$\dot{P}_{\rm rot}$ ($\rm s\,s^{-1}$)	Distance (kpc)	$h_0^{\rm sd}$	$C_{21}^{95\%}$	$C_{22}^{95\%}$	$h_0^{95\%}$	$Q_{22}^{95\%}$ ($\rm kg\,m^2$)	$\varepsilon^{95\%}$	$h_0^{95\%}/h_0^{\rm sd}$	$\mathcal{O}_{m=1,2}^{l=2}$	$\mathcal{O}_{m=2}^{l=2}$
J0023+0923[aε]	327.8	1.0×10^{-20}	1.11 (a)	1.3×10^{-27}	9.6×10^{-27}	8.5×10^{-27}	1.7×10^{-26}	3.3×10^{30}	4.2×10^{-8}	13	-3.2	-1.0
J0030+0451[aε]	205.5	1.0×10^{-20}	0.33 (a)	3.6×10^{-27}	8.7×10^{-27}	3.1×10^{-27}	6.5×10^{-27}	9.2×10^{29}	1.2×10^{-8}	1.8	-4.4	-2.3
J0034−0534[aε]	532.7	4.2×10^{-21}	1.35 (b)	8.9×10^{-28}	1.1×10^{-26}	5.2×10^{-27}	1.1×10^{-26}	9.2×10^{29}	1.2×10^{-8}	12	-4.7	-2.4
J0101−6422[aδ]	388.6	3.7×10^{-21}	1.00 (b)	9.7×10^{-28}	1.0×10^{-26}	3.2×10^{-27}	7.4×10^{-27}	9.0×10^{29}	1.2×10^{-8}	7.6	-4.7	-2.5
J0102+4839[ε]	337.4	1.1×10^{-20}	2.31 (b)	6.8×10^{-28}	1.3×10^{-26}	6.3×10^{-27}	1.3×10^{-26}	4.7×10^{30}	6.1×10^{-8}	19	-3.7	-1.6
J0117+5914[aα]	9.9	5.9×10^{-15}	1.77 (b)	1.1×10^{-25}	...	...	1.7×10^{-25}	5.8×10^{34}	7.5×10^{-4}	1.6	...	-2.5
J0125−2327[ε]	272.1	1.8×10^{-20}	0.92 (b)	2.0×10^{-27}	1.2×10^{-26}	4.2×10^{-27}	8.5×10^{-27}	1.9×10^{30}	2.5×10^{-8}	4.3	-4.1	-2.1
J0154+1833[aε]	422.9	1.1×10^{-21}	1.62 (b)	3.4×10^{-28}	1.6×10^{-26}	3.6×10^{-27}	9.7×10^{-27}	1.6×10^{30}	2.1×10^{-8}	29	-4.3	-2.5
J0218+4232[aε]	430.5	7.6×10^{-20}	3.15 (c)	1.5×10^{-27}	1.2×10^{-26}	4.0×10^{-27}	8.9×10^{-27}	2.8×10^{30}	3.6×10^{-8}	6.1	-4.5	-2.5
J0340+4130[aε]	303.1	6.7×10^{-21}	1.60 (b)	7.2×10^{-28}	1.7×10^{-26}	3.2×10^{-27}	6.8×10^{-27}	2.2×10^{30}	2.8×10^{-8}	9.5	-3.7	-2.4
J0348+0432[aε]	25.6	2.3×10^{-19}	2.10 (d)	9.3×10^{-28}	9.6×10^{-26}	7.0×10^{-27}	1.4×10^{-26}	8.1×10^{32}	1.1×10^{-5}	15	-4.5	-2.4
J0406+3039[ε]	383.3	8.3×10^{-21}	...	...	1.6×10^{-26}	4.2×10^{-27}	8.5×10^{-27}	...	...	...	-3.9	-2.4
J0407+1607[ε]	38.9	7.9×10^{-20}	1.34 (b)	1.1×10^{-27}	1.9×10^{-26}	3.0×10^{-27}	6.7×10^{-27}	1.1×10^{32}	1.4×10^{-6}	6.4	-5.4	-2.6
J0453+1559[aε]	21.8	1.8×10^{-19}	0.52 (b)	3.1×10^{-27}	1.5×10^{-25}	5.4×10^{-27}	1.1×10^{-26}	2.2×10^{32}	2.8×10^{-6}	3.6	-5.5	-3.0
J0509+0856[aε]	246.6	3.8×10^{-21}	0.82 (b)	9.6×10^{-28}	1.3×10^{-26}	3.1×10^{-27}	8.3×10^{-27}	2.0×10^{30}	2.6×10^{-8}	8.6	-4.2	-2.2
J0509+3801[ε]	13.1	7.9×10^{-18}	1.56 (b)	5.3×10^{-27}	2.5×10^{-24}	2.0×10^{-26}	4.4×10^{-26}	7.3×10^{33}	9.5×10^{-5}	8.3	-9.2	-2.7
J0557+1550[ε]	391.2	7.4×10^{-21}	1.83 (b)	7.5×10^{-28}	9.0×10^{-27}	5.1×10^{-27}	1.1×10^{-26}	2.3×10^{30}	3.0×10^{-8}	14	-4.5	-2.2
J0557−2948[δ]	22.9	7.3×10^{-20}	4.27 (b)	2.4×10^{-28}	1.4×10^{-25}	5.9×10^{-27}	1.5×10^{-26}	2.2×10^{33}	2.8×10^{-5}	60	-5.2	-2.7
J0609+2130[α]	18.0	2.4×10^{-19}	0.57 (b)	2.9×10^{-27}	5.7×10^{-25}	8.4×10^{-27}	1.8×10^{-26}	6.0×10^{32}	7.8×10^{-6}	6.4	-8.7	-2.9
J0610−2100[aε]	259.0	1.1×10^{-21}	3.26 (b)	1.3×10^{-28}	1.5×10^{-26}	4.3×10^{-27}	9.4×10^{-27}	8.3×10^{30}	1.1×10^{-7}	71	-3.8	-2.1
J0613−0200[aε]	326.6	8.3×10^{-21}	0.60 (f)	2.2×10^{-27}	1.2×10^{-26}	7.5×10^{-27}	1.6×10^{-26}	1.7×10^{30}	2.2×10^{-8}	7.4	-3.2	-1.2
J0614−3329[aε]	317.6	1.8×10^{-20}	0.63 (g)	3.0×10^{-27}	8.5×10^{-27}	4.2×10^{-27}	8.3×10^{-27}	9.5×10^{29}	1.2×10^{-8}	2.7	-4.5	-2.3
J0621+1002[aε]	34.7	4.6×10^{-20}	0.42 (b)	2.4×10^{-27}	3.4×10^{-26}	3.7×10^{-27}	7.7×10^{-27}	4.9×10^{31}	6.4×10^{-7}	3.2	-5.3	-2.6
J0636+5129[aε]	348.6	3.4×10^{-21}	0.21 (b)	4.2×10^{-27}	9.7×10^{-27}	3.8×10^{-27}	7.8×10^{-27}	2.5×10^{29}	3.2×10^{-9}	1.9	-5.2	-2.5
J0636−3044[δ]	253.4	2.1×10^{-20}	0.71 (b)	2.6×10^{-27}	7.5×10^{-27}	3.8×10^{-27}	7.5×10^{-27}	1.5×10^{30}	2.0×10^{-8}	2.8	-4.5	-2.3
J0645+5158[aε]	112.9	2.7×10^{-21}	1.20 (a)	3.7×10^{-28}	7.6×10^{-27}	3.1×10^{-27}	6.6×10^{-27}	1.1×10^{31}	1.5×10^{-7}	18	-4.4	-2.1
J0709+0458[aε]	29.0	3.8×10^{-19}	1.20 (b)	2.2×10^{-27}	4.2×10^{-26}	4.8×10^{-27}	1.3×10^{-26}	3.3×10^{32}	4.3×10^{-6}	5.7	-5.7	-2.5
J0721−2038[ε]	64.3	4.4×10^{-20}	2.68 (b)	5.1×10^{-28}	1.2×10^{-26}	2.6×10^{-27}	6.4×10^{-27}	7.5×10^{31}	9.8×10^{-7}	13	-4.7	-2.2
J0732+2314[ε]	244.5	6.0×10^{-21}	1.15 (b)	8.5×10^{-28}	7.9×10^{-27}	2.8×10^{-27}	8.3×10^{-27}	2.9×10^{30}	3.8×10^{-8}	9.7	-4.5	-2.2
J0740+6620[aε]	346.5	6.4×10^{-21}	1.14 (h)	1.1×10^{-27}	9.5×10^{-27}	2.8×10^{-27}	6.3×10^{-27}	1.1×10^{30}	1.4×10^{-8}	5.9	-5.5	-2.7
J0751+1807[aε]	287.5	6.7×10^{-21}	0.60 (i)	1.9×10^{-27}	1.1×10^{-26}	5.0×10^{-27}	1.0×10^{-26}	1.3×10^{30}	1.7×10^{-8}	5.4	-4.1	-2.1

Table 3 *continued*

Table 3 *(continued)*

Pulsar Name (J2000)	$f_{\rm rot}$ (Hz)	$\dot{P}_{\rm rot}$ ($\rm s\,s^{-1}$)	Distance (kpc)	$h_0^{\rm sd}$	$C_{21}^{95\%}$	$C_{22}^{95\%}$	$h_0^{95\%}$	$Q_{22}^{95\%}$ ($\rm kg\,m^2$)	$\varepsilon^{95\%}$	$h_0^{95\%}/h_0^{\rm sd}$	$\mathcal{O}_{m=1,2}^{l=2}$	$\mathcal{O}_{m=2}^{l=2}$
J0824+0028[aε]	101.4	1.4×10^{-19}	1.69 (b)	1.8×10^{-27}	8.6×10^{-27}	3.5×10^{-27}	7.6×10^{-27}	2.3×10^{31}	3.0×10^{-7}	4.2	-4.2	-2.0
J0900−3144[aε]	90.0	4.9×10^{-20}	0.89 (i)	1.9×10^{-27}	1.3×10^{-26}	2.8×10^{-27}	6.2×10^{-27}	1.3×10^{31}	1.6×10^{-7}	3.3	-5.0	-3.0
J0921−5202[δ]	103.3	2.1×10^{-20}	0.40 (k)	2.9×10^{-27}	9.3×10^{-27}	2.3×10^{-27}	5.8×10^{-27}	4.0×10^{30}	5.1×10^{-8}	2	-4.4	-2.2
J0931−1902[aε]	215.6	3.2×10^{-21}	3.72 (b)	1.8×10^{-28}	7.9×10^{-27}	3.6×10^{-27}	7.7×10^{-27}	1.1×10^{31}	1.5×10^{-7}	43	-4.3	-2.1
J0955−6150[δ]	500.2	1.4×10^{-20}	2.17 (b)	9.9×10^{-28}	1.1×10^{-26}	5.6×10^{-27}	1.8×10^{-26}	2.8×10^{30}	3.6×10^{-8}	18	-4.8	-2.2
J1012+5307[aε]	190.3	1.0×10^{-20}	0.70 (j)	1.6×10^{-27}	9.5×10^{-27}	4.0×10^{-27}	7.8×10^{-27}	2.8×10^{30}	3.6×10^{-8}	4.8	-4.2	-2.1
J1012−4235[δ]	322.5	6.5×10^{-21}	0.37 (b)	3.1×10^{-27}	9.3×10^{-27}	7.1×10^{-27}	1.6×10^{-26}	1.0×10^{30}	1.3×10^{-8}	5	-3.8	-1.8
J1017−7156[aδ]	427.6	2.8×10^{-21}	3.50 (f)	2.5×10^{-28}	7.7×10^{-27}	4.1×10^{-27}	8.8×10^{-27}	3.1×10^{30}	4.0×10^{-8}	35	-4.7	-2.4
J1022+1001[aδ]	60.8	3.5×10^{-20}	0.64 (f)	1.8×10^{-27}	1.4×10^{-26}	3.8×10^{-27}	7.7×10^{-27}	2.4×10^{31}	3.2×10^{-7}	4.2	-4.6	-1.9
J1024−0719[bε]	193.7	···	1.20 (f)	···	1.6×10^{-26}	3.7×10^{-27}	7.2×10^{-27}	4.2×10^{30}	5.4×10^{-8}	···	-3.4	-2.2
J1035−6720[aδ]	348.2	4.5×10^{-20}	1.46 (b)	2.2×10^{-27}	9.9×10^{-27}	4.4×10^{-27}	1.3×10^{-26}	2.8×10^{30}	3.6×10^{-8}	5.8	-5.2	-2.2
J1036−8317[δ]	293.4	3.1×10^{-20}	0.93 (b)	2.6×10^{-27}	1.2×10^{-26}	3.3×10^{-27}	7.1×10^{-27}	1.4×10^{30}	1.8×10^{-8}	2.7	-4.4	-2.4
J1038+0032[ε]	34.7	6.7×10^{-20}	5.95 (b)	2.1×10^{-28}	3.8×10^{-26}	3.2×10^{-27}	6.9×10^{-27}	6.3×10^{32}	8.1×10^{-6}	33	-5.3	-2.6
J1045−4509[aδ]	133.8	1.8×10^{-20}	0.59 (f)	2.1×10^{-27}	1.5×10^{-26}	5.0×10^{-27}	9.6×10^{-27}	5.8×10^{30}	7.5×10^{-8}	4.6	-2.7	-1.3
J1101−6424[δ]	195.7	1.8×10^{-21}	2.17 (b)	2.2×10^{-28}	8.7×10^{-27}	2.3×10^{-27}	5.7×10^{-27}	5.9×10^{30}	7.6×10^{-8}	26	-4.6	-2.7
J1103−5403[δ]	294.7	3.7×10^{-21}	1.68 (b)	5.0×10^{-28}	1.0×10^{-26}	3.4×10^{-27}	9.6×10^{-27}	3.4×10^{30}	4.4×10^{-8}	19	-4.7	-3.5
J1125+7819[bε]	238.0	···	0.88 (b)	···	7.7×10^{-27}	3.4×10^{-27}	7.3×10^{-27}	2.1×10^{30}	2.7×10^{-8}	···	-4.5	-2.3
J1125−5825[aδ]	322.4	6.0×10^{-20}	1.74 (b)	2.0×10^{-27}	8.6×10^{-27}	3.7×10^{-27}	9.2×10^{-27}	2.8×10^{30}	3.6×10^{-8}	4.5	-4.7	-2.3
J1125−6014[δ]	380.2	4.0×10^{-21}	1.40 (f)	7.1×10^{-28}	8.0×10^{-27}	3.8×10^{-27}	8.2×10^{-27}	1.5×10^{30}	1.9×10^{-8}	12	-4.7	-2.4
J1142+0119[bε]	197.0	···	2.17 (b)	···	1.6×10^{-26}	3.6×10^{-27}	7.4×10^{-27}	7.6×10^{30}	9.8×10^{-8}	···	-3.4	-2.1
J1207−5050[aδ]	206.5	5.7×10^{-21}	1.27 (b)	6.9×10^{-28}	9.5×10^{-27}	4.4×10^{-27}	1.1×10^{-26}	6.0×10^{30}	7.8×10^{-8}	16	-4.1	-1.9
J1216−6410[δ]	282.5	1.6×10^{-21}	1.10 (b)	5.0×10^{-28}	9.7×10^{-27}	2.8×10^{-27}	7.3×10^{-27}	1.8×10^{30}	2.4×10^{-8}	15	-4.5	-2.4
J1231−1411[aε]	271.5	8.3×10^{-21}	0.42 (b)	2.9×10^{-27}	1.3×10^{-26}	5.6×10^{-27}	1.1×10^{-26}	1.1×10^{30}	1.4×10^{-8}	3.7	-3.8	-2.1
J1300+1240[bε]	160.8	···	0.60 (j)	···	1.2×10^{-26}	5.2×10^{-27}	1.1×10^{-26}	4.6×10^{30}	6.0×10^{-8}	···	-3.5	-1.6
J1302−3258[ε]	265.2	6.6×10^{-21}	1.43 (b)	7.4×10^{-28}	2.1×10^{-26}	4.1×10^{-27}	7.5×10^{-27}	2.8×10^{30}	3.6×10^{-8}	10	-3.3	-2.3
J1312+0051[aε]	236.5	8.2×10^{-21}	1.47 (b)	7.6×10^{-28}	9.6×10^{-27}	2.9×10^{-27}	6.3×10^{-27}	3.0×10^{30}	3.9×10^{-8}	8.3	-4.5	-2.4
J1327+3423[ε]	24.1	1.3×10^{-19}	···	···	1.3×10^{-25}	5.2×10^{-27}	1.6×10^{-26}	···	···	···	-5.1	-2.6
J1327−0755[bε]	373.4	···	25.00 (b)	···	1.0×10^{-26}	3.9×10^{-27}	7.9×10^{-27}	2.6×10^{31}	3.3×10^{-7}	···	-4.6	-2.4
J1337−6423[aδ]	106.1	1.8×10^{-20}	5.94 (b)	1.9×10^{-28}	1.3×10^{-26}	3.1×10^{-27}	6.7×10^{-27}	6.4×10^{31}	8.3×10^{-7}	36	-4.2	-2.1
J1400−1431[aε]	324.2	9.0×10^{-23}	0.27 (n)	5.1×10^{-28}	8.2×10^{-27}	3.9×10^{-27}	8.3×10^{-27}	3.9×10^{29}	5.0×10^{-9}	16	-4.6	-2.3
J1411+2551[aε]	16.0	8.9×10^{-20}	1.13 (b)	8.5×10^{-28}	9.7×10^{-25}	1.7×10^{-26}	3.2×10^{-26}	2.6×10^{33}	3.3×10^{-5}	37	-9.3	-2.7
J1420−5625[δ]	29.3	6.8×10^{-20}	1.33 (b)	8.5×10^{-28}	6.0×10^{-26}	4.1×10^{-27}	1.1×10^{-26}	3.2×10^{32}	4.1×10^{-6}	13	-5.1	-2.7
J1421−4409[aδ]	156.6	6.0×10^{-21}	2.08 (b)	3.8×10^{-28}	1.0×10^{-26}	2.8×10^{-27}	6.6×10^{-27}	1.0×10^{31}	1.3×10^{-7}	18	-4.3	-2.2

Table 3 *continued*

Table 3 *(continued)*

Pulsar Name (J2000)	$f_{\rm rot}$ (Hz)	$\dot{P}_{\rm rot}$ ($\rm s\,s^{-1}$)	Distance (kpc)	$h_0^{\rm sd}$	$C_{21}^{95\%}$	$C_{22}^{95\%}$	$h_0^{95\%}$	$Q_{22}^{95\%}$ ($\rm kg\,m^2$)	$\varepsilon^{95\%}$	$h_0^{95\%}/h_0^{\rm sd}$	$\mathcal{O}_{m=1,2}^{l=2}$	$\mathcal{O}_{m=2}^{l=2}$
J1431−4715[aδ]	497.0	1.1×10^{-20}	1.53 (p)	1.3×10^{-27}	1.5×10^{-26}	6.2×10^{-27}	1.6×10^{-26}	1.8×10^{30}	2.3×10^{-8}	13	-4.4	-2.2
J1431−5740[δ]	243.3	6.4×10^{-21}	3.55 (b)	2.8×10^{-28}	9.7×10^{-27}	3.1×10^{-27}	6.7×10^{-27}	7.4×10^{30}	9.5×10^{-8}	24	-4.4	-2.4
J1435−6100[δ]	107.0	2.4×10^{-20}	2.81 (b)	4.6×10^{-28}	8.2×10^{-27}	3.6×10^{-27}	8.0×10^{-27}	3.6×10^{31}	4.7×10^{-7}	17	-3.9	-1.8
J1439−5501[δ]	34.9	1.4×10^{-19}	0.65 (b)	2.7×10^{-27}	3.5×10^{-26}	4.9×10^{-27}	1.0×10^{-26}	1.0×10^{32}	1.3×10^{-6}	3.8	-5.1	-2.3
J1446−4701[aδ]	455.6	9.6×10^{-21}	1.50 (f)	1.1×10^{-27}	1.1×10^{-26}	5.6×10^{-27}	1.2×10^{-26}	1.6×10^{30}	2.1×10^{-8}	11	-4.3	-2.2
J1453+1902[aϵ]	172.6	9.2×10^{-21}	1.27 (b)	8.0×10^{-28}	1.3×10^{-26}	4.6×10^{-27}	8.0×10^{-27}	6.3×10^{30}	8.1×10^{-8}	10	-4.1	-2.7
J1455−3330[aϵ]	125.2	2.3×10^{-20}	1.01 (q)	1.3×10^{-27}	9.2×10^{-27}	2.6×10^{-27}	5.4×10^{-27}	6.4×10^{30}	8.3×10^{-8}	4.1	-4.3	-2.3
J1502−6752[aδ]	37.4	2.2×10^{-19}	7.73 (b)	3.0×10^{-28}	3.1×10^{-26}	3.1×10^{-27}	7.0×10^{-27}	7.1×10^{32}	9.2×10^{-6}	24	-5.6	-2.6
J1513−2550[ϵ]	471.9	2.2×10^{-20}	3.96 (b)	6.5×10^{-28}	1.6×10^{-26}	5.9×10^{-27}	1.2×10^{-26}	4.0×10^{30}	5.2×10^{-8}	19	-3.9	-2.3
J1514−4946[aδ]	278.6	1.1×10^{-20}	0.91 (b)	1.6×10^{-27}	1.2×10^{-26}	3.3×10^{-27}	1.0×10^{-26}	2.2×10^{30}	2.9×10^{-8}	6.6	-4.2	-2.2
J1518+0204A[cϵ]	180.1	4.4×10^{-20}	8.00 (r)	2.8×10^{-28}	9.0×10^{-27}	4.9×10^{-27}	9.7×10^{-27}	4.4×10^{31}	5.7×10^{-7}	34	-5.1	-2.2
J1518+4904[aϵ]	24.4	2.3×10^{-20}	0.96 (b)	6.3×10^{-28}	1.2×10^{-25}	4.5×10^{-27}	9.4×10^{-27}	2.8×10^{32}	3.6×10^{-6}	15	-5.0	-3.0
J1525−5545[δ]	88.0	1.3×10^{-19}	3.14 (b)	8.7×10^{-28}	1.1×10^{-26}	2.4×10^{-27}	8.9×10^{-27}	6.6×10^{31}	8.6×10^{-7}	10	-4.5	-1.8
J1528−3146[ϵ]	16.4	2.5×10^{-19}	0.77 (b)	2.1×10^{-27}	1.0×10^{-24}	8.6×10^{-27}	1.8×10^{-26}	9.5×10^{32}	1.2×10^{-5}	8.6	-9.6	-2.9
J1529−3828[δ]	117.8	2.7×10^{-20}	4.30 (b)	3.3×10^{-28}	1.1×10^{-26}	2.7×10^{-27}	7.0×10^{-27}	4.0×10^{31}	5.1×10^{-7}	21	-4.3	-2.1
J1536−4948[aδ]	324.7	2.1×10^{-20}	0.98 (b)	2.1×10^{-27}	9.4×10^{-27}	4.7×10^{-27}	9.7×10^{-27}	1.6×10^{30}	2.1×10^{-8}	4.5	-4.3	-2.2
J1537+1155[aϵ]	26.4	2.4×10^{-18}	1.05 (s)	6.1×10^{-27}	7.6×10^{-26}	6.6×10^{-27}	1.2×10^{-26}	3.3×10^{32}	4.2×10^{-6}	2	-5.0	-2.7
J1537−5312[δ]	144.4	1.6×10^{-20}	3.05 (b)	4.0×10^{-28}	1.2×10^{-26}	2.1×10^{-27}	4.5×10^{-27}	1.2×10^{31}	1.6×10^{-7}	11	-4.4	-2.4
J1543−5149[aδ]	486.2	1.6×10^{-20}	1.15 (b)	2.0×10^{-27}	1.5×10^{-26}	4.6×10^{-27}	1.1×10^{-26}	9.9×10^{29}	1.3×10^{-8}	5.7	-4.5	-2.4
J1544+4937[ϵ]	463.1	2.9×10^{-21}	2.99 (b)	3.1×10^{-28}	1.5×10^{-26}	7.1×10^{-27}	1.5×10^{-26}	3.8×10^{30}	5.0×10^{-8}	48	-4.0	-2.0
J1545−4550[δ]	279.7	5.3×10^{-20}	2.20 (f)	1.4×10^{-27}	1.0×10^{-26}	3.1×10^{-27}	6.7×10^{-27}	3.4×10^{30}	4.4×10^{-8}	4.8	-4.5	-2.4
J1547−5709[δ]	233.0	7.4×10^{-21}	2.69 (b)	3.9×10^{-28}	7.2×10^{-27}	3.1×10^{-27}	7.9×10^{-27}	7.2×10^{30}	9.3×10^{-8}	20	-4.5	-2.3
J1551−0658[γ]	141.0	2.0×10^{-20}	1.32 (b)	1.0×10^{-27}	8.9×10^{-27}	2.7×10^{-27}	5.7×10^{-27}	6.9×10^{30}	9.0×10^{-8}	5.6	-4.3	-2.3
J1600−3053[aϵ]	277.9	7.9×10^{-21}	3.00 (f)	4.0×10^{-28}	1.3×10^{-26}	3.9×10^{-27}	8.3×10^{-27}	5.9×10^{30}	7.6×10^{-8}	21	-4.1	-2.3
J1603−7202[aδ]	67.4	1.7×10^{-20}	3.40 (f)	2.5×10^{-28}	1.3×10^{-26}	2.5×10^{-27}	5.2×10^{-27}	7.1×10^{31}	9.1×10^{-7}	20	-4.6	-2.3
J1614−2230[aϵ]	317.4	3.7×10^{-21}	0.70 (q)	1.3×10^{-27}	1.2×10^{-26}	4.6×10^{-27}	9.9×10^{-27}	1.3×10^{30}	1.6×10^{-8}	7.9	-4.2	-2.2
J1618−3921[ϵ]	83.4	5.4×10^{-20}	5.52 (b)	3.1×10^{-28}	2.1×10^{-26}	2.1×10^{-27}	5.2×10^{-27}	7.6×10^{31}	9.8×10^{-7}	17	-3.6	-2.2
J1618−4624[δ]	168.6	3.1×10^{-21}	3.04 (b)	1.9×10^{-28}	1.3×10^{-26}	2.6×10^{-27}	6.9×10^{-27}	1.3×10^{31}	1.7×10^{-7}	36	-4.4	-2.4
J1622−6617[aδ]	42.3	5.1×10^{-20}	4.05 (b)	2.9×10^{-28}	2.9×10^{-26}	2.5×10^{-27}	5.7×10^{-27}	2.4×10^{32}	3.1×10^{-6}	20	-5.2	-2.6
J1623−2631[cϵ]	90.3	8.8×10^{-20}	1.80 (t)	1.3×10^{-27}	2.0×10^{-26}	4.8×10^{-27}	1.1×10^{-26}	4.4×10^{31}	5.7×10^{-7}	8.6	-3.2	-1.5
J1628−3205[bδ]	311.4	···	1.23 (b)	···	1.2×10^{-26}	3.1×10^{-27}	8.9×10^{-27}	2.1×10^{30}	2.7×10^{-8}	···	-4.3	-2.4
J1629−6902[δ]	166.6	1.0×10^{-20}	0.96 (b)	1.1×10^{-27}	9.7×10^{-27}	3.2×10^{-27}	6.5×10^{-27}	4.1×10^{30}	5.3×10^{-8}	6	-4.4	-2.4
J1630+3734[aα]	301.4	8.5×10^{-21}	1.19 (b)	1.1×10^{-27}	1.1×10^{-26}	3.0×10^{-27}	8.6×10^{-27}	2.1×10^{30}	2.7×10^{-8}	7.9	-4.4	-2.3

Table 3 *continued*

Table 3 *(continued)*

Pulsar Name (J2000)	$f_{\rm rot}$ (Hz)	$\dot{P}_{\rm rot}$ ($\rm s\,s^{-1}$)	Distance (kpc)	$h_0^{\rm sd}$	$C_{21}^{95\%}$	$C_{22}^{95\%}$	$h_0^{95\%}$	$Q_{22}^{95\%}$ ($\rm kg\,m^2$)	$\varepsilon^{95\%}$	$h_0^{95\%}/h_0^{\rm sd}$	$\mathcal{O}_{m=1,2}^{l=2}$	$\mathcal{O}_{m=2}^{l=2}$
J1640+2224[aε]	316.1	1.3×10^{-21}	1.52 (u)	3.4×10^{-28}	1.2×10^{-26}	3.6×10^{-27}	7.5×10^{-27}	2.1×10^{30}	2.7×10^{-8}	22	-4.3	-2.4
J1641+3627A[cα]	96.4	8.2×10^{-20}	7.10 (r)	3.2×10^{-28}	1.1×10^{-26}	2.3×10^{-27}	5.5×10^{-27}	7.7×10^{31}	1.0×10^{-6}	17	-4.5	-2.3
J1643−1224[aε]	216.4	1.8×10^{-20}	1.20 (f)	1.3×10^{-27}	9.9×10^{-27}	4.8×10^{-27}	9.6×10^{-27}	4.5×10^{30}	5.8×10^{-8}	7.3	-3.8	-1.8
J1652−4838[δ]	264.2	1.1×10^{-20}	...	...	1.0×10^{-26}	4.5×10^{-27}	9.9×10^{-27}	...	...	...	-4.1	-2.1
J1653−2054[δ]	242.2	1.1×10^{-20}	2.63 (b)	5.0×10^{-28}	8.8×10^{-27}	2.8×10^{-27}	6.6×10^{-27}	5.4×10^{30}	7.0×10^{-8}	13	-4.5	-2.4
J1658−5324[aδ]	410.0	1.1×10^{-20}	0.88 (b)	1.9×10^{-27}	9.7×10^{-27}	3.7×10^{-27}	8.3×10^{-27}	7.9×10^{29}	1.0×10^{-8}	4.3	-4.6	-2.5
J1705−1903[δ]	403.2	2.1×10^{-20}	2.40 (b)	9.8×10^{-28}	1.1×10^{-26}	4.3×10^{-27}	9.9×10^{-27}	2.7×10^{30}	3.4×10^{-8}	10	-4.5	-2.4
J1708−3506[aε]	222.0	8.6×10^{-21}	3.32 (b)	3.3×10^{-28}	9.9×10^{-27}	2.6×10^{-27}	5.7×10^{-27}	7.0×10^{30}	9.1×10^{-8}	17	-4.4	-2.4
J1709+2313[aε]	215.9	1.3×10^{-21}	2.18 (b)	1.9×10^{-28}	1.7×10^{-26}	3.9×10^{-27}	8.1×10^{-27}	6.9×10^{30}	8.9×10^{-8}	42	-3.7	-2.1
J1713+0747[aε]	218.8	7.8×10^{-21}	1.00 (f)	1.1×10^{-27}	9.0×10^{-27}	3.3×10^{-27}	6.9×10^{-27}	2.6×10^{30}	3.4×10^{-8}	6.5	-4.4	-2.3
J1719−1438[aε]	172.7	7.3×10^{-21}	0.34 (b)	2.7×10^{-27}	1.0×10^{-26}	3.2×10^{-27}	7.2×10^{-27}	1.5×10^{30}	1.9×10^{-8}	2.7	-4.8	-2.8
J1721−2457[bε]	286.0	...	1.36 (b)	...	1.2×10^{-26}	3.7×10^{-27}	7.6×10^{-27}	2.3×10^{30}	3.0×10^{-8}	...	-4.4	-2.3
J1727−2946[aδ]	36.9	2.4×10^{-19}	1.88 (b)	1.3×10^{-27}	4.5×10^{-26}	2.5×10^{-27}	6.6×10^{-27}	1.7×10^{32}	2.2×10^{-6}	5.1	-4.9	-2.7
J1729−2117[γ]	15.1	1.7×10^{-19}	0.97 (b)	1.3×10^{-27}	1.5×10^{-24}	1.5×10^{-26}	3.1×10^{-26}	2.4×10^{33}	3.2×10^{-5}	23	-9.2	-2.7
J1730−2304[aε]	123.1	1.1×10^{-20}	0.47 (f)	2.0×10^{-27}	8.8×10^{-27}	2.3×10^{-27}	5.0×10^{-27}	2.8×10^{30}	3.7×10^{-8}	2.5	-4.6	-2.3
J1731−1847[aε]	426.5	2.3×10^{-20}	4.78 (b)	5.2×10^{-28}	1.3×10^{-26}	3.9×10^{-27}	8.6×10^{-27}	4.2×10^{30}	5.4×10^{-8}	17	-4.5	-2.5
J1732−5049[aδ]	188.2	1.1×10^{-20}	1.88 (b)	6.2×10^{-28}	1.3×10^{-26}	2.3×10^{-27}	6.7×10^{-27}	6.5×10^{30}	8.4×10^{-8}	11	-3.7	-2.3
J1737−0811[δ]	239.5	7.9×10^{-21}	0.21 (b)	5.4×10^{-27}	1.2×10^{-26}	5.3×10^{-27}	1.2×10^{-26}	7.6×10^{29}	9.8×10^{-9}	2.1	-3.5	-1.8
J1738+0333[aε]	170.9	2.2×10^{-20}	1.47 (v)	1.1×10^{-27}	8.5×10^{-27}	2.3×10^{-27}	4.8×10^{-27}	4.5×10^{30}	5.8×10^{-8}	4.5	-5.0	-2.9
J1741+1351[aε]	266.9	2.9×10^{-20}	1.08 (w)	2.1×10^{-27}	1.1×10^{-26}	3.0×10^{-27}	6.6×10^{-27}	1.8×10^{30}	2.4×10^{-8}	3.2	-4.2	-2.4
J1744−1134[aε]	245.4	7.2×10^{-21}	0.41 (f)	2.6×10^{-27}	9.5×10^{-27}	4.9×10^{-27}	9.8×10^{-27}	1.2×10^{30}	1.6×10^{-8}	3.7	-4.1	-2.1
J1745+1017[aε]	377.1	2.2×10^{-21}	1.21 (b)	6.0×10^{-28}	9.2×10^{-27}	3.8×10^{-27}	8.3×10^{-27}	1.3×10^{30}	1.7×10^{-8}	14	-4.6	-2.4
J1747−4036[aδ]	607.7	1.1×10^{-20}	7.15 (b)	2.9×10^{-28}	1.6×10^{-26}	4.9×10^{-27}	1.1×10^{-26}	4.0×10^{30}	5.1×10^{-8}	38	-4.5	-2.5
J1748−2446A[cγ]	86.5	9.2×10^{-20}	6.90 (r)	3.3×10^{-28}	1.2×10^{-26}	3.7×10^{-27}	7.1×10^{-27}	1.2×10^{32}	1.5×10^{-6}	22	-4.3	-2.0
J1748−3009[bγ]	103.3	...	5.05 (b)	...	1.0×10^{-26}	2.2×10^{-27}	7.5×10^{-27}	6.5×10^{31}	8.4×10^{-7}	...	-4.4	-2.1
J1750−2536[γ]	28.8	1.4×10^{-19}	3.22 (b)	5.1×10^{-28}	5.5×10^{-26}	6.0×10^{-27}	1.1×10^{-26}	7.5×10^{32}	9.8×10^{-6}	21	-5.2	-2.7
J1751−2857[aε]	255.4	1.0×10^{-20}	1.09 (b)	1.2×10^{-27}	1.6×10^{-26}	8.7×10^{-27}	2.0×10^{-26}	6.1×10^{30}	7.9×10^{-8}	17	-3.4	-1.7
J1753−1914[γ]	15.9	2.0×10^{-18}	2.92 (b)	1.6×10^{-27}	1.3×10^{-24}	1.2×10^{-26}	2.6×10^{-26}	5.5×10^{33}	7.1×10^{-5}	17	-9.4	-3.0
J1753−2240[γ]	10.5	9.7×10^{-19}	3.23 (b)	8.0×10^{-28}	1.3×10^{-23}	5.7×10^{-26}	1.2×10^{-25}	6.4×10^{34}	8.2×10^{-4}	150	-8.3	-2.6
J1755−3716[δ]	78.2	3.1×10^{-20}	8.18 (b)	1.5×10^{-28}	1.3×10^{-26}	2.9×10^{-27}	5.8×10^{-27}	1.4×10^{32}	1.8×10^{-6}	38	-4.4	-2.2
J1757−1854[δ]	46.5	2.6×10^{-18}	19.56 (b)	4.6×10^{-28}	1.7×10^{-26}	2.7×10^{-27}	7.1×10^{-27}	1.2×10^{33}	1.5×10^{-5}	16	-5.1	-2.3
J1757−5322[δ]	112.7	2.6×10^{-20}	0.94 (b)	1.5×10^{-27}	9.3×10^{-27}	5.3×10^{-27}	9.0×10^{-27}	1.2×10^{31}	1.6×10^{-7}	6.1	-3.6	-1.8
J1801−1417[aε]	275.9	3.8×10^{-21}	1.10 (b)	7.4×10^{-28}	7.4×10^{-27}	3.2×10^{-27}	6.9×10^{-27}	1.8×10^{30}	2.4×10^{-8}	9.3	-4.6	-2.3

Table 3 *continued*

Table 3 *(continued)*

Pulsar Name (J2000)	$f_{\rm rot}$ (Hz)	$\dot{P}_{\rm rot}$ ($\rm s\,s^{-1}$)	Distance (kpc)	$h_0^{\rm sd}$	$C_{21}^{95\%}$	$C_{22}^{95\%}$	$h_0^{95\%}$	$Q_{22}^{95\%}$ ($\rm kg\,m^2$)	$\varepsilon^{95\%}$	$h_0^{95\%}/h_0^{\rm sd}$	$\mathcal{O}_{m=1,2}^{l=2}$	$\mathcal{O}_{m=2}^{l=2}$
J1801−3210$^{b\delta}$	134.2	···	6.11 (b)	···	8.5×10^{-27}	4.7×10^{-27}	1.2×10^{-26}	7.3×10^{31}	9.5×10^{-7}	···	-3.7	-1.5
J1802−2124$^{a\epsilon}$	79.1	7.1×10^{-20}	0.76 (i)	2.5×10^{-27}	9.5×10^{-27}	2.2×10^{-27}	4.9×10^{-27}	1.1×10^{31}	1.4×10^{-7}	2	-4.8	-2.3
J1804−0735$^{c\gamma}$	43.3	1.8×10^{-19}	7.80 (r)	2.9×10^{-28}	2.2×10^{-26}	6.8×10^{-27}	1.8×10^{-26}	1.4×10^{33}	1.8×10^{-5}	62	-4.6	-1.2
J1804−2717$^{a\epsilon}$	107.0	3.5×10^{-20}	0.81 (b)	1.9×10^{-27}	8.0×10^{-27}	2.6×10^{-27}	5.9×10^{-27}	7.5×10^{30}	9.8×10^{-8}	3	-4.3	-2.2
J1804−2858$^{b\delta}$	669.9	···	8.19 (b)	···	1.5×10^{-26}	7.3×10^{-27}	1.8×10^{-26}	6.0×10^{30}	7.7×10^{-8}	···	-4.5	-2.2
J1807−2459A$^{c\gamma}$	326.9	2.4×10^{-20}	3.00 (r)	7.6×10^{-28}	7.7×10^{-27}	5.9×10^{-27}	1.2×10^{-26}	6.3×10^{30}	8.1×10^{-8}	16	-4.1	-1.7
J1810+1744$^{\gamma}$	601.4	4.4×10^{-21}	2.36 (b)	5.5×10^{-28}	1.4×10^{-26}	6.2×10^{-27}	1.5×10^{-26}	1.8×10^{30}	2.3×10^{-8}	27	-4.5	-2.3
J1810−2005$^{a\delta}$	30.5	5.3×10^{-20}	3.51 (b)	2.9×10^{-28}	3.9×10^{-26}	3.9×10^{-27}	9.2×10^{-27}	6.3×10^{32}	8.2×10^{-6}	31	-5.6	-2.8
J1811−2405$^{a\epsilon}$	375.9	1.3×10^{-20}	1.83 (b)	9.9×10^{-28}	1.3×10^{-26}	7.5×10^{-27}	1.5×10^{-26}	3.5×10^{30}	4.5×10^{-8}	15	-3.8	-1.9
J1813−2621$^{b\gamma}$	225.7	···	3.16 (b)	···	1.4×10^{-26}	2.6×10^{-27}	6.0×10^{-27}	6.8×10^{30}	8.8×10^{-8}	···	-4.0	-2.4
J1821+0155$^{\alpha}$	29.6	2.9×10^{-20}	1.72 (b)	4.3×10^{-28}	5.1×10^{-26}	4.1×10^{-27}	1.1×10^{-26}	4.1×10^{32}	5.3×10^{-6}	26	-5.5	-2.8
J1823−3021A$^{c\epsilon}$	183.8	4.3×10^{-20}	7.90 (r)	2.9×10^{-28}	1.2×10^{-26}	2.7×10^{-27}	5.7×10^{-27}	2.4×10^{31}	3.1×10^{-7}	20	-4.2	-2.3
J1824−2452A$^{c\gamma}$	327.4	2.4×10^{-20}	5.50 (z)	4.1×10^{-28}	1.1×10^{-26}	6.6×10^{-27}	1.7×10^{-26}	1.6×10^{31}	2.1×10^{-7}	41	-4.0	-1.7
J1825−0319$^{\delta}$	219.6	6.8×10^{-21}	3.86 (b)	2.6×10^{-28}	9.5×10^{-27}	4.1×10^{-27}	9.5×10^{-27}	1.4×10^{31}	1.8×10^{-7}	37	-4.1	-2.0
J1826−2415$^{\delta}$	213.0	1.7×10^{-20}	2.73 (b)	5.7×10^{-28}	8.5×10^{-27}	5.8×10^{-27}	1.2×10^{-26}	1.3×10^{31}	1.7×10^{-7}	21	-3.6	-1.5
J1829+2456$^{\alpha}$	24.4	5.3×10^{-20}	0.92 (b)	1.0×10^{-27}	1.0×10^{-25}	5.3×10^{-27}	1.1×10^{-26}	3.1×10^{32}	4.0×10^{-6}	11	-5.2	-2.8
J1832−0836$^{b\epsilon}$	367.8	···	1.60 (f)	···	9.8×10^{-27}	3.8×10^{-27}	8.3×10^{-27}	1.8×10^{30}	2.3×10^{-8}	···	-4.8	-2.4
J1833−0827$^{a\eta}$	11.7	9.2×10^{-15}	4.50 (j)	5.9×10^{-26}	6.4×10^{-24}	4.6×10^{-26}	9.3×10^{-26}	5.5×10^{34}	7.2×10^{-4}	1.6	-8.1	-2.1
J1835−0114$^{\delta}$	195.5	7.0×10^{-21}	3.45 (b)	2.7×10^{-28}	1.8×10^{-26}	3.1×10^{-27}	5.6×10^{-27}	9.3×10^{30}	1.2×10^{-7}	21	-1.7	-2.5
J1840−0643$^{\gamma}$	28.1	9.5×10^{-20}	4.99 (b)	2.6×10^{-28}	5.1×10^{-26}	8.1×10^{-27}	1.8×10^{-26}	2.0×10^{33}	2.6×10^{-5}	67	-4.0	-2.0
J1841+0130$^{\gamma}$	33.6	8.2×10^{-18}	4.23 (b)	3.2×10^{-27}	3.6×10^{-26}	3.3×10^{-27}	7.4×10^{-27}	5.0×10^{32}	6.5×10^{-6}	2.3	-5.1	-2.6
J1843−1113$^{a\epsilon}$	541.8	9.3×10^{-21}	1.26 (i)	1.4×10^{-27}	1.1×10^{-26}	6.4×10^{-27}	1.3×10^{-26}	1.0×10^{30}	1.4×10^{-8}	9.2	-4.5	-2.3
J1843−1448$^{b\delta}$	182.8	···	3.47 (b)	···	1.2×10^{-26}	6.0×10^{-27}	1.3×10^{-26}	2.5×10^{31}	3.2×10^{-7}	···	-3.0	-1.2
J1853+1303$^{a\epsilon}$	244.4	8.6×10^{-21}	1.32 (b)	8.9×10^{-28}	9.3×10^{-27}	4.5×10^{-27}	1.0×10^{-26}	4.1×10^{30}	5.3×10^{-8}	11	-4.1	-2.1
J1857+0943$^{a\epsilon}$	186.5	1.7×10^{-20}	1.18 (f)	1.2×10^{-27}	1.0×10^{-26}	3.3×10^{-27}	6.6×10^{-27}	4.1×10^{30}	5.3×10^{-8}	5.4	-4.3	-2.2
J1858−2216$^{\delta}$	419.5	3.8×10^{-21}	0.92 (b)	1.1×10^{-27}	1.0×10^{-26}	3.6×10^{-27}	7.8×10^{-27}	7.4×10^{29}	9.6×10^{-9}	7	-4.7	-2.4
J1902−5105$^{a\eta}$	573.9	8.7×10^{-21}	1.65 (b)	1.1×10^{-27}	1.3×10^{-26}	7.1×10^{-27}	1.4×10^{-26}	1.3×10^{30}	1.7×10^{-8}	13	-4.5	-2.3
J1903+0327$^{a\epsilon}$	465.1	1.9×10^{-20}	6.12 (b)	3.9×10^{-28}	1.6×10^{-26}	5.5×10^{-27}	1.0×10^{-26}	5.4×10^{30}	7.0×10^{-8}	27	-4.2	-2.4
J1903−7051$^{a\delta}$	277.9	7.7×10^{-21}	0.93 (b)	1.3×10^{-27}	9.0×10^{-27}	5.9×10^{-27}	1.1×10^{-26}	2.3×10^{30}	3.0×10^{-8}	8.4	-4.0	-2.0
J1904+0412$^{\gamma}$	14.1	1.1×10^{-19}	4.58 (b)	2.2×10^{-28}	2.5×10^{-24}	2.2×10^{-26}	4.5×10^{-26}	1.9×10^{34}	2.5×10^{-4}	200	-9.0	-2.6
J1905+0400$^{a\gamma}$	264.2	4.2×10^{-21}	1.06 (b)	8.0×10^{-28}	1.3×10^{-26}	2.6×10^{-27}	6.5×10^{-27}	1.8×10^{30}	2.3×10^{-8}	8.1	-4.1	-2.5
J1909−3744$^{a\delta}$	339.3	2.6×10^{-21}	1.15 (f)	6.6×10^{-28}	1.1×10^{-26}	5.7×10^{-27}	1.2×10^{-26}	2.1×10^{30}	2.8×10^{-8}	18	-4.4	-2.1
J1910+1256$^{a\epsilon}$	200.7	8.8×10^{-21}	1.50 (b)	7.2×10^{-28}	2.6×10^{-26}	5.0×10^{-27}	1.0×10^{-26}	7.0×10^{30}	9.0×10^{-8}	14	-2.5	-2.0

Table 3 *continued*

Table 3 *(continued)*

Pulsar Name (J2000)	$f_{\rm rot}$ (Hz)	$\dot{P}_{\rm rot}$ ($\rm s\,s^{-1}$)	Distance (kpc)	$h_0^{\rm sd}$	$C_{21}^{95\%}$	$C_{22}^{95\%}$	$h_0^{95\%}$	$Q_{22}^{95\%}$ ($\rm kg\,m^2$)	$\varepsilon^{95\%}$	$h_0^{95\%}/h_0^{\rm sd}$	$\mathcal{O}_{m=1,2}^{l=2}$	$\mathcal{O}_{m=2}^{l=2}$
J1911+1347[aε]	216.2	1.7×10^{-20}	1.36 (b)	1.1×10^{-27}	9.3×10^{-27}	2.6×10^{-27}	5.6×10^{-27}	3.0×10^{30}	3.9×10^{-8}	5	-4.6	-2.4
J1911−1114[aε]	275.8	1.1×10^{-20}	1.07 (b)	1.3×10^{-27}	9.1×10^{-27}	3.0×10^{-27}	6.4×10^{-27}	1.6×10^{30}	2.1×10^{-8}	4.8	-4.6	-2.4
J1914+0659[γ]	54.0	3.1×10^{-20}	8.47 (b)	1.2×10^{-28}	1.8×10^{-26}	2.8×10^{-27}	5.9×10^{-27}	3.1×10^{32}	4.0×10^{-6}	48	-5.0	-2.4
J1915+1606[aγ]	16.9	8.6×10^{-18}	5.25 (b)	1.9×10^{-27}	6.1×10^{-25}	1.6×10^{-26}	3.3×10^{-26}	1.1×10^{34}	1.4×10^{-4}	18	-8.4	-1.8
J1918−0642[aε]	130.8	2.4×10^{-20}	1.10 (a)	1.3×10^{-27}	8.8×10^{-27}	4.8×10^{-27}	1.0×10^{-26}	1.2×10^{31}	1.5×10^{-7}	7.7	-3.8	-1.4
J1923+2515[aα]	264.0	7.0×10^{-21}	1.20 (b)	9.1×10^{-28}	1.1×10^{-26}	2.8×10^{-27}	6.5×10^{-27}	2.0×10^{30}	2.6×10^{-8}	7.1	-4.4	-2.5
J1933−6211[aδ]	282.2	2.9×10^{-21}	0.65 (b)	1.1×10^{-27}	1.3×10^{-26}	3.1×10^{-27}	6.2×10^{-27}	9.2×10^{29}	1.2×10^{-8}	5.5	-4.1	-2.5
J1939+2134[aγ]	641.9	1.1×10^{-19}	4.80 (f)	1.4×10^{-27}	1.8×10^{-26}	1.5×10^{-26}	2.2×10^{-26}	4.7×10^{30}	6.1×10^{-8}	16	-2.8	-2.0
J1943+2210[γ]	196.7	8.8×10^{-21}	6.77 (b)	1.6×10^{-28}	9.9×10^{-27}	2.3×10^{-27}	5.8×10^{-27}	1.9×10^{31}	2.4×10^{-7}	37	-4.5	-2.4
J1944+0907[aε]	192.9	6.5×10^{-21}	1.22 (b)	7.4×10^{-28}	9.3×10^{-27}	2.9×10^{-27}	6.2×10^{-27}	3.7×10^{30}	4.8×10^{-8}	8.3	-4.4	-2.4
J1946+3417[aε]	315.4	1.0×10^{-21}	6.94 (b)	6.5×10^{-29}	7.8×10^{-27}	5.5×10^{-27}	1.2×10^{-26}	1.5×10^{31}	1.9×10^{-7}	180	-4.2	-2.0
J1946−5403[δ]	368.9	2.7×10^{-21}	1.15 (b)	7.0×10^{-28}	9.9×10^{-27}	5.4×10^{-27}	1.2×10^{-26}	1.8×10^{30}	2.4×10^{-8}	17	-4.2	-2.1
J1949+3106[aε]	76.1	9.3×10^{-20}	7.47 (b)	2.9×10^{-28}	1.2×10^{-26}	3.9×10^{-27}	7.8×10^{-27}	1.8×10^{32}	2.4×10^{-6}	27	-4.4	-2.1
J1950+2414[aγ]	232.3	2.0×10^{-20}	7.27 (b)	2.4×10^{-28}	1.2×10^{-26}	5.1×10^{-27}	9.1×10^{-27}	2.2×10^{31}	2.9×10^{-7}	38	-3.7	-2.2
J1955+2527[aε]	205.2	1.1×10^{-20}	8.18 (b)	1.5×10^{-28}	1.1×10^{-26}	4.8×10^{-27}	9.8×10^{-27}	3.5×10^{31}	4.5×10^{-7}	65	-3.5	-1.6
J1955+2908[aε]	163.0	3.1×10^{-20}	6.30 (b)	2.9×10^{-28}	8.7×10^{-27}	2.5×10^{-27}	5.5×10^{-27}	2.4×10^{31}	3.1×10^{-7}	19	-4.6	-2.5
J1959+2048[aε]	622.1	1.2×10^{-20}	1.40 (cc)	1.6×10^{-27}	1.8×10^{-26}	6.9×10^{-27}	1.3×10^{-26}	8.7×10^{29}	1.1×10^{-8}	8.3	-4.2	-2.4
J2007+2722[γ]	40.8	9.6×10^{-19}	7.10 (b)	7.1×10^{-28}	1.8×10^{-26}	7.9×10^{-27}	1.6×10^{-26}	1.2×10^{33}	1.6×10^{-5}	23	-4.1	-1.8
J2010−1323[aε]	191.5	3.0×10^{-21}	1.16 (b)	5.3×10^{-28}	1.1×10^{-26}	7.3×10^{-27}	1.4×10^{-26}	8.3×10^{30}	1.1×10^{-7}	27	-2.6	-0.8
J2017+0603[aε]	345.3	8.0×10^{-21}	1.40 (b)	9.6×10^{-28}	1.1×10^{-26}	3.5×10^{-27}	7.7×10^{-27}	1.7×10^{30}	2.1×10^{-8}	8	-5.2	-2.6
J2019+2425[aε]	254.2	1.6×10^{-21}	1.16 (b)	4.4×10^{-28}	7.5×10^{-27}	5.1×10^{-27}	1.1×10^{-26}	3.5×10^{30}	4.5×10^{-8}	24	-4.4	-2.1
J2022+2534[ε]	377.9	6.2×10^{-21}	...	...	9.2×10^{-27}	5.2×10^{-27}	1.5×10^{-26}	...	...	...	-4.6	-1.9
J2033+1734[aε]	168.1	8.4×10^{-21}	1.74 (b)	5.5×10^{-28}	1.0×10^{-26}	3.6×10^{-27}	6.7×10^{-27}	7.6×10^{30}	9.8×10^{-8}	12	-4.4	-2.4
J2039−3616[ε]	305.3	8.4×10^{-21}	1.70 (b)	7.6×10^{-28}	7.5×10^{-27}	4.9×10^{-27}	1.0×10^{-26}	3.4×10^{30}	4.3×10^{-8}	13	-4.3	-2.0
J2043+1711[aε]	420.2	4.1×10^{-21}	1.60 (a)	6.6×10^{-28}	1.6×10^{-26}	5.0×10^{-27}	1.1×10^{-26}	1.8×10^{30}	2.3×10^{-8}	16	-4.4	-2.4
J2043+2740[α]	10.4	1.3×10^{-15}	1.48 (b)	6.3×10^{-26}	1.7×10^{-23}	7.9×10^{-26}	1.6×10^{-25}	4.1×10^{34}	5.3×10^{-4}	2.6	-7.9	-2.4
J2045+3633[aε]	31.6	5.9×10^{-19}	5.63 (b)	6.2×10^{-28}	5.2×10^{-26}	2.9×10^{-27}	6.5×10^{-27}	6.8×10^{32}	8.7×10^{-6}	11	-5.3	-2.8
J2047+1053[γ]	233.3	2.1×10^{-20}	2.79 (b)	6.4×10^{-28}	1.0×10^{-26}	3.5×10^{-27}	7.1×10^{-27}	6.6×10^{30}	8.6×10^{-8}	11	-4.2	-2.3
J2051−0827[aε]	221.8	1.2×10^{-20}	1.47 (b)	9.0×10^{-28}	1.6×10^{-26}	2.5×10^{-27}	5.7×10^{-27}	3.1×10^{30}	4.0×10^{-8}	6.3	-3.9	-2.5
J2053+4650[aε]	79.5	1.7×10^{-19}	3.81 (b)	7.8×10^{-28}	1.4×10^{-26}	2.4×10^{-27}	5.3×10^{-27}	5.8×10^{31}	7.5×10^{-7}	6.8	-4.3	-2.2
J2055+3829[aε]	478.6	8.5×10^{-22}	4.59 (b)	1.1×10^{-28}	8.5×10^{-27}	5.6×10^{-27}	1.2×10^{-26}	4.4×10^{30}	5.6×10^{-8}	110	-4.7	-2.3
J2124−3358[aε]	202.8	8.0×10^{-21}	0.44 (f)	2.3×10^{-27}	1.1×10^{-26}	3.3×10^{-27}	7.1×10^{-27}	1.4×10^{30}	1.8×10^{-8}	3	-4.1	-2.3
J2129−5721[aδ]	268.4	1.9×10^{-20}	7.00 (f)	2.6×10^{-28}	1.0×10^{-26}	3.9×10^{-27}	7.3×10^{-27}	1.3×10^{31}	1.7×10^{-7}	28	-4.3	-2.3
J2144−5237[δ]	198.4	8.9×10^{-21}	1.66 (b)	6.5×10^{-28}	7.8×10^{-27}	3.6×10^{-27}	6.9×10^{-27}	5.3×10^{30}	6.9×10^{-8}	11	-4.5	-2.4

Table 3 *continued*

Table 3 *(continued)*

Pulsar Name (J2000)	$f_{\rm rot}$ (Hz)	$\dot{P}_{\rm rot}$ ($\rm s\,s^{-1}$)	Distance (kpc)	$h_0^{\rm sd}$	$C_{21}^{95\%}$	$C_{22}^{95\%}$	$h_0^{95\%}$	$Q_{22}^{95\%}$ ($\rm kg\,m^2$)	$\varepsilon^{95\%}$	$h_0^{95\%}/h_0^{\rm sd}$	$\mathcal{O}_{m=1,2}^{l=2}$	$\mathcal{O}_{m=2}^{l=2}$
J2145−0750[aϵ]	62.3	2.7×10^{-20}	0.83 (f)	1.3×10^{-27}	1.9×10^{-26}	4.5×10^{-27}	8.9×10^{-27}	3.5×10^{31}	4.5×10^{-7}	7.1	-4.0	-1.9
J2150−0326[ϵ]	284.8	8.2×10^{-21}	...	...	9.6×10^{-27}	3.1×10^{-27}	6.6×10^{-27}	...	...	...	-4.5	-2.4
J2205+6012[ϵ]	414.0	2.0×10^{-20}	3.53 (b)	6.5×10^{-28}	7.9×10^{-27}	6.1×10^{-27}	1.3×10^{-26}	4.8×10^{30}	6.2×10^{-8}	20	-4.2	-1.9
J2214+3000[aϵ]	320.6	1.3×10^{-20}	0.60 (dd)	2.7×10^{-27}	8.0×10^{-27}	3.9×10^{-27}	8.3×10^{-27}	8.9×10^{29}	1.1×10^{-8}	3	-4.6	-2.3
J2222−0137[aϵ]	30.5	1.5×10^{-20}	0.27 (ee)	2.0×10^{-27}	5.1×10^{-26}	7.1×10^{-27}	1.4×10^{-26}	7.3×10^{31}	9.4×10^{-7}	6.8	-5.0	-2.5
J2229+2643[aϵ]	335.8	1.4×10^{-21}	1.80 (b)	3.1×10^{-28}	2.0×10^{-26}	3.2×10^{-27}	6.7×10^{-27}	1.9×10^{30}	2.5×10^{-8}	21	-3.5	-2.5
J2234+0611[aϵ]	279.6	8.4×10^{-21}	1.50 (a)	8.2×10^{-28}	9.1×10^{-27}	3.6×10^{-27}	7.6×10^{-27}	2.7×10^{30}	3.5×10^{-8}	9.2	-4.5	-2.4
J2234+0944[aϵ]	275.7	1.3×10^{-20}	0.80 (a)	1.9×10^{-27}	1.3×10^{-26}	4.2×10^{-27}	8.6×10^{-27}	1.6×10^{30}	2.1×10^{-8}	4.4	-4.1	-2.2
J2235+1506[aα]	16.7	9.2×10^{-20}	1.54 (b)	6.5×10^{-28}	1.0×10^{-24}	8.8×10^{-27}	1.9×10^{-26}	1.9×10^{33}	2.5×10^{-5}	29	-9.5	-2.8
J2236−5527[δ]	144.8	9.6×10^{-21}	2.05 (b)	4.6×10^{-28}	9.2×10^{-27}	3.1×10^{-27}	5.4×10^{-27}	9.6×10^{30}	1.2×10^{-7}	12	-4.2	-2.3
J2241−5236[aδ]	457.3	5.1×10^{-21}	1.05 (f)	1.2×10^{-27}	1.3×10^{-26}	4.0×10^{-27}	8.8×10^{-27}	8.1×10^{29}	1.0×10^{-8}	7.5	-4.6	-2.5
J2256−1024[aϵ]	435.8	1.0×10^{-20}	1.33 (b)	1.3×10^{-27}	1.5×10^{-26}	4.9×10^{-27}	1.0×10^{-26}	1.3×10^{30}	1.7×10^{-8}	8.3	-4.2	-2.4
J2302+4442[aϵ]	192.6	1.4×10^{-20}	0.86 (b)	1.5×10^{-27}	7.0×10^{-27}	3.7×10^{-27}	7.8×10^{-27}	3.3×10^{30}	4.3×10^{-8}	5.1	-4.2	-2.1
J2317+1439[aϵ]	290.3	2.7×10^{-21}	2.16 (b)	3.3×10^{-28}	8.7×10^{-27}	5.4×10^{-27}	1.1×10^{-26}	5.1×10^{30}	6.6×10^{-8}	33	-4.2	-2.0
J2322+2057[aϵ]	208.0	3.2×10^{-21}	1.01 (b)	6.5×10^{-28}	8.3×10^{-27}	2.9×10^{-27}	6.2×10^{-27}	2.7×10^{30}	3.4×10^{-8}	9.6	-4.4	-2.3
J2322−2650[aδ]	288.8	4.1×10^{-22}	0.23 (gg)	1.2×10^{-27}	9.5×10^{-27}	4.8×10^{-27}	1.1×10^{-26}	5.7×10^{29}	7.3×10^{-9}	9.3	-4.2	-2.0

References—The following is a list of references for pulsar distances and intrinsic period derivatives, and they should be consulted for information on the associated uncertainties on these quantities: (a) Arzoumanian et al. (2018), (b) Yao et al. (2017), (c) Verbiest & Lorimer (2014), (d) Antoniadis et al. (2013), (e) Reardon et al. (2016), (f) Reardon et al. (2021), (g) Bassa et al. (2016), (h) Fonseca et al. (2021), (i) Desvignes et al. (2016), (j) Verbiest et al. (2012), (k) Lorimer et al. (2021), (l) Reynoso et al. (2006), (m) Negueruela et al. (2011), (n) Swiggum et al. (2017), (o) Halpern et al. (2013), (p) Bates et al. (2015), (q) Matthews et al. (2016), (r) Harris (2010), (s) Fonseca et al. (2014), (t) Braga et al. (2015), (u) Vigeland et al. (2018), (v) Freire et al. (2012), (w) Espinoza et al. (2013), (x) Ferdman et al. (2014), (y) Camilo et al. (2021), (z) Testa et al. (2001), (aa) Lin et al. (2009), (bb) Gotthelf et al. (2011), (cc) Brownsberger & Romani (2014), (dd) Guillemot et al. (2016), (ee) Deller et al. (2013), (ff) Halpern et al. (2001), (gg) Spiewak et al. (2018).

References—The following is a list of references for pulsar ephemeris data used in this analysis: CHIME: α, Hobart: β, Jodrell Bank: γ, MeerKAT: δ, Nancay: ϵ, NICER: ζ, UTMOST: η, .

[a] The observed $\dot{P}$ has been corrected to account for the relative motion between the pulsar and observer.

[b] The corrected pulsar $\dot{P}$ value is negative, so no value is given and no spin-down limit has been calculated.

[c] This is a globular cluster pulsar for which a proxy period derivative has been derived assuming a characteristic age of 10^9 years and a braking index of $n = 5$.

Table 4. Limits on Gravitational-wave Amplitude, and Other Derived Quantities, for 23 High-value Pulsars from the Three Analysis Methods.

Pulsar Name	$f_{\rm rot}$	$\dot{P}_{\rm rot}$	Distance	$h_0^{\rm sd}$	Analysis	$C_{21}^{95\%}$	$C_{22}^{95\%}$	$h_0^{95\%}$	$Q_{22}^{95\%}$	$\varepsilon^{95\%}$	$h_0^{95\%}/h_0^{\rm sd}$	Statistic[a]	Statistic[b]
(J2000)	(Hz)	($\rm s\,s^{-1}$)	(kpc)		Method				(kg m^2)			l=2,m=1,2	l=2,m=2
J0437−4715[cδ]	173.7	1.4×10^{-20}	0.16 (e)	8.0×10^{-27}	Bayesian	1.3×10^{-26}	3.8×10^{-27}	6.9×10^{-27}	6.6×10^{29}	8.5×10^{-9}	0.87	-4.4	-2.8
					$\mathcal{F}$-statistic	2.3×10^{-26}	3.5×10^{-27}	8.9×10^{-27}	8.7×10^{29}	1.1×10^{-8}	1.12	0.08	0.29
					5n-vector	...	...	...	...	...	...	...	...
J0534+2200[cγ]	29.6	4.2×10^{-13}	2.00	1.4×10^{-24}	Bayesian	$7.9(6.2)\times10^{-26}$	$6.5(6.1)\times10^{-27}$	$1.3(1.2)\times10^{-26}$	$5.6(5.0)\times10^{32}$	$7.2(6.5)\times10^{-6}$	0.0094(0.0085)	-4.8(-4.9)	-2.6(-2.7)
					$\mathcal{F}$-statistic	$7.0(3.1)\times10^{-26}$	$8.8(5.5)\times10^{-27}$	$1.7(1.0)\times10^{-26}$	$6.9(4.4)\times10^{32}$	$8.9(5.7)\times10^{-6}$	0.01(0.01)	0.65(0.52)	0.56(0.24)
					5n-vector	$1.4(1.3)\times10^{-25}$	...	$9.0(8.7)\times10^{-27}$	$3.7(3.6)\times10^{32}$	$4.9(4.7)\times10^{-6}$	0.0064(0.0062)	0.02(0.02)	0.73(0.73)
J0537−6910[*]	61.9	5.2×10^{-14}	49.6	3.0×10^{-26}	Bayesian	$2.2(1.8)\times10^{-26}$	$5.6(5.0)\times10^{-27}$	$1.1(1.0)\times10^{-26}$	...	$3.4(3.1)\times10^{-5}$	0.37(0.33)	-8.3(-8.3)	-4.3(-4.5)
					$\mathcal{F}$-statistic	...	...	...	...	...	...	...	...
					5n-vector	...	...	...	...	...	...	...	...
J0711−6830[cδ]	182.1	1.4×10^{-20}	0.11 (b)	1.2×10^{-26}	Bayesian	1.6×10^{-26}	2.4×10^{-27}	7.0×10^{-27}	4.1×10^{29}	5.3×10^{-9}	0.57	-3.9	-2.3
					$\mathcal{F}$-statistic	1.9×10^{-26}	5.2×10^{-27}	9.9×10^{-27}	6.0×10^{29}	7.8×10^{-9}	0.83	0.17	0.34
					5n-vector	9.8×10^{-27}	...	5.0×10^{-27}	3.1×10^{29}	4.0×10^{-9}	0.42	0.90	0.96
J0835−4510[cβ]	11.2	1.2×10^{-13}	0.28 (i)	3.4×10^{-24}	Bayesian	$1.6(0.8)\times10^{-23}$	$8.8(8.6)\times10^{-26}$	$1.8(1.7)\times10^{-25}$	$7.2(7.0)\times10^{33}$	$9.3(9.1)\times10^{-5}$	0.052(0.051)	-6.2(-2.7)	-1.1(-1.0)
					$\mathcal{F}$-statistic	$1.7(1.3)\times10^{-23}$	$1.0(0.16)\times10^{-25}$	$2.0(0.67)\times10^{-25}$	$8.2(2.7)\times10^{33}$	$1.1(0.36)\times10^{-4}$	0.06(0.02)	0.24(0.17)	0.09(0.02)
					5n-vector	$1.1(1.4)\times10^{-23}$	...	$1.8(1.1)\times10^{-25}$	$7.3(4.5)\times10^{33}$	$9.5(5.8)\times10^{-5}$	0.05(0.03)	0.83(0.83)	0.20(0.20)
J0908−4913[η]	9.4	1.5×10^{-14}	1.00 (i)	3.0×10^{-25}	Bayesian	...	...	2.7×10^{-25}	5.6×10^{34}	7.2×10^{-4}	0.89	...	-2.7
					$\mathcal{F}$-statistic	1.1×10^{-22}	2.2×10^{-25}	4.8×10^{-25}	1.0×10^{35}	1.3×10^{-3}	1.6	0.31	0.16
					5n-vector	...	...	5.9×10^{-25}	1.2×10^{35}	1.6×10^{-3}	1.97	...	0.69
J1101−6101[ζ]	15.9	8.6×10^{-15}	7.00 (m)	4.3×10^{-26}	Bayesian	6.8×10^{-25}	1.2×10^{-26}	2.6×10^{-26}	1.3×10^{34}	1.7×10^{-4}	0.61	-9.8	-2.9
					$\mathcal{F}$-statistic	8.9×10^{-25}	6.5×10^{-27}	1.3×10^{-26}	6.6×10^{33}	8.5×10^{-5}	0.3	0.68	0.88
					5n-vector	9.5×10^{-25}	...	2.1×10^{-26}	1.1×10^{34}	1.4×10^{-4}	0.50	0.77	0.84
J1105−6107[η]	15.8	1.6×10^{-14}	2.36 (b)	1.7×10^{-25}	Bayesian	1.1×10^{-24}	2.9×10^{-26}	5.8×10^{-26}	1.0×10^{34}	1.3×10^{-4}	0.34	-3.5	-1.3
					$\mathcal{F}$-statistic	1.2×10^{-24}	2.9×10^{-26}	5.8×10^{-26}	1.0×10^{34}	1.3×10^{-4}	0.34	0.48	0.11
					5n-vector	...	...	...	...	...	...	...	...
J1302−6350[cη]	20.9	2.3×10^{-15}	2.30 (n)	7.7×10^{-26}	Bayesian	2.5×10^{-25}	1.2×10^{-26}	2.4×10^{-26}	2.3×10^{33}	3.0×10^{-5}	0.32	-4.7	-2.3
					$\mathcal{F}$-statistic	4.2×10^{-25}	1.6×10^{-26}	3.2×10^{-26}	3.1×10^{33}	4.0×10^{-5}	0.41	0.18	0.03
					5n-vector	...	...	...	...	...	...	...	...
J1412+7922[ζ]	16.9	3.3×10^{-15}	2.00 (o)	9.5×10^{-26}	Bayesian	1.2×10^{-24}	1.2×10^{-26}	2.5×10^{-26}	3.2×10^{33}	4.1×10^{-5}	0.26	-8.7	-2.7
					$\mathcal{F}$-statistic	1.4×10^{-24}	1.2×10^{-26}	2.4×10^{-26}	3.0×10^{33}	3.9×10^{-5}	0.25	0.32	0.66
					5n-vector	1.5×10^{-24}	...	2.2×10^{-26}	2.9×10^{33}	3.7×10^{-5}	0.24	0.07	0.66

Table 4 *continued*

Table 4 *(continued)*

Pulsar Name (J2000)	$f_{\rm rot}$ (Hz)	$\dot{P}_{\rm rot}$ ($\rm s\,s^{-1}$)	Distance (kpc)	$h_0^{\rm sd}$	Analysis Method	$C_{21}^{95\%}$	$C_{22}^{95\%}$	$h_0^{95\%}$	$Q_{22}^{95\%}$ ($\rm kg\,m^2$)	$\varepsilon^{95\%}$	$h_0^{95\%}/h_0^{\rm sd}$	Statistic[a] l=2,m=1,2	Statistic[b] l=2,m=2
J1745−0952[cϵ]	51.6	8.6×10^{-20}	0.23 (b)	7.5×10^{-27}	Bayesian	1.5×10^{-26}	2.2×10^{-27}	4.7×10^{-27}	7.3×10^{30}	9.5×10^{-8}	0.63	-5.1	-2.5
					$\mathcal{F}$-statistic	2.1×10^{-26}	1.0×10^{-27}	3.7×10^{-27}	5.8×10^{30}	7.5×10^{-8}	0.49	0.60	0.90
					5n-vector	...	...	...	...	...	...	...	...
J1756−2251[cϵ]	35.1	1.0×10^{-18}	0.73 (y)	6.6×10^{-27}	Bayesian	3.9×10^{-26}	2.8×10^{-27}	6.1×10^{-27}	6.6×10^{31}	8.6×10^{-7}	0.93	-5.3	-2.7
					$\mathcal{F}$-statistic	4.4×10^{-26}	1.1×10^{-27}	3.7×10^{-27}	4.0×10^{31}	5.2×10^{-7}	0.56	0.34	0.92
					5n-vector	...	...	...	...	...	...	...	...
J1809−1917[cγ]	12.1	2.6×10^{-14}	3.27 (b)	1.4×10^{-25}	Bayesian	7.5×10^{-24}	4.6×10^{-26}	9.0×10^{-26}	3.7×10^{34}	4.8×10^{-4}	0.66	-8.2	-2.1
					$\mathcal{F}$-statistic	7.0×10^{-24}	6.3×10^{-26}	1.3×10^{-25}	5.2×10^{34}	6.8×10^{-4}	0.91	0.37	0.11
					5n-vector	7.5×10^{-24}	...	9.8×10^{-26}	4.0×10^{34}	5.2×10^{-4}	0.70	0.40	0.52
J1813−1749[cζ]	22.4	1.3×10^{-13}	6.20 (z)	2.2×10^{-25}	Bayesian	1.9×10^{-25}	7.7×10^{-27}	1.5×10^{-26}	3.5×10^{33}	4.5×10^{-5}	0.07	-4.7	-2.5
					$\mathcal{F}$-statistic	1.9×10^{-25}	3.6×10^{-27}	7.2×10^{-27}	1.6×10^{33}	2.1×10^{-5}	0.03	0.42	0.87
					5n-vector	2.2×10^{-25}	...	9.9×10^{-27}	2.2×10^{33}	2.9×10^{-5}	0.05	0.79	0.94
J1828−1101[γ]	13.9	1.5×10^{-14}	4.77 (b)	7.7×10^{-26}	Bayesian	3.3×10^{-24}	1.9×10^{-26}	4.2×10^{-26}	1.9×10^{34}	2.5×10^{-4}	0.55	-8.9	-2.6
					$\mathcal{F}$-statistic	4.1×10^{-24}	1.4×10^{-26}	2.3×10^{-26}	1.0×10^{34}	1.3×10^{-4}	0.30	0.76	0.89
					5n-vector	8.7×10^{-24}	...	4.3×10^{-26}	1.9×10^{34}	2.5×10^{-4}	0.55	0.29	0.71
J1838−0655[ζ]	14.2	4.9×10^{-14}	6.60 (cc)	1.0×10^{-25}	Bayesian	3.4×10^{-24}	1.6×10^{-26}	3.7×10^{-26}	2.2×10^{34}	2.9×10^{-4}	0.36	-8.7	-2.7
					$\mathcal{F}$-statistic	2.1×10^{-24}	6.3×10^{-26}	1.0×10^{-25}	6.0×10^{34}	7.8×10^{-4}	1.00	0.67	0.96
					5n-vector	3.1×10^{-24}	...	4.1×10^{-26}	2.5×10^{34}	3.2×10^{-4}	0.41	0.26	0.68
J1849−0001[ζ]	26.0	1.4×10^{-14}	7.00 (bb)	7.0×10^{-26}	Bayesian	7.3×10^{-26}	5.0×10^{-27}	1.0×10^{-26}	1.9×10^{33}	2.5×10^{-5}	0.15	-5.3	-2.7
					$\mathcal{F}$-statistic	3.4×10^{-26}	9.3×10^{-27}	1.9×10^{-26}	3.5×10^{33}	4.6×10^{-5}	0.27	0.92	0.13
					5n-vector	1.5×10^{-25}	...	1.6×10^{-26}	3.0×10^{33}	3.8×10^{-5}	0.22	0.37	0.42
J1856+0245[γ]	12.4	6.2×10^{-14}	6.32 (b)	1.1×10^{-25}	Bayesian	6.2×10^{-24}	2.2×10^{-26}	5.2×10^{-26}	3.9×10^{34}	5.0×10^{-4}	0.46	-8.6	-2.7
					$\mathcal{F}$-statistic	1.2×10^{-23}	1.9×10^{-26}	4.6×10^{-26}	3.5×10^{34}	4.5×10^{-4}	0.42	0.07	0.82
					5n-vector	7.9×10^{-24}	...	1.0×10^{-25}	7.6×10^{34}	9.8×10^{-4}	0.91	0.09	0.27
J1913+1011[γ]	27.8	3.4×10^{-15}	4.61 (b)	5.4×10^{-26}	Bayesian	8.3×10^{-26}	1.0×10^{-26}	2.4×10^{-26}	2.6×10^{33}	3.4×10^{-5}	0.45	-4.0	-1.5
					$\mathcal{F}$-statistic	8.7×10^{-26}	1.0×10^{-26}	2.2×10^{-26}	2.4×10^{33}	3.1×10^{-5}	0.40	0.53	0.08
					5n-vector	1.1×10^{-25}	...	1.3×10^{-26}	1.4×10^{33}	1.8×10^{-5}	0.23	0.50	0.44
J1925+1720[γ]	13.2	1.0×10^{-14}	5.06 (b)	5.9×10^{-26}	Bayesian	4.0×10^{-24}	1.6×10^{-26}	3.7×10^{-26}	2.0×10^{34}	2.5×10^{-4}	0.63	-8.9	-2.9
					$\mathcal{F}$-statistic	6.0×10^{-24}	2.2×10^{-26}	4.3×10^{-26}	2.3×10^{34}	2.9×10^{-4}	0.72	0.10	0.73
					5n-vector	3.7×10^{-24}	...	3.7×10^{-26}	1.9×10^{34}	2.5×10^{-4}	0.62	0.72	0.93
J1928+1746[γ]	14.5	1.3×10^{-14}	4.34 (b)	8.1×10^{-26}	Bayesian	1.1×10^{-24}	1.6×10^{-26}	3.4×10^{-26}	1.3×10^{34}	1.7×10^{-4}	0.42	-9.3	-3.1
					$\mathcal{F}$-statistic	7.8×10^{-25}	2.1×10^{-26}	4.3×10^{-26}	1.6×10^{34}	2.1×10^{-4}	0.53	0.90	0.55
					5n-vector	3.5×10^{-24}	...	3.3×10^{-26}	1.2×10^{34}	1.6×10^{-4}	0.40	0.02	0.86

Table 4 *continued*

Table 4 *(continued)*

Pulsar Name (J2000)	$f_{\rm rot}$ (Hz)	$\dot{P}_{\rm rot}$ ($\rm s\,s^{-1}$)	Distance (kpc)	$h_0^{\rm sd}$	Analysis Method	$C_{21}^{95\%}$	$C_{22}^{95\%}$	$h_0^{95\%}$	$Q_{22}^{95\%}$ ($\rm kg\,m^2$)	$\varepsilon^{95\%}$	$h_0^{95\%}/h_0^{\rm sd}$	Statistic[a] l=2,m=1,2	Statistic[b] l=2,m=2
J1935+2025[γ]	12.5	6.1×10^{-14}	4.60 (b)	1.5×10^{-25}	Bayesian	3.4×10^{-24}	2.5×10^{-26}	5.3×10^{-26}	2.9×10^{34}	3.7×10^{-4}	0.35	-9.1	-2.6
					$\mathcal{F}$-statistic	1.2×10^{-23}	4.2×10^{-26}	8.5×10^{-26}	4.6×10^{34}	5.9×10^{-4}	0.56	1.00	0.43
					5n-vector	3.9×10^{-24}	...	6.4×10^{-26}	3.5×10^{34}	4.5×10^{-4}	0.43	0.90	0.68
J1952+3252[cα]	25.3	5.8×10^{-15}	3.00 (i)	1.0×10^{-25}	Bayesian	$1.0(1.0)\times10^{-25}$	$8.1(8.1)\times10^{-27}$	$1.8(1.6)\times10^{-26}$	$1.5(1.4)\times10^{33}$	$2.0(1.8)\times10^{-5}$	0.17(0.16)	-4.7(-4.6)	-2.1(-2.2)
					$\mathcal{F}$-statistic	1.0×10^{-25}	1.6×10^{-26}	3.0×10^{-26}	2.6×10^{33}	3.4×10^{-5}	0.30	0.54	0.16
					5n-vector	$1.1(1.1)\times10^{-25}$	...	$2.2(2.1)\times10^{-26}$	$1.9(1.8)\times10^{33}$	$2.4(2.3)\times10^{-5}$	0.21(0.21)	0.79(0.79)	0.30(0.30)
J2229+6114[α]	19.4	7.8×10^{-14}	3.00 (hh)	3.3×10^{-25}	Bayesian	$4.1(4.0)\times10^{-25}$	$8.1(5.5)\times10^{-27}$	$1.7(1.1)\times10^{-26}$	$2.5(1.6)\times10^{33}$	$3.2(2.1)\times10^{-5}$	0.052(0.033)	-8.2(-5.2)	-2.9(-3.0)
					$\mathcal{F}$-statistic	$3.2(4.0)\times10^{-25}$	$8.0(6.4)\times10^{-27}$	$1.6(1.2)\times10^{-26}$	$2.3(1.8)\times10^{33}$	$3.0(2.3)\times10^{-5}$	0.05(0.04)	0.78(0.52)	0.74(0.52)
					5n-vector	$4.3(3.4)\times10^{-25}$	...	$1.3(1.4)\times10^{-26}$	$1.9(2.0)\times10^{33}$	$2.5(2.6)\times10^{-5}$	0.04(0.04)	0.72(0.72)	0.85(0.85)

NOTE—For references and other notes see Table 3. Values in parentheses are those produced using the restricted orientation priors described in Section 2.1.2

[a] For the *Bayesian* method this column shows the base-10 logarithm of the Bayesian odds, $\mathcal{O}$, comparing a coherent signal model at both the $l = 2$, $m = 1, 2$ modes to incoherent signal models. For the *$\mathcal{F}$-/$\mathcal{G}$-statistic* method this column shows the false-alarm probability for a signal just at the $l = 2$, $m = 1$ mode, assuming that the $2\mathcal{F}$ value has a χ^2 distribution with 4 degrees-of-freedom and the $2\mathcal{G}$ value has a χ^2 distribution with 2 degrees of freedom. For the *5n-vector* method this column shows the p-value for a search for a signal at just the $l = 2$, $m = 1$ mode, where the null hypothesis being tested is that the data are consistent with pure Gaussian noise.

[b] This is the same as in footnote [a], but for all the methods the assumed signal model is from the $l = m = 2$ mode.

[c] The observed $\dot{P}$ has been corrected to account for the relative motion between the pulsar and observer.

* The pulsar J0537−6910 was not analysed in this study but is included for completion. The values listed here are taken from Abbott et al. (2021c).

Table 5. Limits on Gravitational-wave Amplitude from dipole radiation in Brans-Dicke theory for 23 Pulsars using the $\mathcal{D}$-statistic.

Pulsar Name (J2000)	$f_{\rm rot}$ (Hz)	$\dot{P}_{\rm rot}$ ($\rm s\,s^{-1}$)	Distance (kpc)	$h_{0d}^{95\%}$	FAP
J0437−4715[a]	173.7	1.4×10^{-20}	0.16 (e)	9.7×10^{-27}	0.92
J0534+2200[a]	29.6	4.2×10^{-13}	2.00	$9.5(7.0)\times10^{-26}$	0.95(0.31)
J0711−6830[a]	182.1	1.4×10^{-20}	0.11 (b)	1.9×10^{-26}	0.96
J0835−4510[a]	11.2	1.2×10^{-13}	0.28 (i)	$1.1(0.74)\times10^{-23}$	0.89(0.39)
J0908−4913	9.4	1.5×10^{-14}	1.00 (i)	1.4×10^{-22}	0.89
J1101−6101	15.9	8.6×10^{-15}	7.00 (m)	4.7×10^{-25}	0.99
J1105−6107	15.8	1.6×10^{-14}	2.36 (b)	2.0×10^{-25}	0.99
J1302−6350[a]	20.9	2.3×10^{-15}	2.30 (n)	2.3×10^{-25}	0.93
J1412+7922	16.9	3.3×10^{-15}	2.00 (o)	9.6×10^{-25}	0.54
J1745−0952[a]	51.6	8.6×10^{-20}	0.23 (b)	2.0×10^{-26}	0.97
J1756−2251[a]	35.1	1.0×10^{-18}	0.73 (y)	1.7×10^{-25}	0.99
J1809−1917[a]	12.1	2.6×10^{-14}	3.27 (b)	2.7×10^{-23}	0.97
J1813−1749[a]	22.4	1.3×10^{-13}	6.20 (z)	2.1×10^{-25}	0.95
J1828−1101	13.9	1.5×10^{-14}	4.77 (b)	6.6×10^{-24}	0.96
J1838−0655	14.2	4.9×10^{-14}	6.60 (cc)	4.7×10^{-24}	0.52
J1849−0001	26.0	1.4×10^{-14}	7.00 (bb)	1.7×10^{-26}	0.99
J1856+0245	12.4	6.2×10^{-14}	6.32 (b)	1.1×10^{-23}	0.71
J1913+1011	27.8	3.4×10^{-15}	4.61 (b)	7.5×10^{-26}	0.98
J1925+1720	13.2	1.0×10^{-14}	5.06 (b)	5.7×10^{-24}	0.84
J1928+1746	14.5	1.3×10^{-14}	4.34 (b)	2.6×10^{-24}	0.72
J1935+2025	12.5	6.1×10^{-14}	4.60 (b)	4.2×10^{-24}	0.99
J1952+3252[a]	25.3	5.8×10^{-15}	3.00 (i)	8.1×10^{-26}	0.99
J2229+6114	19.4	7.8×10^{-14}	3.00 (hh)	$5.3(5.8)\times10^{-26}$	0.99(0.95)

NOTE—For references and other notes see Table 3. Values in parentheses are those produced using the restricted orientation priors described in Section 2.1.2. The last column shows the false-alarm probability (FAP) for a signal, assuming that the $2\mathcal{D}$ value has a χ^2 distribution with 2 degrees-of-freedom.

All Authors and Affiliations

R. Abbott,[1] H. Abe,[2] F. Acernese,[3,4] K. Ackley,[5] N. Adhikari,[6] R. X. Adhikari,[1] V. K. Adkins,[7] V. B. Adya,[8] C. Affeldt,[9,10] D. Agarwal,[11] M. Agathos,[12,13] K. Agatsuma,[14] N. Aggarwal,[15] O. D. Aguiar,[16] L. Aiello,[17] A. Ain,[18] P. Ajith,[19] T. Akutsu,[20,21] S. Albanesi,[22,23] R. A. Alfaidi,[24] A. Allocca,[25,4] P. A. Altin,[8] A. Amato,[26] C. Anand,[5] S. Anand,[1] A. Ananyeva,[1] S. B. Anderson,[1] W. G. Anderson,[6] M. Ando,[27,28] T. Andrade,[29] N. Andres,[30] M. Andrés-Carcasona,[31] T. Andrić,[32] S. V. Angelova,[33] S. Ansoldi,[34,35] J. M. Antelis,[36] S. Antier,[37,38] T. Apostolatos,[39] E. Z. Appavuravther,[40,41] S. Appert,[1] S. K. Apple,[42] K. Arai,[1] A. Araya,[43] M. C. Araya,[1] J. S. Areeda,[44] M. Arène,[45] N. Aritomi,[20] N. Arnaud,[46,47] M. Arogeti,[48] S. M. Aronson,[7] K. G. Arun,[49] H. Asada,[50] Y. Asali,[51] G. Ashton,[52] Y. Aso,[53,54] M. Assiduo,[55,56] S. Assis de Souza Melo,[47] S. M. Aston,[57] P. Astone,[58] F. Aubin,[56] K. AultONeal,[36] C. Austin,[7] S. Babak,[45] F. Badaracco,[59] M. K. M. Bader,[60] C. Badger,[61] S. Bae,[62] Y. Bae,[63] A. M. Baer,[64] S. Bagnasco,[23] Y. Bai,[1] M. Bailes,[65] J. Baird,[45] R. Bajpai,[66] T. Baka,[67] M. Ball,[68] G. Ballardin,[47] S. W. Ballmer,[69] A. Balsamo,[64] G. Baltus,[70] S. Banagiri,[15] B. Banerjee,[32] D. Bankar,[11] J. C. Barayoga,[1] C. Barbieri,[71,72,73] B. C. Barish,[1] D. Barker,[74] P. Barneo,[29] F. Barone,[75,4] B. Barr,[24] L. Barsotti,[76] M. Barsuglia,[45] D. Barta,[77] J. Bartlett,[74] M. A. Barton,[24] I. Bartos,[78] S. Basak,[19] R. Bassiri,[79] A. Basti,[80,18] M. Bawaj,[40,81] J. C. Bayley,[24] M. Bazzan,[82,83] B. R. Becher,[84] B. Bécsy,[85] V. M. Bedakihale,[86] F. Beirnaert,[87] M. Bejger,[88] I. Belahcene,[46] V. Benedetto,[89] D. Beniwal,[90] M. G. Benjamin,[91] T. F. Bennett,[92] J. D. Bentley,[14] M. BenYaala,[33] S. Bera,[11] M. Berbel,[93] F. Bergamin,[9,10] B. K. Berger,[79] S. Bernuzzi,[13] D. Bersanetti,[94] A. Bertolini,[60] J. Betzwieser,[57] D. Beveridge,[95] R. Bhandare,[96] A. V. Bhandari,[11] U. Bhardwaj,[38,60] R. Bhatt,[1] D. Bhattacharjee,[97] S. Bhaumik,[78] A. Bianchi,[60,98] I. A. Bilenko,[99] G. Billingsley,[1] S. Bini,[100,101] R. Birney,[102] O. Birnholtz,[103] S. Biscans,[1,76] M. Bischi,[55,56] S. Biscoveanu,[76] A. Bisht,[9,10] B. Biswas,[11] M. Bitossi,[47,18] M.-A. Bizouard,[37] J. K. Blackburn,[1] C. D. Blair,[95] D. G. Blair,[95] R. M. Blair,[74] F. Bobba,[104,105] N. Bode,[9,10] M. Boër,[37] G. Bogaert,[37] M. Boldrini,[106,58] G. N. Bolingbroke,[90] L. D. Bonavena,[82] F. Bondu,[107] E. Bonilla,[79] R. Bonnand,[30] P. Booker,[9,10] B. A. Boom,[60] R. Bork,[1] V. Boschi,[18] N. Bose,[108] S. Bose,[11] V. Bossilkov,[95] V. Boudart,[70] Y. Bouffanais,[82,83] A. Bozzi,[47] C. Bradaschia,[18] P. R. Brady,[6] A. Bramley,[57] A. Branch,[57] M. Branchesi,[32,109] J. E. Brau,[68] M. Breschi,[13] T. Briant,[110] J. H. Briggs,[24] A. Brillet,[37] M. Brinkmann,[9,10] P. Brockill,[6] A. F. Brooks,[1] J. Brooks,[47] D. D. Brown,[90] S. Brunett,[1] G. Bruno,[59] R. Bruntz,[64] J. Bryant,[14] F. Bucci,[56] T. Bulik,[111] H. J. Bulten,[60] A. Buonanno,[112,113] K. Burtnyk,[74] R. Buscicchio,[14] D. Buskulic,[30] C. Buy,[114] R. L. Byer,[79] G. S. Cabourn Davies,[52] G. Cabras,[34,35] R. Cabrita,[59] L. Cadonati,[48] M. Caesar,[115] G. Cagnoli,[26] C. Cahillane,[74] J. Calderón Bustillo,[116] J. D. Callaghan,[24] T. A. Callister,[117,118] E. Calloni,[25,4] J. Cameron,[95] J. B. Camp,[119] M. Canepa,[120,94] S. Canevarolo,[67] M. Cannavacciuolo,[104] K. C. Cannon,[28] H. Cao,[90] Z. Cao,[121] E. Capocasa,[45,20] E. Capote,[69] G. Carapella,[104,105] F. Carbognani,[47] M. Carlassara,[9,10] J. B. Carlin,[122] M. F. Carney,[15] M. Carpinelli,[123,124,47] G. Carrillo,[68] G. Carullo,[80,18] T. L. Carver,[17] J. Casanueva Diaz,[47] C. Casentini,[125,126] G. Castaldi,[127] S. Caudill,[60,67] M. Cavaglià,[97] F. Cavalier,[46] R. Cavalieri,[47] G. Cella,[18] P. Cerdá-Durán,[128] E. Cesarini,[126] W. Chaibi,[37] S. Chalathadka Subrahmanya,[129] E. Champion,[130] C.-H. Chan,[131] C. Chan,[28] C. L. Chan,[132] K. Chan,[132] M. Chan,[133] K. Chandra,[108] I. P. Chang,[131] P. Chanial,[47] S. Chao,[131] C. Chapman-Bird,[24] P. Charlton,[134] E. A. Chase,[15] E. Chassande-Mottin,[45] C. Chatterjee,[95] Debarati Chatterjee,[11] Deep Chatterjee,[6] M. Chaturvedi,[96] S. Chaty,[45] C. Chen,[135,136] D. Chen,[53] H. Y. Chen,[76] J. Chen,[131] K. Chen,[137] X. Chen,[95] Y.-B. Chen,[138] Y.-R. Chen,[139] Z. Chen,[17] H. Cheng,[78] C. K. Cheong,[132] H. Y. Cheung,[132] H. Y. Chia,[78] F. Chiadini,[140,105] C-Y. Chiang,[141] G. Chiarini,[83] R. Chierici,[142] A. Chincarini,[94] M. L. Chiofalo,[80,18] A. Chiummo,[47] R. K. Choudhary,[95] S. Choudhary,[11] N. Christensen,[37] Q. Chu,[95] Y-K. Chu,[141] S. S. Y. Chua,[8] K. W. Chung,[61] G. Ciani,[82,83] P. Ciecielag,[88] M. Cieślar,[88] M. Cifaldi,[125,126] A. A. Ciobanu,[90] R. Ciolfi,[143,83] F. Cipriano,[37] F. Clara,[74] J. A. Clark,[1,48] P. Clearwater,[65] S. Clesse,[144] F. Cleva,[37] E. Coccia,[32,109] E. Codazzo,[32] P.-F. Cohadon,[110] D. E. Cohen,[46] M. Colleoni,[145] C. G. Collette,[146] A. Colombo,[71,72] M. Colpi,[71,72] C. M. Compton,[74] M. Constancio Jr.,[16] L. Conti,[83] S. J. Cooper,[14] P. Corban,[57] T. R. Corbitt,[7] I. Cordero-Carrión,[147] S. Corezzi,[81,40] K. R. Corley,[51] N. J. Cornish,[85] D. Corre,[46] A. Corsi,[148] S. Cortese,[47] C. A. Costa,[16] R. Cotesta,[113] R. Cottingham,[57] M. W. Coughlin,[149] J.-P. Coulon,[37] S. T. Countryman,[51] B. Cousins,[150] P. Couvares,[1] D. M. Coward,[95] M. J. Cowart,[57] D. C. Coyne,[1] R. Coyne,[151] J. D. E. Creighton,[6] T. D. Creighton,[91] A. W. Criswell,[149] M. Croquette,[110] S. G. Crowder,[152] J. R. Cudell,[70] T. J. Cullen,[7] A. Cumming,[24] R. Cummings,[24] L. Cunningham,[24] E. Cuoco,[47,153,18] M. Curyło,[111] P. Dabadie,[26] T. Dal Canton,[46] S. Dall'Osso,[32] G. Dálya,[87,154] A. Dana,[79] B. D'Angelo,[120,94] S. Danilishin,[155,60] S. D'Antonio,[126] K. Danzmann,[9,10] C. Darsow-Fromm,[129] A. Dasgupta,[86] L. E. H. Datrier,[24] Sayak Datta,[11] Sayantani Datta,[49] V. Dattilo,[47] I. Dave,[96] M. Davier,[46] D. Davis,[1] M. C. Davis,[115] E. J. Daw,[156] R. Dean,[115] D. DeBra,[79] M. Deenadayalan,[11] J. Degallaix,[157] M. De Laurentis,[25,4] S. Deléglise,[110] V. Del Favero,[130] F. De Lillo,[59] N. De Lillo,[24] D. Dell'Aquila,[123] W. Del Pozzo,[80,18] L. M. DeMarchi,[15] F. De Matteis,[125,126] V. D'Emilio,[17] N. Demos,[76]

T. Dent,[116] A. Depasse,[59] R. De Pietri,[158,159] R. De Rosa,[25,4] C. De Rossi,[47] R. DeSalvo,[127,160] R. De Simone,[140] S. Dhurandhar,[11] M. C. Díaz,[91] N. A. Didio,[69] T. Dietrich,[113] L. Di Fiore,[4] C. Di Fronzo,[14] C. Di Giorgio,[104,105] F. Di Giovanni,[128] M. Di Giovanni,[32] T. Di Girolamo,[25,4] A. Di Lieto,[80,18] A. Di Michele,[81] B. Ding,[146] S. Di Pace,[106,58] I. Di Palma,[106,58] F. Di Renzo,[80,18] A. K. Divakarla,[78] A. Dmitriev,[14] Z. Doctor,[15] L. Donahue,[161] L. D'Onofrio,[25,4] F. Donovan,[76] K. L. Dooley,[17] S. Doravari,[11] M. Drago,[106,58] J. C. Driggers,[74] Y. Drori,[1] J.-G. Ducoin,[46] P. Dupej,[24] U. Dupletsa,[32] O. Durante,[104,105] D. D'Urso,[123,124] P.-A. Duverne,[46] S. E. Dwyer,[74] C. Eassa,[74] P. J. Easter,[5] M. Ebersold,[162] T. Eckhardt,[129] G. Eddolls,[24] B. Edelman,[68] T. B. Edo,[1] O. Edy,[52] A. Effler,[57] S. Eguchi,[133] J. Eichholz,[8] S. S. Eikenberry,[78] M. Eisenmann,[30,20] R. A. Eisenstein,[76] A. Ejlli,[17] E. Engelby,[44] Y. Enomoto,[27] L. Errico,[25,4] R. C. Essick,[163] H. Estellés,[145] D. Estevez,[164] Z. Etienne,[165] T. Etzel,[1] M. Evans,[76] T. M. Evans,[57] T. Evstafyeva,[12] B. E. Ewing,[150] F. Fabrizi,[55,56] F. Faedi,[56] V. Fafone,[125,126,32] H. Fair,[69] S. Fairhurst,[17] P. C. Fan,[161] A. M. Farah,[166] S. Farinon,[94] B. Farr,[68] W. M. Farr,[117,118] E. J. Fauchon-Jones,[17] G. Favaro,[82] M. Favata,[167] M. Fays,[70] M. Fazio,[168] J. Feicht,[1] M. M. Fejer,[79] E. Fenyvesi,[77,169] D. L. Ferguson,[170] A. Fernandez-Galiana,[76] I. Ferrante,[80,18] T. A. Ferreira,[16] F. Fidecaro,[80,18] P. Figura,[111] A. Fiori,[18,80] I. Fiori,[47] M. Fishbach,[15] R. P. Fisher,[64] R. Fittipaldi,[171,105] V. Fiumara,[172,105] R. Flaminio,[30,20] E. Floden,[149] H. K. Fong,[28] J. A. Font,[128,173] B. Fornal,[160] P. W. F. Forsyth,[8] A. Franke,[129] S. Frasca,[106,58] F. Frasconi,[18] J. P. Freed,[36] Z. Frei,[154] A. Freise,[60,98] O. Freitas,[174] R. Frey,[68] P. Fritschel,[76] V. V. Frolov,[57] G. G. Fronzé,[23] Y. Fujii,[175] Y. Fujikawa,[176] Y. Fujimoto,[177] P. Fulda,[78] M. Fyffe,[57] H. A. Gabbard,[24] B. U. Gadre,[113] J. R. Gair,[113] J. Gais,[132] S. Galaudage,[5] R. Gamba,[13] D. Ganapathy,[76] A. Ganguly,[11] D. Gao,[178] S. G. Gaonkar,[11] B. Garaventa,[94,120] C. García Núñez,[102] C. García-Quirós,[145] F. Garufi,[25,4] B. Gateley,[74] V. Gayathri,[78] G.-G. Ge,[178] G. Gemme,[94] A. Gennai,[18] J. George,[96] O. Gerberding,[129] L. Gergely,[179] P. Gewecke,[129] S. Ghonge,[48] Abhirup Ghosh,[113] Archisman Ghosh,[87] Shaon Ghosh,[167] Shrobana Ghosh,[17] Tathagata Ghosh,[11] B. Giacomazzo,[71,72,73] L. Giacoppo,[106,58] J. A. Giaime,[7,57] K. D. Giardina,[57] D. R. Gibson,[102] C. Gier,[33] M. Giesler,[180] P. Giri,[18,80] F. Gissi,[89] S. Gkaitatzis,[18,80] J. Glanzer,[7] A. E. Gleckl,[44] P. Godwin,[150] E. Goetz,[181] R. Goetz,[78] N. Gohlke,[9,10] J. Golomb,[1] B. Goncharov,[32] G. González,[7] M. Gosselin,[47] R. Gouaty,[30] D. W. Gould,[8] S. Goyal,[19] B. Grace,[8] A. Grado,[182,4] V. Graham,[24] M. Granata,[157] V. Granata,[104] A. Grant,[24] S. Gras,[76] P. Grassia,[1] C. Gray,[74] R. Gray,[24] G. Greco,[40] A. C. Green,[78] R. Green,[17] A. M. Gretarsson,[36] E. M. Gretarsson,[36] D. Griffith,[1] W. L. Griffiths,[17] H. L. Griggs,[48] G. Grignani,[81,40] A. Grimaldi,[100,101] E. Grimes,[36] S. J. Grimm,[32,109] H. Grote,[17] S. Grunewald,[113] P. Gruning,[46] A. S. Gruson,[44] D. Guerra,[128] G. M. Guidi,[55,56] A. R. Guimaraes,[7] G. Guixé,[29] H. K. Gulati,[86] A. M. Gunny,[76] H.-K. Guo,[160] Y. Guo,[60] Anchal Gupta,[1] Anuradha Gupta,[183] I. M. Gupta,[150] P. Gupta,[60,67] S. K. Gupta,[108] R. Gustafson,[184] F. Guzman,[185] S. Ha,[186] I. P. W. Hadiputrawan,[137] L. Haegel,[45] S. Haino,[141] O. Halim,[35] E. D. Hall,[76] E. Z. Hamilton,[162] G. Hammond,[24] W.-B. Han,[187] M. Haney,[162] J. Hanks,[74] C. Hanna,[150] M. D. Hannam,[17] O. Hannuksela,[67,60] H. Hansen,[74] T. J. Hansen,[36] J. Hanson,[57] T. Harder,[37] K. Haris,[60,67] J. Harms,[32,109] G. M. Harry,[42] I. W. Harry,[52] D. Hartwig,[129] K. Hasegawa,[188] B. Haskell,[88] C.-J. Haster,[76] J. S. Hathaway,[130] K. Hattori,[189] K. Haughian,[24] H. Hayakawa,[190] K. Hayama,[133] F. J. Hayes,[24] J. Healy,[130] A. Heidmann,[110] A. Heidt,[9,10] M. C. Heintze,[57] J. Heinze,[9,10] J. Heinzel,[76] H. Heitmann,[37] F. Hellman,[191] P. Hello,[46] A. F. Helmling-Cornell,[68] G. Hemming,[47] M. Hendry,[24] I. S. Heng,[24] E. Hennes,[60] J. Hennig,[192] M. H. Hennig,[192] C. Henshaw,[48] A. G. Hernandez,[92] F. Hernandez Vivanco,[5] M. Heurs,[9,10] A. L. Hewitt,[193] S. Higginbotham,[17] S. Hild,[155,60] P. Hill,[33] Y. Himemoto,[194] A. S. Hines,[185] N. Hirata,[20] C. Hirose,[176] T-C. Ho,[137] W. C. G. Ho,[195] S. Hochheim,[9,10] D. Hofman,[157] J. N. Hohmann,[129] D. G. Holcomb,[115] N. A. Holland,[8] I. J. Hollows,[156] Z. J. Holmes,[90] K. Holt,[57] D. E. Holz,[166] Q. Hong,[131] J. Hough,[24] S. Hourihane,[1] E. J. Howell,[95] C. G. Hoy,[17] D. Hoyland,[14] A. Hreibi,[9,10] B-H. Hsieh,[188] H-F. Hsieh,[196] C. Hsiung,[135] Y. Hsu,[131] H-Y. Huang,[141] P. Huang,[178] Y-C. Huang,[139] Y.-J. Huang,[141] Yiting Huang,[152] Yiwen Huang,[76] M. T. Hübner,[5] A. D. Huddart,[197] B. Hughey,[36] D. C. Y. Hui,[198] V. Hui,[30] S. Husa,[145] S. H. Huttner,[24] R. Huxford,[150] T. Huynh-Dinh,[57] S. Ide,[199] B. Idzkowski,[111] A. Iess,[125,126] K. Inayoshi,[200] Y. Inoue,[137] P. Iosif,[201] M. Isi,[76] K. Isleif,[129] K. Ito,[202] Y. Itoh,[177,203] B. R. Iyer,[19] V. JaberianHamedan,[95] T. Jacqmin,[110] P.-E. Jacquet,[110] S. J. Jadhav,[204] S. P. Jadhav,[11] T. Jain,[12] A. L. James,[17] A. Z. Jan,[170] K. Jani,[205] J. Janquart,[67,60] K. Janssens,[206,37] N. N. Janthalur,[204] P. Jaranowski,[207] D. Jariwala,[78] R. Jaume,[145] A. C. Jenkins,[61] K. Jenner,[90] C. Jeon,[208] W. Jia,[76] J. Jiang,[78] H.-B. Jin,[209,210] G. R. Johns,[64] R. Johnston,[24] A. W. Jones,[95] D. I. Jones,[211] P. Jones,[14] R. Jones,[24] P. Joshi,[150] L. Ju,[95] A. Jue,[160] P. Jung,[63] K. Jung,[186] J. Junker,[9,10] V. Juste,[164] K. Kaihotsu,[202] T. Kajita,[212] M. Kakizaki,[189] C. V. Kalaghatgi,[17,67,60,213] V. Kalogera,[15] B. Kamai,[1] M. Kamiizumi,[190] N. Kanda,[177,203] S. Kandhasamy,[11] G. Kang,[214] J. B. Kanner,[1] Y. Kao,[131] S. J. Kapadia,[19] D. P. Kapasi,[8] C. Karathanasis,[31] S. Karki,[97] R. Kashyap,[150] M. Kasprzack,[1] W. Kastaun,[9,10] T. Kato,[188] S. Katsanevas,[47] E. Katsavounidis,[76] W. Katzman,[57] T. Kaur,[95] K. Kawabe,[74] K. Kawaguchi,[188] F. Kéfélian,[37] D. Keitel,[145] J. S. Key,[215] S. Khadka,[79] F. Y. Khalili,[99] S. Khan,[17] T. Khanam,[148] E. A. Khazanov,[216] N. Khetan,[32,109] M. Khursheed,[96] N. Kijbunchoo,[8] A. Kim,[15] C. Kim,[208] J. C. Kim,[217] J. Kim,[218] K. Kim,[208] W. S. Kim,[63] Y.-M. Kim,[186] C. Kimball,[15] N. Kimura,[190] M. Kinley-Hanlon,[24] R. Kirchhoff,[9,10] J. S. Kissel,[74] S. Klimenko,[78]

T. Klinger,[12] A. M. Knee,[181] T. D. Knowles,[165] N. Knust,[9,10] E. Knyazev,[76] Y. Kobayashi,[177] P. Koch,[9,10] G. Koekoek,[60,155] K. Kohri,[219] K. Kokeyama,[220] S. Koley,[32] P. Kolitsidou,[17] M. Kolstein,[31] K. Komori,[76] V. Kondrashov,[1] A. K. H. Kong,[196] A. Kontos,[84] N. Koper,[9,10] M. Korobko,[129] M. Kovalam,[95] N. Koyama,[176] D. B. Kozak,[1] C. Kozakai,[53] V. Kringel,[9,10] N. V. Krishnendu,[9,10] A. Królak,[221,222] G. Kuehn,[9,10] F. Kuei,[131] P. Kuijer,[60] S. Kulkarni,[183] A. Kumar,[204] Prayush Kumar,[19] Rahul Kumar,[74] Rakesh Kumar,[86] J. Kume,[28] K. Kuns,[76] Y. Kuromiya,[202] S. Kuroyanagi,[223,224] K. Kwak,[186] G. Lacaille,[24] P. Lagabbe,[30] D. Laghi,[114] E. Lalande,[225] M. Lalleman,[206] T. L. Lam,[132] A. Lamberts,[37,226] M. Landry,[74] B. B. Lane,[76] R. N. Lang,[76] J. Lange,[170] B. Lantz,[79] I. La Rosa,[30] A. Lartaux-Vollard,[46] P. D. Lasky,[5] M. Laxen,[57] A. Lazzarini,[1] C. Lazzaro,[82,83] P. Leaci,[106,58] S. Leavey,[9,10] S. LeBohec,[160] Y. K. Lecoeuche,[181] E. Lee,[188] H. M. Lee,[227] H. W. Lee,[217] K. Lee,[228] R. Lee,[139] I. N. Legred,[1] J. Lehmann,[9,10] A. Lemaître,[229] M. Lenti,[56,230] M. Leonardi,[20] E. Leonova,[38] N. Leroy,[46] N. Letendre,[30] C. Levesque,[225] Y. Levin,[5] J. N. Leviton,[184] K. Leyde,[45] A. K. Y. Li,[1] B. Li,[131] J. Li,[15] K. L. L. Li,[231] P. Li,[232] T. G. F. Li,[132] X. Li,[138] C-Y. Lin,[233] E. T. Lin,[196] F-K. Lin,[141] F-L. Lin,[234] H. L. Lin,[137] L. C.-C. Lin,[231] F. Linde,[213,60] S. D. Linker,[127,92] J. N. Linley,[24] T. B. Littenberg,[235] G. C. Liu,[135] J. Liu,[95] K. Liu,[131] X. Liu,[6] F. Llamas,[91] R. K. L. Lo,[1] T. Lo,[131] L. T. London,[38,76] A. Longo,[236] D. Lopez,[162] M. Lopez Portilla,[67] M. Lorenzini,[125,126] V. Loriette,[237] M. Lormand,[57] G. Losurdo,[18] T. P. Lott,[48] J. D. Lough,[9,10] C. O. Lousto,[130] G. Lovelace,[44] J. F. Lucaccioni,[238] H. Lück,[9,10] D. Lumaca,[125,126] A. P. Lundgren,[52] L.-W. Luo,[141] J. E. Lynam,[64] M. Ma'arif,[137] R. Macas,[52] J. B. Machtinger,[15] M. MacInnis,[76] D. M. Macleod,[17] I. A. O. MacMillan,[1] A. Macquet,[37] I. Magaña Hernandez,[6] C. Magazzù,[18] R. M. Magee,[1] R. Maggiore,[14] M. Magnozzi,[94,120] S. Mahesh,[165] E. Majorana,[106,58] I. Maksimovic,[237] S. Maliakal,[1] A. Malik,[96] N. Man,[37] V. Mandic,[149] V. Mangano,[106,58] G. L. Mansell,[74,76] M. Manske,[6] M. Mantovani,[47] M. Mapelli,[82,83] F. Marchesoni,[41,40,239] D. Marín Pina,[29] F. Marion,[30] Z. Mark,[138] S. Márka,[51] Z. Márka,[51] C. Markakis,[12] A. S. Markosyan,[79] A. Markowitz,[1] E. Maros,[1] A. Marquina,[147] S. Marsat,[45] F. Martelli,[55,56] I. W. Martin,[24] R. M. Martin,[167] M. Martinez,[31] V. A. Martinez,[78] V. Martinez,[26] K. Martinovic,[61] D. V. Martynov,[14] E. J. Marx,[76] H. Masalehdan,[129] K. Mason,[76] E. Massera,[156] A. Masserot,[30] M. Masso-Reid,[24] S. Mastrogiovanni,[45] A. Matas,[113] M. Mateu-Lucena,[145] F. Matichard,[1,76] M. Matiushechkina,[9,10] N. Mavalvala,[76] J. J. McCann,[95] R. McCarthy,[74] D. E. McClelland,[8] P. K. McClincy,[150] S. McCormick,[57] L. McCuller,[76] G. I. McGhee,[24] S. C. McGuire,[57] C. McIsaac,[52] J. McIver,[181] T. McRae,[8] S. T. McWilliams,[165] D. Meacher,[6] M. Mehmet,[9,10] A. K. Mehta,[113] Q. Meijer,[67] A. Melatos,[122] D. A. Melchor,[44] G. Mendell,[74] A. Menendez-Vazquez,[31] C. S. Menoni,[168] R. A. Mercer,[6] L. Mereni,[157] K. Merfeld,[68] E. L. Merilh,[57] J. D. Merritt,[68] M. Merzougui,[37] S. Meshkov,[1,*] C. Messenger,[24] C. Messick,[76] P. M. Meyers,[122] F. Meylahn,[9,10] A. Mhaske,[11] A. Miani,[100,101] H. Miao,[14] I. Michaloliakos,[78] C. Michel,[157] Y. Michimura,[27] H. Middleton,[122] D. P. Mihaylov,[113] L. Milano,[25,†] A. L. Miller,[59] A. Miller,[92] B. Miller,[38,60] M. Millhouse,[122] J. C. Mills,[17] E. Milotti,[240,35] Y. Minenkov,[126] N. Mio,[241] Ll. M. Mir,[31] M. Miravet-Tenés,[128] A. Mishkin,[78] C. Mishra,[242] T. Mishra,[78] T. Mistry,[156] S. Mitra,[11] V. P. Mitrofanov,[99] G. Mitselmakher,[78] R. Mittleman,[76] O. Miyakawa,[190] K. Miyo,[190] S. Miyoki,[190] Geoffrey Mo,[76] L. M. Modafferi,[145] E. Moguel,[238] K. Mogushi,[97] S. R. P. Mohapatra,[76] S. R. Mohite,[6] I. Molina,[44] M. Molina-Ruiz,[191] M. Mondin,[92] M. Montani,[55,56] C. J. Moore,[14] J. Moragues,[145] D. Moraru,[74] F. Morawski,[88] A. More,[11] C. Moreno,[36] G. Moreno,[74] Y. Mori,[202] S. Morisaki,[6] N. Morisue,[177] Y. Moriwaki,[189] B. Mours,[164] C. M. Mow-Lowry,[60,98] S. Mozzon,[52] F. Muciaccia,[106,58] Arunava Mukherjee,[243] D. Mukherjee,[150] Soma Mukherjee,[91] Subroto Mukherjee,[86] Suvodip Mukherjee,[163,38] N. Mukund,[9,10] A. Mullavey,[57] J. Munch,[90] E. A. Muñiz,[69] P. G. Murray,[24] R. Musenich,[94,120] S. Muusse,[90] S. L. Nadji,[9,10] K. Nagano,[244] A. Nagar,[23,245] K. Nakamura,[20] H. Nakano,[246] M. Nakano,[188] Y. Nakayama,[202] V. Napolano,[47] I. Nardecchia,[125,126] T. Narikawa,[188] H. Narola,[67] L. Naticchioni,[58] B. Nayak,[92] R. K. Nayak,[247] B. F. Neil,[95] J. Neilson,[89,105] A. Nelson,[185] T. J. N. Nelson,[57] M. Nery,[9,10] P. Neubauer,[238] A. Neunzert,[215] K. Y. Ng,[76] S. W. S. Ng,[90] C. Nguyen,[45] P. Nguyen,[68] T. Nguyen,[76] L. Nguyen Quynh,[248] J. Ni,[149] W.-T. Ni,[209,178,139] S. A. Nichols,[7] T. Nishimoto,[188] A. Nishizawa,[28] S. Nissanke,[38,60] E. Nitoglia,[142] F. Nocera,[47] M. Norman,[17] C. North,[17] S. Nozaki,[189] G. Nurbek,[91] L. K. Nuttall,[52] Y. Obayashi,[188] J. Oberling,[74] B. D. O'Brien,[78] J. O'Dell,[197] E. Oelker,[24] W. Ogaki,[188] G. Oganesyan,[32,109] J. J. Oh,[63] K. Oh,[198] S. H. Oh,[63] M. Ohashi,[190] T. Ohashi,[177] M. Ohkawa,[176] F. Ohme,[9,10] H. Ohta,[28] M. A. Okada,[16] Y. Okutani,[199] C. Olivetto,[47] K. Oohara,[188,249] R. Oram,[57] B. O'Reilly,[57] R. G. Ormiston,[149] N. D. Ormsby,[64] R. O'Shaughnessy,[130] E. O'Shea,[180] S. Oshino,[190] S. Ossokine,[113] C. Osthelder,[1] S. Otabe,[2] D. J. Ottaway,[90] H. Overmier,[57] A. E. Pace,[150] G. Pagano,[80,18] R. Pagano,[7] M. A. Page,[95] G. Pagliaroli,[32,109] A. Pai,[108] S. A. Pai,[96] S. Pal,[247] J. R. Palamos,[68] O. Palashov,[216] C. Palomba,[58] H. Pan,[131] K.-C. Pan,[139,196] P. K. Panda,[204] P. T. H. Pang,[60,67] C. Pankow,[15] F. Pannarale,[106,58] B. C. Pant,[96] F. H. Panther,[95] F. Paoletti,[18] A. Paoli,[47] A. Paolone,[58,250] G. Pappas,[201] A. Parisi,[135] H. Park,[6] J. Park,[251] W. Parker,[57] D. Pascucci,[60,87] A. Pasqualetti,[47] R. Passaquieti,[80,18] D. Passuello,[18] M. Patel,[64] M. Pathak,[90] B. Patricelli,[47,18] A. S. Patron,[7] S. Paul,[68] E. Payne,[5] M. Pedraza,[1] R. Pedurand,[105] M. Pegoraro,[83] A. Pele,[57] F. E. Peña Arellano,[190] S. Penano,[79] S. Penn,[252] A. Perego,[100,101] A. Pereira,[26]

T. Pereira,[253] C. J. Perez,[74] C. Périgois,[30] C. C. Perkins,[78] A. Perreca,[100,101] S. Perriès,[142] D. Pesios,[201] J. Petermann,[129] D. Petterson,[1] H. P. Pfeiffer,[113] H. Pham,[57] K. A. Pham,[149] K. S. Phukon,[60,213] H. Phurailatpam,[132] O. J. Piccinni,[58] M. Pichot,[37] M. Piendibene,[80,18] F. Piergiovanni,[55,56] L. Pierini,[106,58] V. Pierro,[89,105] G. Pillant,[47] M. Pillas,[46] F. Pilo,[18] L. Pinard,[157] C. Pineda-Bosque,[92] I. M. Pinto,[89,105,254] M. Pinto,[47] B. J. Piotrzkowski,[6] K. Piotrzkowski,[59] M. Pirello,[74] M. D. Pitkin,[193] A. Placidi,[40,81] E. Placidi,[106,58] M. L. Planas,[145] W. Plastino,[255,236] C. Pluchar,[256] R. Poggiani,[80,18] E. Polini,[30] D. Y. T. Pong,[132] S. Ponrathnam,[11] E. K. Porter,[45] R. Poulton,[47] A. Poverman,[84] J. Powell,[65] M. Pracchia,[30] T. Pradier,[164] A. K. Prajapati,[86] K. Prasai,[79] R. Prasanna,[204] G. Pratten,[14] M. Principe,[89,254,105] G. A. Prodi,[257,101] L. Prokhorov,[14] P. Prosposito,[125,126] L. Prudenzi,[113] A. Puecher,[60,67] M. Punturo,[40] F. Puosi,[18,80] P. Puppo,[58] M. Pürrer,[113] H. Qi,[17] N. Quartey,[64] V. Quetschke,[91] P. J. Quinonez,[36] R. Quitzow-James,[97] F. J. Raab,[74] G. Raaijmakers,[38,60] H. Radkins,[74] N. Radulesco,[37] P. Raffai,[154] S. X. Rail,[225] S. Raja,[96] C. Rajan,[96] K. E. Ramirez,[57] T. D. Ramirez,[44] A. Ramos-Buades,[113] J. Rana,[150] P. Rapagnani,[106,58] A. Ray,[6] V. Raymond,[17] N. Raza,[181] M. Razzano,[80,18] J. Read,[44] L. A. Rees,[42] T. Regimbau,[30] L. Rei,[94] S. Reid,[33] S. W. Reid,[64] D. H. Reitze,[1,78] P. Relton,[17] A. Renzini,[1] P. Rettegno,[22,23] B. Revenu,[45] A. Reza,[60] M. Rezac,[44] F. Ricci,[106,58] D. Richards,[197] J. W. Richardson,[258] L. Richardson,[185] G. Riemenschneider,[22,23] K. Riles,[184] S. Rinaldi,[80,18] K. Rink,[181] N. A. Robertson,[1] R. Robie,[1] F. Robinet,[46] A. Rocchi,[126] S. Rodriguez,[44] L. Rolland,[30] J. G. Rollins,[1] M. Romanelli,[107] R. Romano,[3,4] C. L. Romel,[74] A. Romero,[31] I. M. Romero-Shaw,[5] J. H. Romie,[57] S. Ronchini,[32,109] L. Rosa,[4,25] C. A. Rose,[6] D. Rosińska,[111] M. P. Ross,[259] S. Rowan,[24] S. J. Rowlinson,[14] S. Roy,[67] Santosh Roy,[11] Soumen Roy,[260] D. Rozza,[123,124] P. Ruggi,[47] K. Ruiz-Rocha,[205] K. Ryan,[74] S. Sachdev,[150] T. Sadecki,[74] J. Sadiq,[116] S. Saha,[196] Y. Saito,[190] K. Sakai,[261] M. Sakellariadou,[61] S. Sakon,[150] O. S. Salafia,[73,72,71] F. Salces-Carcoba,[1] L. Salconi,[47] M. Saleem,[149] F. Salemi,[100,101] A. Samajdar,[72] E. J. Sanchez,[1] J. H. Sanchez,[44] L. E. Sanchez,[1] N. Sanchis-Gual,[262] J. R. Sanders,[263] A. Sanuy,[29] T. R. Saravanan,[11] N. Sarin,[5] B. Sassolas,[157] H. Satari,[95] O. Sauter,[78] R. L. Savage,[74] V. Savant,[11] T. Sawada,[177] H. L. Sawant,[11] S. Sayah,[157] D. Schaetzl,[1] M. Scheel,[138] J. Scheuer,[15] M. G. Schiworski,[90] P. Schmidt,[14] S. Schmidt,[67] R. Schnabel,[129] M. Schneewind,[9,10] R. M. S. Schofield,[68] A. Schönbeck,[129] B. W. Schulte,[9,10] B. F. Schutz,[17,9,10] E. Schwartz,[17] J. Scott,[24] S. M. Scott,[8] M. Seglar-Arroyo,[30] Y. Sekiguchi,[264] D. Sellers,[57] A. S. Sengupta,[260] D. Sentenac,[47] E. G. Seo,[132] V. Sequino,[25,4] A. Sergeev,[216] Y. Setyawati,[9,10,67] T. Shaffer,[74] M. S. Shahriar,[15] M. A. Shaikh,[19] B. Shams,[160] L. Shao,[200] A. Sharma,[32,109] P. Sharma,[96] P. Shawhan,[112] N. S. Shcheblanov,[229] A. Sheela,[242] Y. Shikano,[265,266] M. Shikauchi,[28] H. Shimizu,[267] K. Shimode,[190] H. Shinkai,[268] T. Shishido,[54] A. Shoda,[20] D. H. Shoemaker,[76] D. M. Shoemaker,[170] S. ShyamSundar,[96] M. Sieniawska,[59] D. Sigg,[74] L. Silenzi,[40,41] L. P. Singer,[119] D. Singh,[150] M. K. Singh,[19] N. Singh,[111] A. Singha,[155,60] A. M. Sintes,[145] V. Sipala,[123,124] V. Skliris,[17] B. J. J. Slagmolen,[8] T. J. Slaven-Blair,[95] J. Smetana,[14] J. R. Smith,[44] L. Smith,[24] R. J. E. Smith,[5] J. Soldateschi,[230,269,56] S. N. Somala,[270] K. Somiya,[2] I. Song,[196] K. Soni,[11] V. Sordini,[142] F. Sorrentino,[94] N. Sorrentino,[80,18] R. Soulard,[37] T. Souradeep,[271,11] E. Sowell,[148] V. Spagnuolo,[155,60] A. P. Spencer,[24] M. Spera,[82,83] P. Spinicelli,[47] A. K. Srivastava,[86] V. Srivastava,[69] K. Staats,[15] C. Stachie,[37] F. Stachurski,[24] D. A. Steer,[45] J. Steinlechner,[155,60] S. Steinlechner,[155,60] N. Stergioulas,[201] D. J. Stops,[14] M. Stover,[238] K. A. Strain,[24] L. C. Strang,[122] G. Stratta,[272,58] M. D. Strong,[7] A. Strunk,[74] R. Sturani,[253] A. L. Stuver,[115] M. Suchenek,[88] S. Sudhagar,[11] V. Sudhir,[76] R. Sugimoto,[273,244] H. G. Suh,[6] A. G. Sullivan,[51] T. Z. Summerscales,[274] L. Sun,[8] S. Sunil,[86] A. Sur,[88] J. Suresh,[28] P. J. Sutton,[17] Takamasa Suzuki,[176] Takanori Suzuki,[2] Toshikazu Suzuki,[188] B. L. Swinkels,[60] M. J. Szczepańczyk,[78] P. Szewczyk,[111] M. Tacca,[60] H. Tagoshi,[188] S. C. Tait,[24] H. Takahashi,[275] R. Takahashi,[20] S. Takano,[27] H. Takeda,[27] M. Takeda,[177] C. J. Talbot,[33] C. Talbot,[1] K. Tanaka,[276] Taiki Tanaka,[188] Takahiro Tanaka,[277] A. J. Tanasijczuk,[59] S. Tanioka,[190] D. B. Tanner,[78] D. Tao,[1] L. Tao,[78] R. D. Tapia,[150] E. N. Tapia San Martín,[60] C. Taranto,[125] A. Taruya,[278] J. D. Tasson,[161] R. Tenorio,[145] J. E. S. Terhune,[115] L. Terkowski,[129] M. P. Thirugnanasambandam,[11] M. Thomas,[57] P. Thomas,[74] E. E. Thompson,[48] J. E. Thompson,[17] S. R. Thondapu,[96] K. A. Thorne,[57] E. Thrane,[5] Shubhanshu Tiwari,[162] Srishti Tiwari,[11] V. Tiwari,[17] A. M. Toivonen,[149] A. E. Tolley,[52] T. Tomaru,[20] T. Tomura,[190] M. Tonelli,[80,18] Z. Tornasi,[24] A. Torres-Forné,[128] C. I. Torrie,[1] I. Tosta e Melo,[124] D. Töyrä,[8] A. Trapananti,[41,40] F. Travasso,[40,41] G. Traylor,[57] M. Trevor,[112] M. C. Tringali,[47] A. Tripathee,[184] L. Troiano,[279,105] A. Trovato,[45] L. Trozzo,[4,190] R. J. Trudeau,[1] D. Tsai,[131] K. W. Tsang,[60,280,67] T. Tsang,[281] J-S. Tsao,[234] M. Tse,[76] R. Tso,[138] S. Tsuchida,[177] L. Tsukada,[150] D. Tsuna,[28] T. Tsutsui,[28] K. Turbang,[282,206] M. Turconi,[37] D. Tuyenbayev,[177] A. S. Ubhi,[14] N. Uchikata,[188] T. Uchiyama,[190] R. P. Udall,[1] A. Ueda,[283] T. Uehara,[284,285] K. Ueno,[28] G. Ueshima,[286] C. S. Unnikrishnan,[287] A. L. Urban,[7] T. Ushiba,[190] A. Utina,[155,60] G. Vajente,[1] A. Vajpeyi,[5] G. Valdes,[185] M. Valentini,[183,100,101] V. Valsan,[6] N. van Bakel,[60] M. van Beuzekom,[60] M. van Dael,[60,288] J. F. J. van den Brand,[155,98,60] C. Van Den Broeck,[67,60] D. C. Vander-Hyde,[69] H. van Haevermaet,[206] J. V. van Heijningen,[59] M. H. P. M. van Putten,[289] N. van Remortel,[206] M. Vardaro,[213,60] A. F. Vargas,[122] V. Varma,[113] M. Vasúth,[77] A. Vecchio,[14] G. Vedovato,[83] J. Veitch,[24] P. J. Veitch,[90] J. Venneberg,[9,10] G. Venugopalan,[1] D. Verkindt,[30] P. Verma,[222] Y. Verma,[96] S. M. Vermeulen,[17] D. Veske,[51] F. Vetrano,[55] A. Viceré,[55,56] S. Vidyant,[69] A. D. Viets,[290]

A. Vijaykumar,[19] V. Villa-Ortega,[116] J.-Y. Vinet,[37] A. Virtuoso,[240,35] S. Vitale,[76] H. Vocca,[81,40] E. R. G. von Reis,[74] J. S. A. von Wrangel,[9,10] C. Vorvick,[74] S. P. Vyatchanin,[99] L. E. Wade,[238] M. Wade,[238] K. J. Wagner,[130] R. C. Walet,[60] M. Walker,[64] G. S. Wallace,[33] L. Wallace,[1] J. Wang,[178] J. Z. Wang,[184] W. H. Wang,[91] R. L. Ward,[8] J. Warner,[74] M. Was,[30] T. Washimi,[20] N. Y. Washington,[1] J. Watchi,[146] B. Weaver,[74] C. R. Weaving,[52] S. A. Webster,[24] M. Weinert,[9,10] A. J. Weinstein,[1] R. Weiss,[76] C. M. Weller,[259] R. A. Weller,[205] F. Wellmann,[9,10] L. Wen,[95] P. Wessels,[9,10] K. Wette,[8] J. T. Whelan,[130] D. D. White,[44] B. F. Whiting,[78] C. Whittle,[76] D. Wilken,[9,10] D. Williams,[24] M. J. Williams,[24] A. R. Williamson,[52] J. L. Willis,[1] B. Willke,[9,10] D. J. Wilson,[256] C. C. Wipf,[1] T. Wlodarczyk,[113] G. Woan,[24] J. Woehler,[9,10] J. K. Wofford,[130] D. Wong,[181] I. C. F. Wong,[132] M. Wright,[24] C. Wu,[139] D. S. Wu,[9,10] H. Wu,[139] D. M. Wysocki,[6] L. Xiao,[1] T. Yamada,[267] H. Yamamoto,[1] K. Yamamoto,[189] T. Yamamoto,[190] K. Yamashita,[202] R. Yamazaki,[199] F. W. Yang,[160] K. Z. Yang,[149] L. Yang,[168] Y.-C. Yang,[131] Y. Yang,[291] Yang Yang,[78] M. J. Yap,[8] D. W. Yeeles,[17] S.-W. Yeh,[139] A. B. Yelikar,[130] M. Ying,[131] J. Yokoyama,[28,27] T. Yokozawa,[190] J. Yoo,[180] T. Yoshioka,[202] Hang Yu,[138] Haocun Yu,[76] H. Yuzurihara,[188] A. Zadrożny,[222] M. Zanolin,[36] S. Zeidler,[292] T. Zelenova,[47] J.-P. Zendri,[83] M. Zevin,[166] M. Zhan,[178] H. Zhang,[234] J. Zhang,[95] L. Zhang,[1] R. Zhang,[78] T. Zhang,[14] Y. Zhang,[185] C. Zhao,[95] G. Zhao,[146] Y. Zhao,[188,20] Yue Zhao,[160] R. Zhou,[191] Z. Zhou,[15] X. J. Zhu,[5] Z.-H. Zhu,[121,232] M. E. Zucker,[1,76] J. Zweizig,[1] D. Antonopoulou,[293] Z. Arzoumanian,[294] A. Basu,[293] S. Bogdanov,[295] I. Cognard,[296,297] K. Crowter,[298] T. Enoto,[299] C. M. L. Flynn,[65] D. C. Good,[300,301] L. Guillemot,[296,297] S. Guillot,[302,303] A. K. Harding,[304] M. J. Keith,[293] L. Kuiper,[305] M. E. Lower,[306,65] A. G. Lyne,[293] J. W. McKee,[307] B. W. Meyers,[298] J. L. Palfreyman,[308] R. M. Shannon,[65] B. Shaw,[293] I. H. Stairs,[298] B. W. Stappers,[293] C. M. Tan,[309,310] G. Theureau[296,297,311] And P. Weltevrede[293]

The LIGO Scientific Collaboration, the Virgo Collaboration, and the KAGRA Collaboration

[1] *LIGO Laboratory, California Institute of Technology, Pasadena, CA 91125, USA*
[2] *Graduate School of Science, Tokyo Institute of Technology, Meguro-ku, Tokyo 152-8551, Japan*
[3] *Dipartimento di Farmacia, Università di Salerno, I-84084 Fisciano, Salerno, Italy*
[4] *INFN, Sezione di Napoli, Complesso Universitario di Monte S. Angelo, I-80126 Napoli, Italy*
[5] *OzGrav, School of Physics & Astronomy, Monash University, Clayton 3800, Victoria, Australia*
[6] *University of Wisconsin-Milwaukee, Milwaukee, WI 53201, USA*
[7] *Louisiana State University, Baton Rouge, LA 70803, USA*
[8] *OzGrav, Australian National University, Canberra, Australian Capital Territory 0200, Australia*
[9] *Max Planck Institute for Gravitational Physics (Albert Einstein Institute), D-30167 Hannover, Germany*
[10] *Leibniz Universität Hannover, D-30167 Hannover, Germany*
[11] *Inter-University Centre for Astronomy and Astrophysics, Pune 411007, India*
[12] *University of Cambridge, Cambridge CB2 1TN, United Kingdom*
[13] *Theoretisch-Physikalisches Institut, Friedrich-Schiller-Universität Jena, D-07743 Jena, Germany*
[14] *University of Birmingham, Birmingham B15 2TT, United Kingdom*
[15] *Northwestern University, Evanston, IL 60208, USA*
[16] *Instituto Nacional de Pesquisas Espaciais, 12227-010 São José dos Campos, São Paulo, Brazil*
[17] *Cardiff University, Cardiff CF24 3AA, United Kingdom*
[18] *INFN, Sezione di Pisa, I-56127 Pisa, Italy*
[19] *International Centre for Theoretical Sciences, Tata Institute of Fundamental Research, Bengaluru 560089, India*
[20] *Gravitational Wave Science Project, National Astronomical Observatory of Japan (NAOJ), Mitaka City, Tokyo 181-8588, Japan*
[21] *Advanced Technology Center, National Astronomical Observatory of Japan (NAOJ), Mitaka City, Tokyo 181-8588, Japan*
[22] *Dipartimento di Fisica, Università degli Studi di Torino, I-10125 Torino, Italy*
[23] *INFN Sezione di Torino, I-10125 Torino, Italy*
[24] *SUPA, University of Glasgow, Glasgow G12 8QQ, United Kingdom*
[25] *Università di Napoli "Federico II", Complesso Universitario di Monte S. Angelo, I-80126 Napoli, Italy*
[26] *Université de Lyon, Université Claude Bernard Lyon 1, CNRS, Institut Lumière Matière, F-69622 Villeurbanne, France*
[27] *Department of Physics, The University of Tokyo, Bunkyo-ku, Tokyo 113-0033, Japan*
[28] *Research Center for the Early Universe (RESCEU), The University of Tokyo, Bunkyo-ku, Tokyo 113-0033, Japan*
[29] *Institut de Ciències del Cosmos (ICCUB), Universitat de Barcelona, C/ Martí i Franquès 1, Barcelona, 08028, Spain*
[30] *Univ. Savoie Mont Blanc, CNRS, Laboratoire d'Annecy de Physique des Particules - IN2P3, F-74000 Annecy, France*
[31] *Institut de Física d'Altes Energies (IFAE), Barcelona Institute of Science and Technology, and ICREA, E-08193 Barcelona, Spain*
[32] *Gran Sasso Science Institute (GSSI), I-67100 L'Aquila, Italy*
[33] *SUPA, University of Strathclyde, Glasgow G1 1XQ, United Kingdom*
[34] *Dipartimento di Scienze Matematiche, Informatiche e Fisiche, Università di Udine, I-33100 Udine, Italy*
[35] *INFN, Sezione di Trieste, I-34127 Trieste, Italy*

[36] *Embry-Riddle Aeronautical University, Prescott, AZ 86301, USA*
[37] *Artemis, Université Côte d'Azur, Observatoire de la Côte d'Azur, CNRS, F-06304 Nice, France*
[38] *GRAPPA, Anton Pannekoek Institute for Astronomy and Institute for High-Energy Physics, University of Amsterdam, Science Park 904, 1098 XH Amsterdam, Netherlands*
[39] *National and Kapodistrian University of Athens, School of Science Building, 2nd floor, Panepistimiopolis, 15771 Ilissia, Greece*
[40] *INFN, Sezione di Perugia, I-06123 Perugia, Italy*
[41] *Università di Camerino, Dipartimento di Fisica, I-62032 Camerino, Italy*
[42] *American University, Washington, D.C. 20016, USA*
[43] *Earthquake Research Institute, The University of Tokyo, Bunkyo-ku, Tokyo 113-0032, Japan*
[44] *California State University Fullerton, Fullerton, CA 92831, USA*
[45] *Université de Paris, CNRS, Astroparticule et Cosmologie, F-75006 Paris, France*
[46] *Université Paris-Saclay, CNRS/IN2P3, IJCLab, 91405 Orsay, France*
[47] *European Gravitational Observatory (EGO), I-56021 Cascina, Pisa, Italy*
[48] *Georgia Institute of Technology, Atlanta, GA 30332, USA*
[49] *Chennai Mathematical Institute, Chennai 603103, India*
[50] *Department of Mathematics and Physics,*
[51] *Columbia University, New York, NY 10027, USA*
[52] *University of Portsmouth, Portsmouth, PO1 3FX, United Kingdom*
[53] *Kamioka Branch, National Astronomical Observatory of Japan (NAOJ), Kamioka-cho, Hida City, Gifu 506-1205, Japan*
[54] *The Graduate University for Advanced Studies (SOKENDAI), Mitaka City, Tokyo 181-8588, Japan*
[55] *Università degli Studi di Urbino "Carlo Bo", I-61029 Urbino, Italy*
[56] *INFN, Sezione di Firenze, I-50019 Sesto Fiorentino, Firenze, Italy*
[57] *LIGO Livingston Observatory, Livingston, LA 70754, USA*
[58] *INFN, Sezione di Roma, I-00185 Roma, Italy*
[59] *Université catholique de Louvain, B-1348 Louvain-la-Neuve, Belgium*
[60] *Nikhef, Science Park 105, 1098 XG Amsterdam, Netherlands*
[61] *King's College London, University of London, London WC2R 2LS, United Kingdom*
[62] *Korea Institute of Science and Technology Information, Daejeon 34141, Republic of Korea*
[63] *National Institute for Mathematical Sciences, Daejeon 34047, Republic of Korea*
[64] *Christopher Newport University, Newport News, VA 23606, USA*
[65] *OzGrav, Swinburne University of Technology, Hawthorn VIC 3122, Australia*
[66] *School of High Energy Accelerator Science, The Graduate University for Advanced Studies (SOKENDAI), Tsukuba City, Ibaraki 305-0801, Japan*
[67] *Institute for Gravitational and Subatomic Physics (GRASP), Utrecht University, Princetonplein 1, 3584 CC Utrecht, Netherlands*
[68] *University of Oregon, Eugene, OR 97403, USA*
[69] *Syracuse University, Syracuse, NY 13244, USA*
[70] *Université de Liège, B-4000 Liège, Belgium*
[71] *Università degli Studi di Milano-Bicocca, I-20126 Milano, Italy*
[72] *INFN, Sezione di Milano-Bicocca, I-20126 Milano, Italy*
[73] *INAF, Osservatorio Astronomico di Brera sede di Merate, I-23807 Merate, Lecco, Italy*
[74] *LIGO Hanford Observatory, Richland, WA 99352, USA*
[75] *Dipartimento di Medicina, Chirurgia e Odontoiatria "Scuola Medica Salernitana", Università di Salerno, I-84081 Baronissi, Salerno, Italy*
[76] *LIGO Laboratory, Massachusetts Institute of Technology, Cambridge, MA 02139, USA*
[77] *Wigner RCP, RMKI, H-1121 Budapest, Konkoly Thege Miklós út 29-33, Hungary*
[78] *University of Florida, Gainesville, FL 32611, USA*
[79] *Stanford University, Stanford, CA 94305, USA*
[80] *Università di Pisa, I-56127 Pisa, Italy*
[81] *Università di Perugia, I-06123 Perugia, Italy*
[82] *Università di Padova, Dipartimento di Fisica e Astronomia, I-35131 Padova, Italy*
[83] *INFN, Sezione di Padova, I-35131 Padova, Italy*
[84] *Bard College, Annandale-On-Hudson, NY 12504, USA*
[85] *Montana State University, Bozeman, MT 59717, USA*
[86] *Institute for Plasma Research, Bhat, Gandhinagar 382428, India*
[87] *Universiteit Gent, B-9000 Gent, Belgium*
[88] *Nicolaus Copernicus Astronomical Center, Polish Academy of Sciences, 00-716, Warsaw, Poland*
[89] *Dipartimento di Ingegneria, Università del Sannio, I-82100 Benevento, Italy*

[90] *OzGrav, University of Adelaide, Adelaide, South Australia 5005, Australia*
[91] *The University of Texas Rio Grande Valley, Brownsville, TX 78520, USA*
[92] *California State University, Los Angeles, Los Angeles, CA 90032, USA*
[93] *Departamento de Matemáticas, Universitat Autònoma de Barcelona, Edificio C Facultad de Ciencias 08193 Bellaterra (Barcelona), Spain*
[94] *INFN, Sezione di Genova, I-16146 Genova, Italy*
[95] *OzGrav, University of Western Australia, Crawley, Western Australia 6009, Australia*
[96] *RRCAT, Indore, Madhya Pradesh 452013, India*
[97] *Missouri University of Science and Technology, Rolla, MO 65409, USA*
[98] *Vrije Universiteit Amsterdam, 1081 HV Amsterdam, Netherlands*
[99] *Lomonosov Moscow State University, Moscow 119991, Russia*
[100] *Università di Trento, Dipartimento di Fisica, I-38123 Povo, Trento, Italy*
[101] *INFN, Trento Institute for Fundamental Physics and Applications, I-38123 Povo, Trento, Italy*
[102] *SUPA, University of the West of Scotland, Paisley PA1 2BE, United Kingdom*
[103] *Bar-Ilan University, Ramat Gan, 5290002, Israel*
[104] *Dipartimento di Fisica "E.R. Caianiello", Università di Salerno, I-84084 Fisciano, Salerno, Italy*
[105] *INFN, Sezione di Napoli, Gruppo Collegato di Salerno, Complesso Universitario di Monte S. Angelo, I-80126 Napoli, Italy*
[106] *Università di Roma "La Sapienza", I-00185 Roma, Italy*
[107] *Univ Rennes, CNRS, Institut FOTON - UMR6082, F-3500 Rennes, France*
[108] *Indian Institute of Technology Bombay, Powai, Mumbai 400 076, India*
[109] *INFN, Laboratori Nazionali del Gran Sasso, I-67100 Assergi, Italy*
[110] *Laboratoire Kastler Brossel, Sorbonne Université, CNRS, ENS-Université PSL, Collège de France, F-75005 Paris, France*
[111] *Astronomical Observatory Warsaw University, 00-478 Warsaw, Poland*
[112] *University of Maryland, College Park, MD 20742, USA*
[113] *Max Planck Institute for Gravitational Physics (Albert Einstein Institute), D-14476 Potsdam, Germany*
[114] *L2IT, Laboratoire des 2 Infinis - Toulouse, Université de Toulouse, CNRS/IN2P3, UPS, F-31062 Toulouse Cedex 9, France*
[115] *Villanova University, Villanova, PA 19085, USA*
[116] *IGFAE, Universidade de Santiago de Compostela, 15782 Spain*
[117] *Stony Brook University, Stony Brook, NY 11794, USA*
[118] *Center for Computational Astrophysics, Flatiron Institute, New York, NY 10010, USA*
[119] *NASA Goddard Space Flight Center, Greenbelt, MD 20771, USA*
[120] *Dipartimento di Fisica, Università degli Studi di Genova, I-16146 Genova, Italy*
[121] *Department of Astronomy, Beijing Normal University, Beijing 100875, China*
[122] *OzGrav, University of Melbourne, Parkville, Victoria 3010, Australia*
[123] *Università degli Studi di Sassari, I-07100 Sassari, Italy*
[124] *INFN, Laboratori Nazionali del Sud, I-95125 Catania, Italy*
[125] *Università di Roma Tor Vergata, I-00133 Roma, Italy*
[126] *INFN, Sezione di Roma Tor Vergata, I-00133 Roma, Italy*
[127] *University of Sannio at Benevento, I-82100 Benevento, Italy and INFN, Sezione di Napoli, I-80100 Napoli, Italy*
[128] *Departamento de Astronomía y Astrofísica, Universitat de València, E-46100 Burjassot, València, Spain*
[129] *Universität Hamburg, D-22761 Hamburg, Germany*
[130] *Rochester Institute of Technology, Rochester, NY 14623, USA*
[131] *National Tsing Hua University, Hsinchu City, 30013 Taiwan, Republic of China*
[132] *The Chinese University of Hong Kong, Shatin, NT, Hong Kong*
[133] *Department of Applied Physics, Fukuoka University, Jonan, Fukuoka City, Fukuoka 814-0180, Japan*
[134] *OzGrav, Charles Sturt University, Wagga Wagga, New South Wales 2678, Australia*
[135] *Department of Physics, Tamkang University, Danshui Dist., New Taipei City 25137, Taiwan*
[136] *Department of Physics and Institute of Astronomy, National Tsing Hua University, Hsinchu 30013, Taiwan*
[137] *Department of Physics, Center for High Energy and High Field Physics, National Central University, Zhongli District, Taoyuan City 32001, Taiwan*
[138] *CaRT, California Institute of Technology, Pasadena, CA 91125, USA*
[139] *Department of Physics, National Tsing Hua University, Hsinchu 30013, Taiwan*
[140] *Dipartimento di Ingegneria Industriale (DIIN), Università di Salerno, I-84084 Fisciano, Salerno, Italy*
[141] *Institute of Physics, Academia Sinica, Nankang, Taipei 11529, Taiwan*
[142] *Université Lyon, Université Claude Bernard Lyon 1, CNRS, IP2I Lyon / IN2P3, UMR 5822, F-69622 Villeurbanne, France*
[143] *INAF, Osservatorio Astronomico di Padova, I-35122 Padova, Italy*
[144] *Université libre de Bruxelles, Avenue Franklin Roosevelt 50 - 1050 Bruxelles, Belgium*

[145] *IAC3–IEEC, Universitat de les Illes Balears, E-07122 Palma de Mallorca, Spain*
[146] *Université Libre de Bruxelles, Brussels 1050, Belgium*
[147] *Departamento de Matemáticas, Universitat de València, E-46100 Burjassot, València, Spain*
[148] *Texas Tech University, Lubbock, TX 79409, USA*
[149] *University of Minnesota, Minneapolis, MN 55455, USA*
[150] *The Pennsylvania State University, University Park, PA 16802, USA*
[151] *University of Rhode Island, Kingston, RI 02881, USA*
[152] *Bellevue College, Bellevue, WA 98007, USA*
[153] *Scuola Normale Superiore, Piazza dei Cavalieri, 7 - 56126 Pisa, Italy*
[154] *Eötvös University, Budapest 1117, Hungary*
[155] *Maastricht University, P.O. Box 616, 6200 MD Maastricht, Netherlands*
[156] *The University of Sheffield, Sheffield S10 2TN, United Kingdom*
[157] *Université Lyon, Université Claude Bernard Lyon 1, CNRS, Laboratoire des Matériaux Avancés (LMA), IP2I Lyon / IN2P3, UMR 5822, F-69622 Villeurbanne, France*
[158] *Dipartimento di Scienze Matematiche, Fisiche e Informatiche, Università di Parma, I-43124 Parma, Italy*
[159] *INFN, Sezione di Milano Bicocca, Gruppo Collegato di Parma, I-43124 Parma, Italy*
[160] *The University of Utah, Salt Lake City, UT 84112, USA*
[161] *Carleton College, Northfield, MN 55057, USA*
[162] *University of Zurich, Winterthurerstrasse 190, 8057 Zurich, Switzerland*
[163] *Perimeter Institute, Waterloo, ON N2L 2Y5, Canada*
[164] *Université de Strasbourg, CNRS, IPHC UMR 7178, F-67000 Strasbourg, France*
[165] *West Virginia University, Morgantown, WV 26506, USA*
[166] *University of Chicago, Chicago, IL 60637, USA*
[167] *Montclair State University, Montclair, NJ 07043, USA*
[168] *Colorado State University, Fort Collins, CO 80523, USA*
[169] *Institute for Nuclear Research, Bem t'er 18/c, H-4026 Debrecen, Hungary*
[170] *University of Texas, Austin, TX 78712, USA*
[171] *CNR-SPIN, c/o Università di Salerno, I-84084 Fisciano, Salerno, Italy*
[172] *Scuola di Ingegneria, Università della Basilicata, I-85100 Potenza, Italy*
[173] *Observatori Astronòmic, Universitat de València, E-46980 Paterna, València, Spain*
[174] *Centro de Física das Universidades do Minho e do Porto, Universidade do Minho, Campus de Gualtar, PT-4710 - 057 Braga, Portugal*
[175] *Department of Astronomy, The University of Tokyo, Mitaka City, Tokyo 181-8588, Japan*
[176] *Faculty of Engineering, Niigata University, Nishi-ku, Niigata City, Niigata 950-2181, Japan*
[177] *Department of Physics, Graduate School of Science, Osaka City University, Sumiyoshi-ku, Osaka City, Osaka 558-8585, Japan*
[178] *State Key Laboratory of Magnetic Resonance and Atomic and Molecular Physics, Innovation Academy for Precision Measurement Science and Technology (APM), Chinese Academy of Sciences, Xiao Hong Shan, Wuhan 430071, China*
[179] *University of Szeged, Dóm tér 9, Szeged 6720, Hungary*
[180] *Cornell University, Ithaca, NY 14850, USA*
[181] *University of British Columbia, Vancouver, BC V6T 1Z4, Canada*
[182] *INAF, Osservatorio Astronomico di Capodimonte, I-80131 Napoli, Italy*
[183] *The University of Mississippi, University, MS 38677, USA*
[184] *University of Michigan, Ann Arbor, MI 48109, USA*
[185] *Texas A&M University, College Station, TX 77843, USA*
[186] *Ulsan National Institute of Science and Technology, Ulsan 44919, Republic of Korea*
[187] *Shanghai Astronomical Observatory, Chinese Academy of Sciences, Shanghai 200030, China*
[188] *Institute for Cosmic Ray Research (ICRR), KAGRA Observatory, The University of Tokyo, Kashiwa City, Chiba 277-8582, Japan*
[189] *Faculty of Science, University of Toyama, Toyama City, Toyama 930-8555, Japan*
[190] *Institute for Cosmic Ray Research (ICRR), KAGRA Observatory, The University of Tokyo, Kamioka-cho, Hida City, Gifu 506-1205, Japan*
[191] *University of California, Berkeley, CA 94720, USA*
[192] *Maastricht University, 6200 MD, Maastricht, Netherlands*
[193] *Lancaster University, Lancaster LA1 4YW, United Kingdom*
[194] *College of Industrial Technology, Nihon University, Narashino City, Chiba 275-8575, Japan*
[195] *Department of Physics and Astronomy, Haverford College, 370 Lancaster Avenue, Haverford, PA 19041, USA*
[196] *Institute of Astronomy, National Tsing Hua University, Hsinchu 30013, Taiwan*
[197] *Rutherford Appleton Laboratory, Didcot OX11 0DE, United Kingdom*
[198] *Department of Astronomy & Space Science, Chungnam National University, Yuseong-gu, Daejeon 34134, Republic of Korea*

[199] *Department of Physical Sciences, Aoyama Gakuin University, Sagamihara City, Kanagawa 252-5258, Japan*
[200] *Kavli Institute for Astronomy and Astrophysics, Peking University, Haidian District, Beijing 100871, China*
[201] *Aristotle University of Thessaloniki, University Campus, 54124 Thessaloniki, Greece*
[202] *Graduate School of Science and Engineering, University of Toyama, Toyama City, Toyama 930-8555, Japan*
[203] *Nambu Yoichiro Institute of Theoretical and Experimental Physics (NITEP), Osaka City University, Sumiyoshi-ku, Osaka City, Osaka 558-8585, Japan*
[204] *Directorate of Construction, Services & Estate Management, Mumbai 400094, India*
[205] *Vanderbilt University, Nashville, TN 37235, USA*
[206] *Universiteit Antwerpen, Prinsstraat 13, 2000 Antwerpen, Belgium*
[207] *University of Białystok, 15-424 Białystok, Poland*
[208] *Ewha Womans University, Seoul 03760, Republic of Korea*
[209] *National Astronomical Observatories, Chinese Academic of Sciences, Chaoyang District, Beijing, China*
[210] *School of Astronomy and Space Science, University of Chinese Academy of Sciences, Chaoyang District, Beijing, China*
[211] *University of Southampton, Southampton SO17 1BJ, United Kingdom*
[212] *Institute for Cosmic Ray Research (ICRR), The University of Tokyo, Kashiwa City, Chiba 277-8582, Japan*
[213] *Institute for High-Energy Physics, University of Amsterdam, Science Park 904, 1098 XH Amsterdam, Netherlands*
[214] *Chung-Ang University, Seoul 06974, Republic of Korea*
[215] *University of Washington Bothell, Bothell, WA 98011, USA*
[216] *Institute of Applied Physics, Nizhny Novgorod, 603950, Russia*
[217] *Inje University Gimhae, South Gyeongsang 50834, Republic of Korea*
[218] *Department of Physics, Myongji University, Yongin 17058, Republic of Korea*
[219] *Institute of Particle and Nuclear Studies (IPNS), High Energy Accelerator Research Organization (KEK), Tsukuba City, Ibaraki 305-0801, Japan*
[220] *School of Physics and Astronomy, Cardiff University, Cardiff, CF24 3AA, UK*
[221] *Institute of Mathematics, Polish Academy of Sciences, 00656 Warsaw, Poland*
[222] *National Center for Nuclear Research, 05-400 Świerk-Otwock, Poland*
[223] *Instituto de Fisica Teorica, 28049 Madrid, Spain*
[224] *Department of Physics, Nagoya University, Chikusa-ku, Nagoya, Aichi 464-8602, Japan*
[225] *Université de Montréal/Polytechnique, Montreal, Quebec H3T 1J4, Canada*
[226] *Laboratoire Lagrange, Université Côte d'Azur, Observatoire Côte d'Azur, CNRS, F-06304 Nice, France*
[227] *Seoul National University, Seoul 08826, Republic of Korea*
[228] *Sungkyunkwan University, Seoul 03063, Republic of Korea*
[229] *NAVIER, École des Ponts, Univ Gustave Eiffel, CNRS, Marne-la-Vallée, France*
[230] *Università di Firenze, Sesto Fiorentino I-50019, Italy*
[231] *Department of Physics, National Cheng Kung University, Tainan City 701, Taiwan*
[232] *School of Physics and Technology, Wuhan University, Wuhan, Hubei, 430072, China*
[233] *National Center for High-performance computing, National Applied Research Laboratories, Hsinchu Science Park, Hsinchu City 30076, Taiwan*
[234] *Department of Physics, National Taiwan Normal University, sec. 4, Taipei 116, Taiwan*
[235] *NASA Marshall Space Flight Center, Huntsville, AL 35811, USA*
[236] *INFN, Sezione di Roma Tre, I-00146 Roma, Italy*
[237] *ESPCI, CNRS, F-75005 Paris, France*
[238] *Kenyon College, Gambier, OH 43022, USA*
[239] *School of Physics Science and Engineering, Tongji University, Shanghai 200092, China*
[240] *Dipartimento di Fisica, Università di Trieste, I-34127 Trieste, Italy*
[241] *Institute for Photon Science and Technology, The University of Tokyo, Bunkyo-ku, Tokyo 113-8656, Japan*
[242] *Indian Institute of Technology Madras, Chennai 600036, India*
[243] *Saha Institute of Nuclear Physics, Bidhannagar, West Bengal 700064, India*
[244] *Institute of Space and Astronautical Science (JAXA), Chuo-ku, Sagamihara City, Kanagawa 252-0222, Japan*
[245] *Institut des Hautes Etudes Scientifiques, F-91440 Bures-sur-Yvette, France*
[246] *Faculty of Law, Ryukoku University, Fushimi-ku, Kyoto City, Kyoto 612-8577, Japan*
[247] *Indian Institute of Science Education and Research, Kolkata, Mohanpur, West Bengal 741252, India*
[248] *Department of Physics, University of Notre Dame, Notre Dame, IN 46556, USA*
[249] *Graduate School of Science and Technology, Niigata University, Nishi-ku, Niigata City, Niigata 950-2181, Japan*
[250] *Consiglio Nazionale delle Ricerche - Istituto dei Sistemi Complessi, Piazzale Aldo Moro 5, I-00185 Roma, Italy*
[251] *Korea Astronomy and Space Science Institute (KASI), Yuseong-gu, Daejeon 34055, Republic of Korea*
[252] *Hobart and William Smith Colleges, Geneva, NY 14456, USA*

[253] International Institute of Physics, Universidade Federal do Rio Grande do Norte, Natal RN 59078-970, Brazil
[254] Museo Storico della Fisica e Centro Studi e Ricerche "Enrico Fermi", I-00184 Roma, Italy
[255] Dipartimento di Matematica e Fisica, Università degli Studi Roma Tre, I-00146 Roma, Italy
[256] University of Arizona, Tucson, AZ 85721, USA
[257] Università di Trento, Dipartimento di Matematica, I-38123 Povo, Trento, Italy
[258] University of California, Riverside, Riverside, CA 92521, USA
[259] University of Washington, Seattle, WA 98195, USA
[260] Indian Institute of Technology, Palaj, Gandhinagar, Gujarat 382355, India
[261] Department of Electronic Control Engineering, National Institute of Technology, Nagaoka College, Nagaoka City, Niigata 940-8532, Japan
[262] Departamento de Matemática da Universidade de Aveiro and Centre for Research and Development in Mathematics and Applications, Campus de Santiago, 3810-183 Aveiro, Portugal
[263] Marquette University, Milwaukee, WI 53233, USA
[264] Faculty of Science, Toho University, Funabashi City, Chiba 274-8510, Japan
[265] Graduate School of Science and Technology, Gunma University, Maebashi, Gunma 371-8510, Japan
[266] Institute for Quantum Studies, Chapman University, Orange, CA 92866, USA
[267] Accelerator Laboratory, High Energy Accelerator Research Organization (KEK), Tsukuba City, Ibaraki 305-0801, Japan
[268] Faculty of Information Science and Technology, Osaka Institute of Technology, Hirakata City, Osaka 573-0196, Japan
[269] INAF, Osservatorio Astrofisico di Arcetri, Largo E. Fermi 5, I-50125 Firenze, Italy
[270] Indian Institute of Technology Hyderabad, Sangareddy, Khandi, Telangana 502285, India
[271] Indian Institute of Science Education and Research, Pune, Maharashtra 411008, India
[272] Istituto di Astrofisica e Planetologia Spaziali di Roma, Via del Fosso del Cavaliere, 100, 00133 Roma RM, Italy
[273] Department of Space and Astronautical Science, The Graduate University for Advanced Studies (SOKENDAI), Sagamihara City, Kanagawa 252-5210, Japan
[274] Andrews University, Berrien Springs, MI 49104, USA
[275] Research Center for Space Science, Advanced Research Laboratories, Tokyo City University, Setagaya, Tokyo 158-0082, Japan
[276] Institute for Cosmic Ray Research (ICRR), Research Center for Cosmic Neutrinos (RCCN), The University of Tokyo, Kashiwa City, Chiba 277-8582, Japan
[277] Department of Physics, Kyoto University, Sakyou-ku, Kyoto City, Kyoto 606-8502, Japan
[278] Yukawa Institute for Theoretical Physics (YITP), Kyoto University, Sakyou-ku, Kyoto City, Kyoto 606-8502, Japan
[279] Dipartimento di Scienze Aziendali - Management and Innovation Systems (DISA-MIS), Università di Salerno, I-84084 Fisciano, Salerno, Italy
[280] Van Swinderen Institute for Particle Physics and Gravity, University of Groningen, Nijenborgh 4, 9747 AG Groningen, Netherlands
[281] Faculty of Science, Department of Physics, The Chinese University of Hong Kong, Shatin, N.T., Hong Kong
[282] Vrije Universiteit Brussel, Pleinlaan 2, 1050 Brussel, Belgium
[283] Applied Research Laboratory, High Energy Accelerator Research Organization (KEK), Tsukuba City, Ibaraki 305-0801, Japan
[284] Department of Communications Engineering, National Defense Academy of Japan, Yokosuka City, Kanagawa 239-8686, Japan
[285] Department of Physics, University of Florida, Gainesville, FL 32611, USA
[286] Department of Information and Management Systems Engineering, Nagaoka University of Technology, Nagaoka City, Niigata 940-2188, Japan
[287] Tata Institute of Fundamental Research, Mumbai 400005, India
[288] Eindhoven University of Technology, Postbus 513, 5600 MB Eindhoven, Netherlands
[289] Department of Physics and Astronomy, Sejong University, Gwangjin-gu, Seoul 143-747, Republic of Korea
[290] Concordia University Wisconsin, Mequon, WI 53097, USA
[291] Department of Electrophysics, National Yang Ming Chiao Tung University, Hsinchu, Taiwan
[292] Department of Physics, Rikkyo University, Toshima-ku, Tokyo 171-8501, Japan
[293] Jodrell Bank Centre for Astrophysics, School of Physics and Astronomy, University of Manchester, Manchester, UK, M13 9PL
[294] Astrophysics Science Division, NASA's Goddard Space Flight Center, Greenbelt, MD 20771, USA
[295] Columbia Astrophysics Laboratory, Columbia University, 550 West 120th Street, New York, NY, 10027, USA
[296] Laboratoire de Physique et Chimie de l'Environnement et de l'Espace, Université d'Orléans/CNRS, F-45071 Orléans Cedex 02, France
[297] Station de radioastronomie de Nançay, Observatoire de Paris, CNRS/INSU, F-18330 Nançay, France
[298] Department of Physics and Astronomy, University of British Columbia, 6224 Agricultural Road, Vancouver, BC V6T 1Z1 Canada
[299] RIKEN Cluster for Pioneering Research, 2-1 Hirosawa, Wako, Saitama 351-0198, Japan
[300] Center for Computational Astrophysics, Flatiron Institute, 162 5th Avenue, New York, New York, 10010, USA
[301] Department of Physics, University of Connecticut, 196 Auditorium Road, U-3046, Storrs, CT 06269-3046, USA
[302] IRAP, CNRS, 9 avenue du Colonel Roche, BP 44346, F-31028 Toulouse Cedex 4, France
[303] Université de Toulouse, CNES, UPS-OMP, F-31028 Toulouse, France
[304] Los Alamos National Laboratory, Los Alamos, NM 87545, USA

[305] *SRON-Netherlands Institute for Space Research, Niels Bohrweg 4, 2333 CA, Leiden, Netherlands*
[306] *CSIRO, Space and Astronomy, PO Box 76, Epping, NSW 1710, Australia*
[307] *Canadian Institute for Theoretical Astrophysics, University of Toronto, 60 St. George Street, Toronto, ON M5S 3H8, Canada*
[308] *School of Natural Sciences, University of Tasmania, Hobart, Australia*
[309] *Department of Physics, McGill University, 3600 rue University, Montréal, QC H3A 2T8, Canada*
[310] *McGill Space Institute, McGill University, 3550 rue University, Montréal, QC H3A 2A7, Canada*
[311] *LUTH, Observatoire de Paris, PSL Research University, CNRS, Université Paris Diderot, Sorbonne Paris Cité, F-92195 Meudon, France*